

Quantum Monte Carlo Calculations of Light Nuclei with Non-Local Potentials

by

Joel E. Lynn

A Dissertation Presented in Partial Fulfillment
of the Requirement for the Degree
Doctor of Philosophy

Approved April 2013 by the
Graduate Supervisory Committee:

Kevin Schmidt, Chair

Ricardo Alarcón

Richard Lebed

Igor Shovkovy

John Shumway

ARIZONA STATE UNIVERSITY

May 2013

ABSTRACT

Monte Carlo methods often used in nuclear physics, such as auxiliary field diffusion Monte Carlo and Green’s function Monte Carlo, have typically relied on phenomenological local real-space potentials containing as few derivatives as possible, such as the Argonne-Urbana family of interactions, to make sampling simple and efficient. Basis set methods such as no-core shell model or coupled-cluster techniques typically use softer non-local potentials because of their more rapid convergence with basis set size. These non-local potentials are typically defined in momentum space and are often based on effective field theory. Comparisons of the results of the two types of methods are complicated by the use of different potentials. This thesis discusses progress made in using such non-local potentials in quantum Monte Carlo calculations of light nuclei. In particular, it shows methods for evaluating the real-space, imaginary-time propagators needed to perform quantum Monte Carlo calculations using non-local potentials and universality properties of these propagators, how to formulate a good trial wave function for non-local potentials, and how to perform a “one-step” Green’s function Monte Carlo calculation for non-local potentials.

I dedicate this thesis to my family, who are the foundation upon which everything else is built.

To my wife and best friend, Jessica: You have always been and always will be my partner in all things. Without your love, support, and infinite patience none of this would have happened: I would not be who I am today without you. We are two birds getting lost upon their way.

To my son, Isaac: You are a continuing source of inspiration. You ask me tough questions, like “what did the universe look like before the big bang?” Seeing your curiosity about our world sharpens my own.

To my son, Owen: Your energy and spirit are rejuvenating. At the end of a day when nothing else may have worked or made sense, coming home and hearing you call my name as you ran to the door set everything right.

To my daughter, Kelsey: Your smile and laughter brightened many cloudy days. You are my Telsey-bird, Telsey-bird oh so sweet!

ACKNOWLEDGEMENTS

This thesis would not have been possible without the support and guidance of my advisor, Professor Kevin Schmidt. It was his suggestion originally that non-local potentials and quantum Monte Carlo might not be mutually exclusive. He was always willing to entertain my ideas even when less than well thought out and allowed me to question everything. Most importantly, he accepted me at the level I was at, and in a relatively short space of time, helped me to gain a much deeper understanding of quantum mechanics and nuclear physics. I have grown to appreciate and embrace the approach he sometimes calls “the dumb guy’s way” and I think of him as my friend as much as my advisor.

To Professor Ricardo Alarcón who often reassured me when the path before me was unclear, I offer my deepest gratitude. One of my professors once called him a “gentleman scholar” and I know now after these years what those words mean. Without him my graduate career would not have been possible.

I also acknowledge my other committee members, Professors Richard Lebed, John Shumway, and Igor Shovkovy for useful and insightful conversations. I would like to make special mention of Professor Richard Lebed. He first introduced me to quantum mechanics years ago and has influenced, for the better, the way I see, think, and do physics ever since.

I gratefully acknowledge support by the National Science Foundation under grant PHY1067777.

TABLE OF CONTENTS

	Page
LIST OF TABLES	vi
LIST OF FIGURES	vii
CHAPTER	
1 INTRODUCTION	1
1.1 Background and Motivation	1
1.2 Outline	3
2 METHODS AND INTERACTIONS	5
2.1 Nuclear Structure Methods	5
2.1.1 The Ab Initio No-Core Shell Model	6
2.1.2 The Coupled-Cluster Decomposition.....	8
2.1.3 The Green's Function Monte Carlo	10
2.2 Nuclear Interactions	16
2.2.1 The Hamiltonian.....	16
2.2.2 Argonne's v ₁₈ Interaction	18
2.2.3 The N ³ LO Interaction	21
2.2.4 The CD-Bonn Interaction	27
3 PROPAGATORS FOR NON-LOCAL POTENTIALS	28
3.1 Introduction.....	28
3.2 Methods for Non-Local Potentials.....	32
3.3 Consistency of the Propagators at Large Imaginary Times	35
3.4 Quantum Monte Carlo with Non-Local Potentials	45
3.5 Conclusions	51
4 GFMC WITH NON-LOCAL POTENTIALS	53
4.1 Introduction.....	53

CHAPTER	Page
4.2 The Wave Function: Standard Form and Techniques	53
4.3 The Wave Function: Non-Local Potentials	57
4.4 Green's Function Monte Carlo	63
4.4.1 Variational Monte Carlo and Non-Local Potentials	63
4.4.2 Green's Function Monte Carlo and Non-Local Potentials	66
5 CHECKING THE METHODS AND CURRENT STATUS	71
5.1 Checks	71
5.2 Current Status and Challenges.....	76
6 CONCLUSION	84
6.1 Summary	84
6.2 Outlook.....	86
REFERENCES	89
APPENDIX	
A EIGENFUNCTION EXPANSIONS OF VARIOUS QUANTITIES	97
A.1 One-Dimensional Examples.....	98
A.2 Three-Dimensional Channel Basis	103

LIST OF TABLES

Table	Page
2.1 Summary of Various Constants Used in the Definition of the AV ₁₈ Potential	20
4.1 Wave Function Parameters for ⁴ He	59
4.2 Deuteron Properties for Three Different Potentials as Calculated from Our Wave Functions Obtained Via Diagonalization Compared with Experiment	63
5.1 A Comparison of the Deuteron Kinetic Energy as Calculated by Three Different Methods: The Channel Calculation, the Growth Calculation, and the Finite Difference Calculation	73
5.2 A Comparison of Green's Function Monte Carlo Results with Argonne's v_{18} Interaction.....	75
5.3 Growth Energy Averages as Calculated in the Channels	76

LIST OF FIGURES

Figure	Page
2.1 A Comparison of Variational Monte Carlo and Green's Function Monte Carlo Energies for Various Nuclei	13
2.2 A Comparison of Green's Function Monte Carlo Energies for Various Nuclei with and Without Three-Body Interactions.....	18
2.3 The Fourier Transform of a Gaussian Is a Gaussian (the Red Dashed Curve). However, Cutting off the Integral at Some Largest Momentum Value k_{\max} Results in “Ringing” (the Solid Black Curve)	24
2.4 The One-Dimensional Regulator Function for $n = 2$	25
2.5 The One-Dimensional Regulator Functions for $n = 2$, Fourier Transformed to Real Space (Normalized So That $f_n(0) = g_n(0) = 1$)	26
2.6 The Absolute Value of the One-Dimensional Regulator Functions for $n = 2$, Fourier Transformed to Real Space (Normalized So That $f_n(0) = g_n(0) = 1$). The y Axis Is Log Scaled to Emphasize the Effect	27
3.1 The Quantum Potential in the 1S_0 Partial Wave as the Propagator Is Calculated for Successively Longer Imaginary Times	37
3.2 The Quantum Potential in the 3P_0 Partial Wave as the Propagator Is Calculated for Successively Longer Imaginary Times	38
3.3 The Quantum Potential in the 3S_1 Partial Wave as the Propagator Is Calculated for Successively Longer Imaginary Times	39
3.4 The Quantum Potential in the 3D_1 Partial Wave as the Propagator Is Calculated for Successively Longer Imaginary Times	40
3.5 The off-Diagonal Propagator in the 1S_0 Partial Wave as the Propagator Is Calculated for Successively Longer Imaginary Times	41

Figure	Page
3.6 The off-Diagonal Propagator in the 3P_0 Partial Wave as the Propagator Is Calculated for Successively Longer Imaginary Times	42
3.7 The off-Diagonal Propagator in the 3S_1 Partial Wave as the Propagator Is Calculated for Successively Longer Imaginary Times	43
3.8 The off-Diagonal Propagator in the 3D_1 Partial Wave as the Propagator Is Calculated for Successively Longer Imaginary Times	43
3.9 The off-Diagonal Propagator in the $^3S_1 - ^3D_1$ Partial Wave as the Propagator Is Calculated for Successively Longer Imaginary Times	44
3.10 The N ³ LO Central Propagator for Initial Separation, $r = 0.5$ fm, and Imaginary Time, $t = (2000 \text{ MeV})^{-1}$	46
3.11 The N ³ LO(600) Central Propagator for Initial Separation, $r = 0.5$ fm, and Imaginary Time, $t = (2000 \text{ MeV})^{-1}$	46
3.12 The Coordinate System Used to Visualize the Central Propagators. O Is the Original Origin, and O' Is the Shifted Origin Such That $r = r'$ Corresponds to the Shifted Origin	47
3.13 The Negative Parts of the N ³ LO Central Propagator for an Initial Separation, $r = 0.5$ fm, and Imaginary Time, $t = (2000 \text{ MeV})^{-1}$	48
3.14 The Negative Parts of the N ³ LO(600) Central Propagator for an Initial Separation, $r = 0.5$ fm, and Imaginary Time, $t = (2000 \text{ MeV})^{-1}$	48
3.15 A Typical Slice Through the N ³ LO Central Propagator for an Initial Separation, $r = 0.5$ fm, and Imaginary Time, $t = (2000 \text{ MeV})^{-1}$	49
3.16 A Typical Slice Through the N ³ LO(600) Central Propagator for an Initial Separation, $r = 0.5$ fm, and Imaginary Time, $t = (2000 \text{ MeV})^{-1}$	49

Figure	Page
4.1 The Correlation $f_c^{(1,0)}(r)$ (the 1S_0 Channel) Calculated Using Our Diagonalization Method for Three Different Potentials: the Boundary-Condition Exponential Is Also Displayed, Where $\alpha = \frac{1}{A-1} = \frac{1}{3}$	60
4.2 The Correlations $f_c^{(0,1)}(r)$ and $f_t^{(0,1)}(r)$ (the 3S_1 - 3D_1 Channel) Calculated Using Our Diagonalization Method for Three Different Potentials: the Boundary-Condition Exponential Is Also Displayed, Where $\alpha = \frac{1}{A-1} = \frac{1}{3}$. The Upper Curves Are the Central Correlations; the Lower Curves Are the Tensor Correlations	61
4.3 A Portion of the Correlation $f_t^{(0,1)}(r)$ Calculated Using Our Diagonalization Method for Three Different Potentials. The y Axis Is Log Scaled to Make the “Ringing” Effect of the N ³ LO Wave Function Clearer	62
5.1 The Ratio f/w for $k = 1.4$ in the Region That Contributes 98% of the Integral: $0 \leq x \leq 2$	78
5.2 The Ratio f/w for $k = 6.0$ in the Region That Contributes 98% of the Integral: $0 \leq x \leq 2$	79
5.3 The AV ₁₈ Channel Propagator $\langle r'L'JS e^{-Ht} rLJS \rangle$ with $L' = 0, L = 0, J = 1, S = 1$, and $t = (2000 \text{ MeV})^{-1}$	80
5.4 The CD-Bonn Channel Propagator $\langle r'L'JS e^{-Ht} rLJS \rangle$ with $L' = 0, L = 0, J = 1, S = 1$, and $t = (2000 \text{ MeV})^{-1}$	80
5.5 The N ³ LO Channel Propagator $\langle r'L'JS e^{-Ht} rLJS \rangle$ with $L' = 0, L = 0, J = 1, S = 1$, and $t = (2000 \text{ MeV})^{-1}$	81
5.6 The S - and D -Wave Energies of Eq. (5.16) for an Initial Separation of $r = 1.0 \text{ fm}$ as a Function of Δ for AV ₁₈ and CD-Bonn.....	82

Figure	Page
5.7 The S - and D -Wave Energies of Eq. (5.16) for an Initial Separation of $r = 1.0$ fm as a Function of Δ for N ³ LO	83
A.1 The Gaussian Eq. (A.6) in Red (Dashed-Dotted Line), and the Eigen- function Expansion Eq. (A.9) Truncated to Different Values of n_{\max} in Black (Solid Line) for Comparison	100

Chapter 1

INTRODUCTION

1.1 Background and Motivation

An important and open goal of contemporary physics is the complete and accurate understanding of the structure of atomic nuclei. Such an understanding would have significant implications for a vast assortment of scientific questions: For example, included are those outlined by the Committee on the Assessment of and Outlook for Nuclear Physics of the National Academies of Science (The NP2010 Committee, 2012). 1) How did visible matter come into being and how does it evolve? 2) How does subatomic matter organize itself and what phenomena emerge? 3) Are the fundamental interactions that are basic to the structure of matter fully understood? 4) How can the knowledge and technological progress provided by nuclear physics best be used to benefit society? A thorough understanding of nuclear structure would make a meaningful contribution to the answer of each of these questions.

For example, understanding nuclear structure thoroughly would imply we could do complete and accurate nuclear matter calculations obtaining the equation of state of nuclear matter. With this we could make better predictions about neutron star evolution and other astrophysical processes. This could help determine which astrophysical processes are involved in the so-called *r* process of nucleosynthesis, which would help directly explain how higher mass number nuclei came into existence. A complete understanding of nuclear structure would mean we could make accurate predictions for nuclear reaction rates and properties of rare isotopes, such as those which will be probed at the Facility for Rare Isotope Beams (FRIB) (York *et al.*,

2010). Furthermore, with such an understanding, we could make predictions about nuclei and processes which are experimentally difficult to probe, or point experiment in the direction of new and interesting nuclear phenomena.

While the field of *ab initio* nuclear structure calculations has made great strides in the past three decades, unresolved questions remain. Among these unresolved questions is how best to arrive at an inter-nucleon potential. Although little doubt remains that quantum chromodynamics (QCD) — the equations of which were written down some forty years ago — is the correct theory underlying the strong interactions between protons and neutrons, it has remained an intractable problem to start from QCD at the relatively low energies important to nuclear physics and arrive at an inter-nucleon potential through direct means. This is a consequence of asymptotic freedom: the fact that at low energies, the strength of the strong interaction grows.

Recently, an idea known as chiral effective field theory, which began with the work of Weinberg (1979) and later Weinberg (1990, 1991), has delivered inter-nucleon potentials (Entem and Machleidt, 2003) which are based on the same symmetries of low-energy QCD (namely broken chiral symmetry) and so show promise of making a more direct connection from QCD to nuclear structure calculations than has been possible previously. These chiral-effective-field-theory potentials have a feature known as non-locality. In essence this means that the interactions between nucleons depend not only on the distance by which they are separated at any given moment, but also on the distance by which they will be separated in the next moment. Another way of saying the same thing is that the interactions between nucleons derived from chiral effective field theory are velocity or momentum dependent.

There exist *ab initio* nuclear structure methods for which this non-locality poses no additional challenge. Basis-set methods, in particular the no-core shell model and the coupled-cluster decomposition, currently favor non-local potentials due to their more

rapid convergence with basis-set size. (Non-local potentials are often called “softer” since they do not induce short-range correlations as strongly as do local potentials.) However, in both of these methods, the initial inter-nucleon interaction is modified in some way from its original form to make it more amenable to the method.

One of the most trusted *ab initio* nuclear structure methods, quantum Monte Carlo, for the very reason that it uses the inter-nucleon interactions in their bare form, is currently formulated in such a way that it is only practically suitable to inter-nucleon potentials which are local (the interactions depend only on the distance by which the nucleons are separated at any given moment). This makes comparisons between nuclear structure methods difficult. This thesis is largely concerned with remedying this shortcoming: How to modify quantum Monte Carlo methods to accommodate non-local potentials.

1.2 Outline

The aim of this work is to perform nuclear structure calculations for light nuclei, with interacting protons and neutrons, using Green’s function Monte Carlo and non-local potentials derived from chiral effective field theory. Doing so would have two immediate effects that contribute to the overarching goal of a complete understanding of nuclear structure. 1) A quantum Monte Carlo calculation (in particular a Green’s function Monte Carlo calculation) of a light nucleus with a nuclear potential derived from chiral effective field theory would make a definite statement about the validity and usefulness of chiral effective field theory to nuclear structure. 2) Such calculations would allow for a more direct comparison of nuclear structure methods. To accomplish this goal, we will need the propagator, a good trial wave function, and Green’s function Monte Carlo. For each of these, modifications must be made to accommodate non-local potentials.

In Chapter 2, we compare and contrast different nuclear structure methods, focusing on those which are able (or in principle are able) to employ non-local potentials, and make an argument in favor of Green’s function Monte Carlo. We give some details on several common nuclear interaction choices with particular attention paid to the next-to-next-to-next-to-leading order in chiral perturbation theory interaction of Entem and Machleidt (2003).

In Chapter 3, we present our work on calculating the imaginary-time two-body (pair) propagator for non-local potentials. Of the three main ingredients we need (a propagator, a wave function, and a quantum Monte Carlo method) the calculation of the pair propagator is the largest hurdle to overcome.

In Chapter 4, we present our work on calculating a good trial wave function for non-local potentials and what modifications to the Green’s function Monte Carlo method must be made to accommodate non-local potentials. In Chapter 5 we present various checks on the methods we have developed and the current status, which includes the current challenges which have prevented a successful ${}^4\text{He}$ calculation to date. In Chapter 6 we conclude by presenting the outlook and future research directions. Appendix A details the eigenfunction expansion technique we have exploited throughout this work.

Chapter 2

METHODS AND INTERACTIONS

2.1 Nuclear Structure Methods

The goal of this work is to demonstrate how to use non-local nucleon-nucleon potentials in quantum Monte Carlo calculations of light nuclei by calculating the ground-state energy of some light nucleus, like ^4He , using the non-local next-to-next-to-next-to-leading order (N^3LO) interaction of Entem and Machleidt (2003). The question arises: Are there other methods that could be used in place of quantum Monte Carlo which are suited for the same purpose? While a number of methods exist for calculations of three- and four-body nuclei (Kamada *et al.*, 2001) — for example Fadeev-Yakubovsky (Yakubovsky, 1967; Glöckle and Kamada, 1993; Kamada and Glöckle, 1992; Nogga *et al.*, 2000), coupled-rearrangement-channel Gaussian-basis variational (Kamimura, 1988; Kameyama *et al.*, 1989; Kamimura and Kameyama, 1990; Hiyama *et al.*, 1999, 2000), stochastic variational (Varga and Suzuki, 1995; Varga *et al.*, 1997; Usukura *et al.*, 1998, 1999), hyperspherical variational (de la Ripelle, 1983; Viviani *et al.*, 1995; Kievsky *et al.*, 1997; Viviani, 1998), Green’s function Monte Carlo (Carlson, 1987, 1988; Pudliner *et al.*, 1997; Wiringa *et al.*, 2000), the no-core shell model (Navrátil and Barrett, 1999; Navrátil *et al.*, 2000a,c,b), coupled-cluster decomposition (Coester, 1958; Coester and Kümmel, 1960; Heisenberg and Mihaila, 1999; Mihaila and Heisenberg, 2000a,b; Dean and Hjorth-Jensen, 2004; Kowalski *et al.*, 2004; Hagen *et al.*, 2008), and effective interaction hyperspherical harmonic (Barnea *et al.*, 2000, 2001) — we want to impose the additional restrictions that the method should be able to handle a non-local potential and should have the possibility to scale up to

larger nuclei. With these additional restrictions in place, there are arguably only three candidates.

2.1.1 The *Ab Initio* No-Core Shell Model

The *ab initio* no-core shell model derives its name from two of its defining features. The A -nucleon non-relativistic Hamiltonian is expanded in a harmonic oscillator basis which allows for the second quantization techniques of the standard shell model to be used. However, unlike a traditional shell model calculation, there is no inert core: all A nucleons are active. See Navrátil *et al.* (2009) for a review of the method and some recent results using chiral two- and three-body interactions.

The starting point is the Hamiltonian

$$H = \sum_{i=1}^A \frac{\mathbf{p}_i^2}{2m} + \sum_{i < j}^A v_{ij} + \sum_{i < j < k}^A V_{ijk}, \quad (2.1)$$

where m is the nucleon mass and v_{ij} and V_{ijk} are the the two- and three-body interactions, respectively. Of course, the center-of-mass motion is unimportant to the calculation and is usually separated out.

$$H = \frac{\mathbf{P}^2}{2mA} + H_A, \quad (2.2)$$

where $\mathbf{P} = \sum_{i=1}^A \mathbf{p}_i$, and

$$H_A = \frac{1}{A} \sum_{i < j}^A \frac{(\mathbf{p}_i - \mathbf{p}_j)^2}{2m} + \sum_{i < j}^A v_{ij} + \sum_{i < j < k}^A V_{ijk}. \quad (2.3)$$

The harmonic oscillator basis used is finite. Typical calculations for p-shell nuclei are limited to between roughly 10 and 20 harmonic oscillator shells (Forssén *et al.*, 2008). For realistic high-accuracy nuclear potentials such as Argonne's v_{18} (AV₁₈) (Wiringa *et al.*, 1995), CD-Bonn(2000) (Machleidt, 2001), and the chiral N³LO (Entem and Machleidt, 2003) potentials, which generate strong short-range correlations,

even these harmonic oscillator basis sets are not sufficient. Therefore, an effective interaction must be generated to help with the convergence with basis set size. Such effective interactions are basis-set size dependent and are often generated via a unitary transformation.

The Hamiltonian is modified to include a center-of-mass harmonic oscillator to assist in the derivation of this effective interaction. $H_{\text{CM}} = T_{\text{CM}} + V_{\text{CM}}$ (the effects of which are to be subtracted out later in the full many-body calculation). T_{CM} is the center-of-mass harmonic oscillator kinetic energy and V_{CM} is the center-of-mass harmonic oscillator potential energy: $V_{\text{CM}} = \frac{1}{2}Am\Omega^2\mathbf{R}^2$, where $\mathbf{R} = \frac{1}{A}\sum_{i=1}^A \mathbf{r}_i$ is the center of mass. The modified Hamiltonian can be written as

$$\begin{aligned} H_A^\Omega &= H_A + H_{\text{CM}} \\ &= \sum_{i=1}^A \left(\frac{\mathbf{p}_i^2}{2m} + \frac{1}{2}m\Omega^2\mathbf{r}_i^2 \right) + \sum_{i < j}^A \left[v_{ij} - \frac{1}{2A}m\Omega^2(\mathbf{r}_i - \mathbf{r}_j)^2 \right]. \end{aligned} \quad (2.4)$$

Clearly, the Hamiltonian now depends on both the basis-set size used and the harmonic oscillator frequency. Convergence, while guaranteed by construction for any particular harmonic oscillator frequency in the limit of infinite basis size, is not trivial. See Forssén *et al.* (2008) for a discussion. The unitary transformation mentioned above is typically the Lee-Suzuki similarity transformation (Ôkubo, 1954; Suzuki and Lee, 1980; Suzuki and Okamoto, 1983). This method allows, in principle, for the construction of an effective Hamiltonian that can faithfully reproduce the non-truncated-space results for a select set of the A -body eigenstates. In practice, however, the effective Hamiltonian is only constructed to reproduce the non-truncated space results for a two- or three- or four-nucleon system. This effective Hamiltonian is then used in the full A -body problem. Furthermore, the similarity transformation generates additional many-body interactions in the effective Hamiltonian.

In short, there are a number of attractive features of the no-core shell model: namely that it can handle a non-local potential and that it can scale up to nuclei with $A > 4$, but the drawbacks include the fact that the results are model-space dependent, bare realistic nucleon-nucleon interactions cannot be used without an additional renormalization method, which generates many-body interactions even if only two- or three-body interactions were present in the original Hamiltonian, and convergence can be problematic.

2.1.2 *The Coupled-Cluster Decomposition*

The coupled-cluster method is a many-body quantum technique that was originally designed for use in nuclear physics problems in the late 1950s (Coester, 1958) but was only developed in earnest for chemistry purposes until the late 1990s and early 2000s with the work on ^{16}O of Heisenberg and Mihaila (Heisenberg and Mihaila, 1999; Mihaila and Heisenberg, 1999, 2000a,b). The idea shares many features with the no-core shell model described above. The energies are calculated in a finite harmonic-oscillator model space and so depend on the manner in which the truncation is made, and the harmonic-oscillator frequency. However, what distinguishes the coupled-cluster method from the shell model is its size extensivity and its size consistency. By size extensivity, it is meant that only linked diagrams appear in the calculation of the expectation value of the energy. It can be shown that all truncation schemes in the standard no-core shell model (known as configuration interaction in quantum chemistry) suffer from the inclusion of disconnected diagrams (Crawford and Schaefer III, 2000). By size consistency, it is meant that the energy of two non-interacting pieces are the same whether computed separately or together. The shell model does not, in general, have this property. See Dean and Hjorth-Jensen (2004) for an overview of the method and some recent results.

The technique begins with an *ansatz* for the full many-body correlated wave function as the exponential of a correlation operator on some reference Slater determinant¹:

$$|\Psi\rangle = \exp(T_{\text{corr}}) |\Psi_0\rangle, \quad (2.5)$$

where T_{corr} is a correlation operator $T_{\text{corr}} = T_{\text{corr}1} + T_{\text{corr}2} + \dots + T_{\text{corr}A}$, and $|\Psi_0\rangle$ is a Slater determinant of single-particle orbitals. The correlation operators are defined in terms of creation and annihilation operators

$$T_{\text{corr}k} = \frac{1}{(k!)^2} \sum_{i_1, \dots, i_k; a_1, \dots, a_k} t_{i_1, \dots, i_k}^{a_1, \dots, a_k} a_{a_1}^\dagger \dots a_{a_k}^\dagger a_{i_k} \dots a_{i_1}, \quad (2.6)$$

where the indices i_1, \dots, i_k label occupied single-particle orbitals and the indices a_1, \dots, a_k label unoccupied orbitals. In particular, many coupled-cluster calculations focus on the single and double correlation operators, which are

$$T_{\text{corr}1} = \sum_{i < \epsilon_f, a > \epsilon_f} t_i^a a_a^\dagger a_i, \quad (2.7a)$$

$$T_{\text{corr}2} = \sum_{i, j < \epsilon_f; a, b > \epsilon_f} t_{ij}^{ab} a_a^\dagger a_b^\dagger a_j a_i. \quad (2.7b)$$

For the correct correlation operator, T_{corr} , the matrix elements

$$\langle \Psi_0 | \exp(-T_{\text{corr}}) H \exp(T_{\text{corr}}) | \Psi_0 \rangle \quad (2.8)$$

equal the energy. The amplitudes t_i^a and t_{ij}^{ab} can be solved for by projecting onto excited Slater determinants.

$$\langle \Psi_i^a | \exp(-T_{\text{corr}}) H \exp(T_{\text{corr}}) | \Psi_0 \rangle = 0, \quad (2.9a)$$

$$\langle \Psi_{ij}^{ab} | \exp(-T_{\text{corr}}) H \exp(T_{\text{corr}}) | \Psi_0 \rangle = 0, \quad (2.9b)$$

¹In the shell-model and coupled-cluster literature, many-body states constructed from antisymmetric products of single-particle states are often called Slater determinants. Of course an actual determinant is the overlap of two such states.

Then, the transformation can be expanded using the so-called “Hadamard Lemma”

$$\begin{aligned} \exp(-T_{\text{corr}})H\exp(T_{\text{corr}}) &= H + [H, T_{\text{corr}\,1}] + [H, T_{\text{corr}\,2}] \\ &\quad + \frac{1}{2}[[H, T_{\text{corr}\,1}], T_{\text{corr}\,1}] + \frac{1}{2}[[H, T_{\text{corr}\,2}], T_{\text{corr}\,2}] \quad (2.10) \\ &\quad + [[H, T_{\text{corr}\,1}], T_{\text{corr}\,2}] + \dots \end{aligned}$$

The expansion terminates at a set level depending on the interactions included in the Hamiltonian. For example, if the Hamiltonian contains only two-body interactions, the expansion terminates at the level of quadruply nested commutators. For three-body interactions, six nested commutators appear. The equations produced by this method are quite involved, but are exact and amenable to iterative techniques and so can be calculated efficiently.

The coupled-cluster method suffers from several drawbacks. Just like the no-core shell model, it has difficulty using bare realistic interactions due to the strong short-range correlations of these interactions. The coupled-cluster method typically “renormalizes” the short range behavior. That is, an effective interaction that can be handled in the finite harmonic-oscillator basis replaces the bare interaction. In addition, the energy is the expectation value of a non-Hermitian operator: $\exp(-T_{\text{corr}})H\exp(T_{\text{corr}})$. Though it is found that for a non-truncated correlation operator T_{corr} the energy-eigenvalue spectrum is in agreement with that of the Hamiltonian, this is not guaranteed when T_{corr} is truncated. Last, in practice, the coupled-cluster method is best suited to closed-shell nuclei where symmetries can reduce the degrees of freedom enough that the calculation is a reasonable size.

2.1.3 The Green’s Function Monte Carlo

Green’s function Monte Carlo is a fully microscopic method for solving the many-body Schrödinger equation, $H\Psi = E\Psi$, capable of handling realistic bare nucleon-nucleon potentials and capable of scaling up to larger nuclei. State of the art cal-

culations go as far as ^{12}C (Pieper, 2005). It is highly accurate and largely regarded as the “gold standard” for calculations of light nuclei with $4 < A \leq 12$. Up until now, a drawback of the method has been that it has been formulated in such a way that it is only practically amenable to interactions that are local in real space: $V_{\text{NN}}(\mathbf{r}, \mathbf{r}') = V_{\text{NN}}(\mathbf{r})\delta^{(3)}(\mathbf{r} - \mathbf{r}')$ plus operators which require, at most, second derivatives. We describe the canonical Green’s function Monte Carlo method in brief here; more details and the necessary deviations (our contributions) to accommodate non-local potentials are presented in Chapter 4.

One would like to start with a variational calculation of the energy of the nuclear system. This is done with so-called variational Monte Carlo (Wiringa, 1991). The method begins with a trial wave function Ψ_T which has many variational parameters. A random position $\mathbf{R} = \{\mathbf{r}_1, \mathbf{r}_2, \dots, \mathbf{r}_A\}$ is generated: the $\{\mathbf{r}_i\}$ are the A position vectors of the nucleons. Then, the Metropolis *et al.* method (Metropolis *et al.*, 1953; Hastings, 1970) is used to generate new positions \mathbf{R}' based on the probability $P = \frac{|\Psi_T(\mathbf{R}')|^2}{|\Psi_T(\mathbf{R})|^2}$. That is, a new position \mathbf{R}' is proposed (often sampled from a Gaussian distribution centered at \mathbf{R}) and the probability P is calculated. If $P > 1$, then the proposed position is accepted. Otherwise the proposed position is accepted with probability P (a uniform random number u between 0 and 1 is generated: if $u \leq P$ the proposed position is accepted, otherwise it is rejected and the original position retained). The process can be viewed as a random walk, and the end result is a set of so-called “walkers” which are distributed according to the trial wave function.

A walker is the set of $3A$ positions and — in the charge basis — $2^A \binom{A}{Z}$ spin-isospin states, where Z is the atomic number of the nucleus: $\sum_{\beta} c_{\beta} |\mathbf{R}\beta\rangle$, where the $\{c_{\beta}\}$ are the $2^A \binom{A}{Z}$ complex coefficients of the states. For example, for ^4He , ^6Li , and ^8Li , there are 96, 1280, and 14336 spin-isospin states, respectively. This number can be

reduced if we work in the good isospin basis, where, instead there are only

$$2^A \frac{2T+1}{\frac{1}{2}A+T+1} \binom{A}{\frac{1}{2}A+T} \quad (2.11)$$

spin-isospin states. (T is the total isospin of the nucleus). Then, we have 32, 320, and 7168 spin-isospin states for ${}^4\text{He}$, ${}^6\text{Li}$, and ${}^8\text{Li}$, respectively. For even- A nuclei, a further reduction can be made. If the $M = 0$ state is needed, just half of the spin components need to be calculated; the other half can be obtained by virtue of the time-reversal invariance of the state (Pieper and Wiringa, 2001). As we move up in mass number A , the savings in the size of the walkers is overwhelmed by the (essentially) exponential growth of the number of spin-isospin components.

The Raleigh-Ritz variational principle is invoked to calculate the trial energy: The variational parameters are adjusted to minimize the trial energy which is an upper bound on the actual ground-state energy.

$$E_T = \frac{\langle \Psi_T | H | \Psi_T \rangle}{\langle \Psi_T | \Psi_T \rangle} \geq E_0. \quad (2.12)$$

However, we do not know the exact many-body wave function and even our best trial wave functions fail to give accurate binding energies for even the lightest nuclei. For example, the best variational energies for ${}^3\text{H}$ and ${}^4\text{He}$ are still some 2% above values given by exact methods such as Faddeev, hyperspherical harmonic or Green's function Monte Carlo (Pudliner *et al.*, 1997). The trend is a worsening of variational Monte Carlo energies as A grows. See Fig. (2.1).

Green's function Monte Carlo allows us to start with a reasonable guess for the wave function and arrive at a wave function which is – in principle – exact. It does this by propagating in imaginary time to project out the ground state. The trial wave function $|\Psi_T\rangle$ can be written as a linear combination of eigenstates

$$|\Psi_T\rangle = \sum_{i=0}^{\infty} \alpha_i |\Psi_i\rangle = \alpha_0 |\Psi_0\rangle + \alpha_1 |\Psi_1\rangle + \dots \quad (2.13)$$

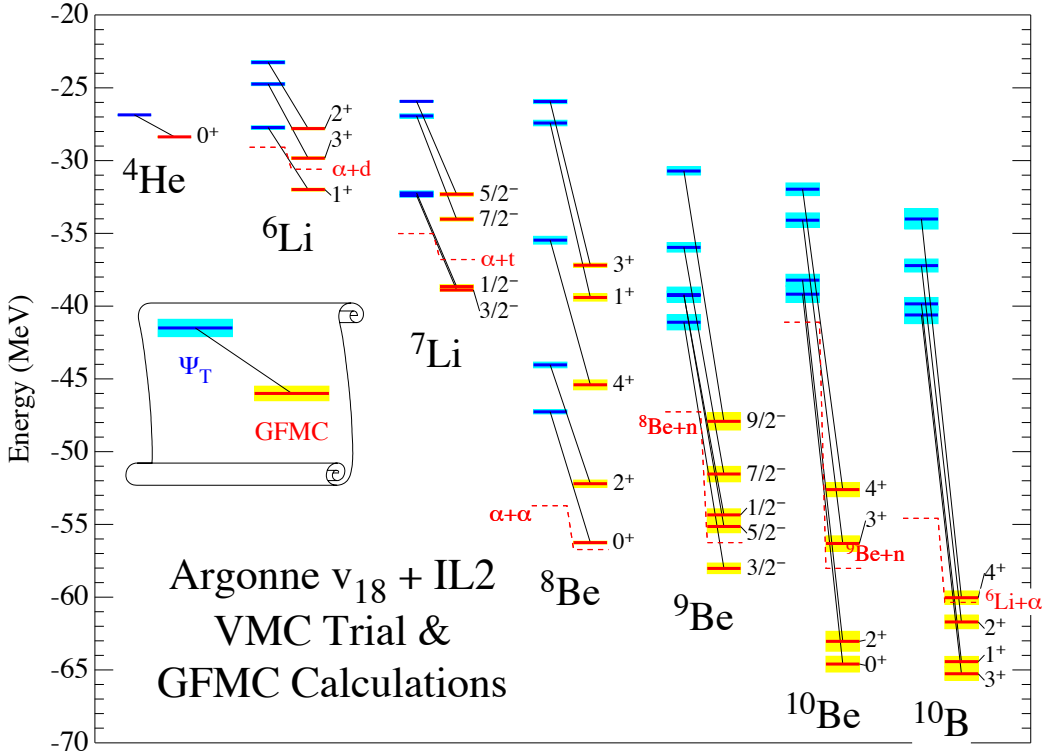


Figure 2.1: A comparison of variational Monte Carlo and Green’s function Monte Carlo energies for various nuclei. The interactions are the two-body AV₁₈ Hamiltonian with the three-body IL2 Hamiltonian. The shading indicates the Monte Carlo statistical errors (Pieper, 2005).

While it certainly should have some large overlap with the exact many-body ground state, $|\Psi_0\rangle$, it inevitably contains an admixture of excited states as well. Propagation with the imaginary-time Green’s function gives

$$|\Psi(t)\rangle = e^{-(H-\tilde{E}_0)t} |\Psi_T\rangle = e^{-(E_0-\tilde{E}_0)t} \left[\alpha_0 |\Psi_0\rangle + \sum_{i=1}^{\infty} \alpha_i e^{-(E_i-E_0)t} |\Psi_i\rangle \right], \quad (2.14)$$

where \tilde{E}_0 is a trial energy: a best estimate for the energy.

In the limit of long imaginary times,

$$\lim_{t \rightarrow \infty} |\Psi(t)\rangle \propto |\Psi_0\rangle. \quad (2.15)$$

Since, for $i > 0$, $E_i > E_0$, the excited states $\{|\Psi_i\rangle\}$ ($i > 0$) all decay away in this limit.

The Green's function, $e^{-(H-\tilde{E}_0)t}$ which we will often refer to as $G_{\alpha\beta}(\mathbf{R}, \mathbf{R}'; t)$, is evaluated by introducing a short imaginary-time Δt ($t = n\Delta t$). It is a matrix in spin-isospin space:

$$G_{\alpha\beta}(\mathbf{R}, \mathbf{R}'; \Delta t) = \langle \mathbf{R}'\alpha | e^{-(H-\tilde{E}_0)\Delta t} | \mathbf{R}\beta \rangle. \quad (2.16)$$

Then, the wave function at a position \mathbf{R}_n evolved to imaginary time t , is the path integral

$$\Psi(\mathbf{R}_n, t) = \int d\mathcal{R} G(\mathbf{R}_n, \mathbf{R}_{n-1}) \cdots G(\mathbf{R}_1, \mathbf{R}_0) \Psi_T(\mathbf{R}_0), \quad (2.17)$$

where $d\mathcal{R} = \prod_{i=0}^{n-1} d\mathbf{R}_i$, suppressing the spin-isospin sums. In Green's function Monte Carlo, this integral is evaluated stochastically; that is, by a random walk. The use of short imaginary times allows us to approximate the many-body propagator by a product over pairs

$$G_{\alpha\beta}(\mathbf{R}, \mathbf{R}'; \Delta t) = G_0(\mathbf{R}, \mathbf{R}'; \Delta t) \langle \alpha | \mathcal{S} \prod_{i < j} \frac{g_{ij}(\mathbf{r}_{ij}, \mathbf{r}'_{ij}; \Delta t)}{g_{0,ij}(\mathbf{r}_{ij}, \mathbf{r}'_{ij}; \Delta t)} | \beta \rangle, \quad (2.18)$$

where \mathbf{r}_{ij} and \mathbf{r}'_{ij} are the initial and final relative coordinates of the pairs, \mathcal{S} is a symmetrization operator,

$$G_0(\mathbf{R}, \mathbf{R}'; \Delta t) = \left(\frac{m}{2\pi\hbar^2\Delta t} \right)^{\frac{3A}{2}} \exp \left[-\frac{m(\mathbf{R} - \mathbf{R}')^2}{2\hbar^2\Delta t} \right], \quad (2.19)$$

is the A -body free-particle propagator,

$$\langle \alpha | g_{ij}(\mathbf{r}_{ij}, \mathbf{r}'_{ij}; \Delta t) | \beta \rangle = \langle \mathbf{r}'_{ij}\alpha | e^{-H\Delta t} | \mathbf{r}_{ij}\beta \rangle, \quad (2.20)$$

is the exact two-body (or pair) propagator, while

$$g_{0,ij}(\mathbf{r}_{ij}, \mathbf{r}'_{ij}; \Delta t) = \left(\frac{m}{2\pi\hbar^2\Delta t} \right)^{3/2} \exp \left[-\frac{m(\mathbf{r}_{ij} - \mathbf{r}'_{ij})^2}{2\hbar^2\Delta t} \right], \quad (2.21)$$

is the two-body free-particle propagator. The pair-product approximation Eq. (2.18) introduces leading errors of order $(\Delta t)^3$ (Ceperley, 1995).

Although in principle, one would now like to calculate expectation values such as $\langle O(t) \rangle = \frac{\langle \Psi(t) | O | \Psi(t) \rangle}{\langle \Psi(t) | \Psi(t) \rangle}$, in practice Green's function Monte Carlo calculates “mixed estimates”

$$\begin{aligned} \langle O(t) \rangle_{\text{Mixed}} &= \frac{\langle \Psi(t) | O | \Psi_T \rangle}{\langle \Psi(t) | \Psi_T \rangle} \\ &= \frac{\int d\mathcal{R} \Psi_T^\dagger(\mathbf{R}_n) G^\dagger(\mathbf{R}_n, \mathbf{R}_{n-1}; \Delta t) \cdots G^\dagger(\mathbf{R}_1, \mathbf{R}_0; \Delta t) O \Psi_T(\mathbf{R}_0)}{\int d\mathcal{R} \Psi_T^\dagger(\mathbf{R}_n) G^\dagger(\mathbf{R}_n, \mathbf{R}_{n-1}; \Delta t) \cdots G^\dagger(\mathbf{R}_1, \mathbf{R}_0; \Delta t) \Psi_T(\mathbf{R}_0)}, \end{aligned} \quad (2.22)$$

since the evaluation of the operator O to the left is difficult. These mixed estimates are related to the desired expectation values to lowest order by

$$\langle O(t) \rangle = \frac{\langle \Psi(t) | O | \Psi(t) \rangle}{\langle \Psi(t) | \Psi(t) \rangle} \approx \langle O(t) \rangle_{\text{Mixed}} + [\langle O(t) \rangle_{\text{Mixed}} - \langle O \rangle_T], \quad (2.23)$$

where $\langle O \rangle_T$ is the variational expectation value (Pudliner *et al.*, 1997). However, for calculating ground-state energies, the operator $O = H$, and, since H and G commute $[H, G] = 0$, we can write the mixed estimate in this case as

$$\langle H \rangle_{\text{Mixed}} = \frac{\langle \Psi_T | e^{-Ht/2} H e^{-Ht/2} | \Psi_T \rangle}{\langle \Psi_T | e^{-Ht/2} e^{-Ht/2} | \Psi_T \rangle}, \quad (2.24)$$

in which case, it is clear that in the limit of large imaginary times,

$$\lim_{t \rightarrow \infty} \langle H \rangle_{\text{Mixed}} = E_0, \quad (2.25)$$

the exact many-body ground-state energy.

Green's function Monte Carlo has the advantage that it works directly with realistic bare nuclear interactions and therefore is a highly trustworthy *ab initio* nuclear

structure method. There are at least two subtleties which may be viewed as drawbacks. One is that, in practice, mixed estimates are calculated for expectation values of operators and therefore they may not be strict upper bounds. However, for ground-state energies, this problem is avoided. An additional issue that arises is the so-called “fermion sign problem”. Statistical errors will grow out of control if a naive unconstrained walk is taken for a fermionic system. There are ways out of this dilemma which involve constraining the path by some means (akin to the fixed-node approximation (Ceperley and Alder, 1980)) and releasing the constraint after the calculation has converged to separate out the effect of the constraint. In practice this appears to work quite well, but again, with the constrained path, the strict variational principle is lost. The method is discussed in more detail in Chapter 4.

2.2 Nuclear Interactions

2.2.1 The Hamiltonian

The nuclear Hamiltonian is taken to be

$$H = \sum_{i=1}^A \frac{-\hbar^2}{2m_i} \nabla_i^2 + \sum_{i < j} v_{ij} + \sum_{i < j < k} V_{ijk} + \dots, \quad (2.26)$$

where v_{ij} and V_{ijk} are the two- and three-body interactions, respectively, m_i is the nucleon mass, and more-body interactions could be included. There is some evidence to suggest that these are small². Charge-independence breaking effects in the kinetic energy operator are included to account for the difference in neutron and proton masses. The kinetic energy operator can be written as a sum of projection operators

²Notably, nuclear structure calculations using two- and three-body interactions seem to account for nuclear structure of nuclei up to ^{12}C quite well without the addition of four- or more-body forces. See Fig. (2.2).

onto protons and neutrons

$$\begin{aligned} T_{\text{ke } i} &= -\frac{\hbar^2}{2} \left[\left(\frac{1 + \tau_{zi}}{2} \right) \frac{1}{m_p} + \left(\frac{1 - \tau_{zi}}{2} \right) \frac{1}{m_n} \right] \nabla_i^2 \\ &= -\frac{\hbar^2}{4} \left(\frac{1}{m_p} + \frac{1}{m_n} \right) \nabla_i^2 - \frac{\hbar^2}{4} \left(\frac{1}{m_p} - \frac{1}{m_n} \right) \tau_{zi} \nabla_i^2. \end{aligned} \quad (2.27)$$

The first term contains the reduced mass and is the dominant contribution to the kinetic energy. The second term is small ($\left(\frac{m_p^{-1} - m_n^{-1}}{m_p^{-1} + m_n^{-1}} \sim \mathcal{O}(10^{-4}) \right)$) and in many cases is treated perturbatively.

The three-body interactions V_{ijk} are mentioned because they form an important part of the standard Green's function Monte Carlo method. Indeed, without a three-body interaction, Green's function calculations of light nuclei (excepting ${}^2\text{H}$) are underbound, worsening rapidly as A grows (Pieper *et al.*, 2001; Pieper, 2005). See Fig. (2.2). However, this dissertation is primarily concerned with two-body interactions v_{ij} for several reasons. 1) The three-body chiral-effective-field-theory interaction is available and used in a local form presently (Navrátil, 2007) (in fact, it has been used in quantum Monte Carlo calculations (Lovato *et al.*, 2012)), while the two-body interaction is decidedly not. 2) While three-body effects are clearly important, two-body interactions are still dominant and should be treated first. 3) The methods we develop here could be adapted, with some modifications, to work with non-local three-body forces.

There are, broadly speaking, two classes of two-body potentials. Local, real-space, phenomenological potentials (of which Argonne's v_{18} figures prominently (Wiringa *et al.*, 1995)) and non-local, momentum-space potentials, which are often based on effective field theory (the N³LO in chiral perturbation theory potential of Entem and Machleidt (2003) is a prime example).

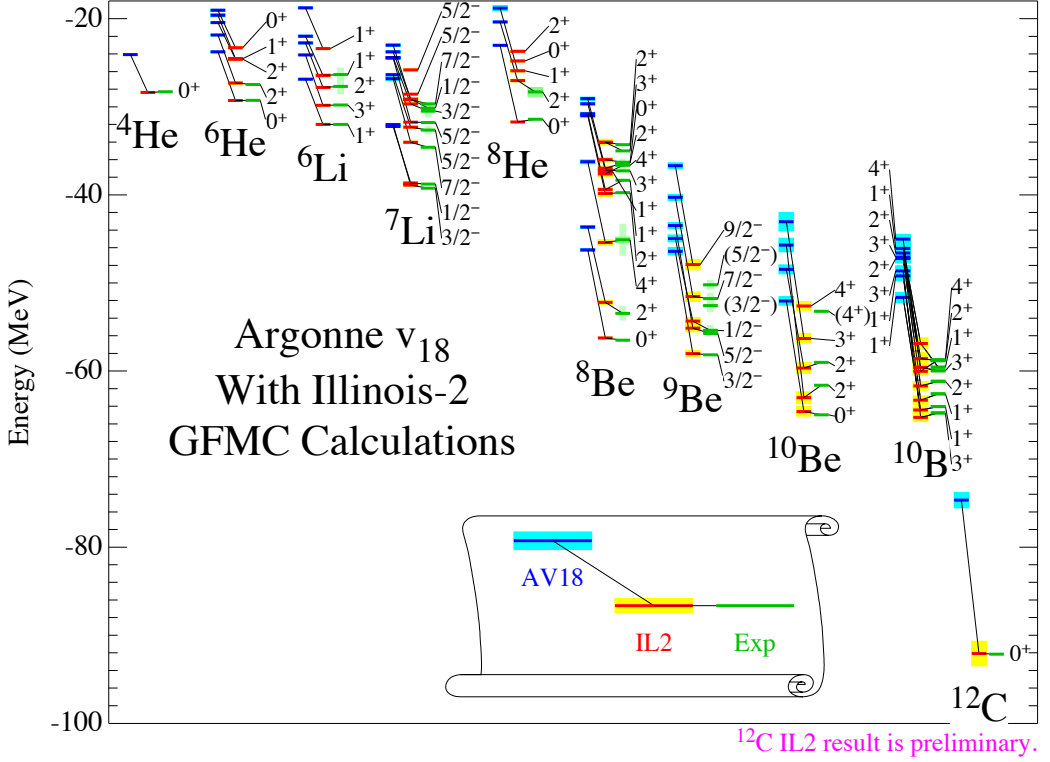


Figure 2.2: A comparison of Green's function Monte Carlo energies for various nuclei with and without three-body interactions. The interactions are the two-body AV₁₈ Hamiltonian with the three-body IL2 Hamiltonian. The shading indicates the Monte Carlo statistical errors (Pieper, 2005).

2.2.2 Argonne's v₁₈ Interaction

The AV₁₈ potential can be written as the sum of three parts

$$v_{ij} = v_{ij}^{\gamma} + v_{ij}^{\pi} + v_{ij}^R, \quad (2.28)$$

where v_{ij}^{γ} is a complete electromagnetic potential, v_{ij}^{π} is the one-pion-exchange potential, and v_{ij}^R is a short-range phenomenological potential. The electromagnetic potential includes one- and two-photon exchange Coulomb interactions ($C1$ and $C2$), vacuum polarization (VP), Darwin-Foldy (DF), and magnetic moment (MM) terms with appropriate proton and neutron form factors. It also includes finite-size effects

to account for the fact that protons and neutrons are not actually point-like particles. For proton-proton, neutron-proton, and neutron-neutron interactions it can be written

$$\begin{aligned} v_{ij}^\gamma(pp) &= V_{C1}(pp) + V_{C2} + V_{VP} + V_{DF} + V_{MM}(pp), \\ v_{ij}^\gamma(np) &= V_{C1}(np) + V_{MM}(np), \\ v_{ij}^\gamma(nn) &= V_{MM}(nn). \end{aligned} \quad (2.29)$$

The one-pion-exchange potential includes charge-dependent effects by inclusion of the differences in neutral and charged pion masses. For proton-proton, neutron-proton, and neutron-neutron interactions it can be written as

$$\begin{aligned} v_{ij}^\pi(pp) &= f^2 v_\pi(m_{\pi^0}), \\ v_{ij}^\pi(np) &= -f^2 v_\pi(m_{\pi^0}) + (-1)^{T+1} 2f^2 v_\pi(m_{\pi^\pm}), \\ v_{ij}^\pi(nn) &= f^2 v_\pi(m_{\pi^0}), \end{aligned} \quad (2.30)$$

where T is the isospin of the pair, f is a charge-independent value of the pion-nucleon coupling constant (see Wiringa *et al.* (1995) for details), and m_{π^0} and m_{π^\pm} are the neutral and charged pion masses, respectively. The potential $v_\pi(m)$ is given by

$$v_\pi(m) = \left(\frac{m}{m_{\pi^\pm}} \right)^2 \frac{1}{3} mc^2 [Y_\mu(r) \boldsymbol{\sigma}_i \cdot \boldsymbol{\sigma}_j + T_\mu(r) S_{ij}], \quad (2.31)$$

where $Y_\mu(r)$ and $T_\mu(r)$ are the standard Yukawa and tensor functions exponentially cut off,

$$\begin{aligned} Y_\mu(r) &= \frac{e^{-\mu r}}{\mu r} \left(1 - e^{-Cr^2} \right), \\ T_\mu(r) &= \left(1 + \frac{3}{\mu r} + \frac{3}{(\mu r)^2} \right) \frac{e^{-\mu r}}{\mu r} \left(1 - e^{-Cr^2} \right)^2, \end{aligned} \quad (2.32)$$

$\mu = mc/\hbar$, c is the speed of light, and C is a shape parameter.

$\boldsymbol{\sigma}_i$ are the standard Pauli spin matrices, and S_{ij} is the tensor operator

$$S_{ij} = 3(\boldsymbol{\sigma}_i \cdot \hat{\mathbf{r}}_{ij})(\boldsymbol{\sigma}_j \cdot \hat{\mathbf{r}}_{ij}) - \boldsymbol{\sigma}_i \cdot \boldsymbol{\sigma}_j, \quad (2.33)$$

with \mathbf{r}_{ij} the relative position vector between two nucleons.

The short-range phenomenological part v_{ij}^R is written as a sum of terms of the form

$$v_{ST}^i(r) = I_{ST}^i T_\mu^2(r) + [P_{ST}^i + \mu r Q_{ST}^i + (\mu r)^2 R_{ST}^i] W(r), \quad (2.34)$$

where the constants I_{ST}^i , P_{ST}^i , Q_{ST}^i , and R_{ST}^i are spin- (S) and isospin- (T) dependent constants to be fit to data, and

$$W(r) = [1 + e^{(r-r_0)/a}]^{-1}, \quad (2.35)$$

is a Woods-Saxon function which provides the short range core. r_0 and a are additional shape parameters. A summary of the parameters used in the definition of the potential can be found in Table (2.1).

Table 2.1: Summary of various constants used in the definition of the AV₁₈ potential.

Fundamental constants		
$\hbar c$	197.32705	MeV fm
m_{π^0}	134.9739	MeV/ c^2
m_{π^\pm}	139.5675	MeV/ c^2
Shape parameters		
C	2.1	fm^{-2}
r_0	0.5	fm
a	0.2	fm

The one-pion-exchange potential and short range potential can be written in an operator form

$$v_{ij}^\pi + v_{ij}^R = \sum_{p=1}^n v_p(r_{ij}) O_{ij}^p, \quad (2.36)$$

where charge-independent operators include

$$O_{ij}^{p=1,14} = [1, (\boldsymbol{\sigma}_i \cdot \boldsymbol{\sigma}_j), S_{ij}, \mathbf{L} \cdot \mathbf{S}, L^2, L^2(\boldsymbol{\sigma}_i \cdot \boldsymbol{\sigma}_j), (\mathbf{L} \cdot \mathbf{S})^2] \otimes [1, (\boldsymbol{\tau}_i \cdot \boldsymbol{\tau}_j)]. \quad (2.37)$$

The $\boldsymbol{\tau}$ are the standard Pauli matrices acting in isospin space, $\mathbf{L} = \frac{1}{2i}(\mathbf{r}_1 - \mathbf{r}_2) \times (\boldsymbol{\nabla}_1 - \boldsymbol{\nabla}_2)$ is the standard relative angular momentum operator, and $\mathbf{S} = \frac{1}{2}(\boldsymbol{\sigma}_1 + \boldsymbol{\sigma}_2)$ is the standard spin operator. Details about such operators can be found in, for example, Wiringa *et al.* (1984). Charge-independence breaking and charge-symmetry breaking in the interaction are introduced through the additional operators

$$O_{ij}^{p=15,18} = [1, (\boldsymbol{\sigma}_i \cdot \boldsymbol{\sigma}_j), S_{ij}] \otimes T_{ij}, (\tau_{zi} + \tau_{zj}), \quad (2.38)$$

where T_{ij} is the isospin tensor operator defined analogously with the spin tensor operator. $T_{ij} = 3\tau_{zi}\tau_{zj} - \boldsymbol{\tau}_i \cdot \boldsymbol{\tau}_j$. Details about these additional operators can be found in Wiringa *et al.* (1995).

The potential is fit to the Nijmegen NN scattering database (Bergervoet *et al.*, 1990; Stoks *et al.*, 1993), which contains 1787 pp and 2514 np data in the range from $E_{\text{lab}} = 0$ to 350 MeV. The χ^2 per datum is 1.09.

2.2.3 The N^3LO Interaction

The N^3LO potential gets its name from the fact that it is a next-to-next-to-next-to-leading order calculation in chiral perturbation theory. Chiral perturbation theory is an effective field theory that describes low-energy pion and pion-nucleon physics. It is based on an effective Lagrangian written in terms of the observed fields (nucleons and pions), which is consistent with the symmetries of low-energy QCD: most

importantly Lorentz invariance and the (broken) chiral symmetry of the light quarks. The Lagrangian is an expansion in the chiral dimension (the number of derivatives or pion mass insertions). Tree diagrams of the theory reproduce well-known current algebra results, which are systematically improved by going to higher order. Loop diagrams are treated covariantly and regularized using dimensional regularization.

The (πN) Lagrangian can be written (Entem and Machleidt, 2002b)

$$\mathcal{L}_{\text{eff}} = \mathcal{L}_{\pi N}^{(1)} + \mathcal{L}_{\pi N}^{(2)} + \mathcal{L}_{\pi N}^{(3)} = \dots, \quad (2.39)$$

where the superscript is the chiral dimension. See Fettes *et al.* (2000, 2001) for a more complete description, details on field content, and a list of operators through dimension 4. As is the case with effective field theories, at each order, undetermined low-energy constants enter which must be fixed by experimental data. Contact is made with non-relativistic physics by using the heavy-baryon approximation of Jenkins and Manohar (1991). To lowest order,

$$\hat{\mathcal{L}}_{\pi N}^{(1)} \approx \bar{N} \left[i\partial_0 - \frac{1}{4f_\pi^2} \boldsymbol{\tau} \cdot (\boldsymbol{\pi} \times \partial_0 \boldsymbol{\pi}) - \frac{g_A}{2f_\pi} \boldsymbol{\tau} \cdot (\boldsymbol{\sigma} \cdot \boldsymbol{\nabla}) \boldsymbol{\pi} \right] N + \dots, \quad (2.40)$$

where N is the nucleon field (a Dirac spinor and a Pauli spinor in isospin space), f_π is the pion decay constant $f_\pi = 92.4$ MeV, $\boldsymbol{\tau}$ is a Pauli matrix in isospin space, $\boldsymbol{\pi}$ is the pion field, g_A is the axial vector coupling constant $g_A = 1.29$, and $\boldsymbol{\sigma}$ is a standard Pauli spin matrix. The πN Lagrangian is ordered according to powers of small momenta $(Q/\Lambda_\chi)^\nu$, where Q is a momentum or pion mass in the diagram, and $\Lambda_\chi \approx 1$ GeV is the chiral symmetry breaking scale. The power ν of a given diagram can be determined by

$$\nu = 2l + \sum_j (d_j - 1), \quad (2.41)$$

where l is the number of loops, d_j , the number of derivatives in the vertex j , and the sum is over all vertices of the diagram.

In order to make contact with nucleon-nucleon scattering, the Bethe-Salpeter equation (Salpeter and Bethe, 1951) is invoked in a specific form (that of Blankenbecler and Sugar (1966)). The Blankenbecler-Sugar form is a set of three-dimensional coupled linear integral equations for relativistic scattering which contains the same information as the Bethe-Salpeter equation but is more agreeable to numerical work. This approach allows for a potential to be defined

$$\bar{V}(\mathbf{p}, \mathbf{p}') \equiv \left\{ \begin{array}{l} \text{sum of irreducible} \\ \boldsymbol{\pi} + 2\boldsymbol{\pi} \text{ contributions} \end{array} \right\} + \text{contacts}, \quad (2.42)$$

which satisfies the relativistic Blankenbecler-Sugar equations. Then, the potential

$$V(\mathbf{p}, \mathbf{p}') \equiv \sqrt{\frac{M_N}{E_{p'}}} \bar{V}(\mathbf{p}, \mathbf{p}') \sqrt{\frac{M_N}{E_p}} \approx \left(1 - \frac{\mathbf{p}'^2 + \mathbf{p}^2}{4M_N^2} \right) \bar{V}(\mathbf{p}, \mathbf{p}'), \quad (2.43)$$

with $E_p \equiv \sqrt{\mathbf{p}^2 + M_N^2}$ the relativistic kinetic energy and M_N the nucleon mass, satisfies the non-relativistic Lipmann-Schwinger equation and can be used in non-relativistic calculations like any other non-relativistic potential (note that we are using the high-energy unit conventions here $\hbar = c = 1$). More details are available in Entem and Machleidt (2002a, 2003).

As we have discussed, N³LO comes from chiral perturbation theory which is a low-momentum expansion and is only valid for momenta in the range $Q \ll \Lambda_\chi \approx 1$ GeV. Thus, Entem and Machleidt (2002a, 2003) note that there is some need to regulate the potential $V(\mathbf{p}, \mathbf{p}')$, so that higher-momentum behavior is suppressed. A choice that generates powers of momentum higher than those in the short-range contact terms is

$$V(\mathbf{p}, \mathbf{p}') \rightarrow V(\mathbf{p}, \mathbf{p}') e^{-(p/\Lambda)^{2n}} e^{-(p'/\Lambda)^{2n}}, \quad (2.44)$$

where $n = 2$ and Λ is chosen to as 500 MeV for the N³LO interaction used throughout this thesis (unless noted otherwise), However, as we will demonstrate in subsequent

chapters, it is likely that this choice Eq. (2.44) has unintended consequences for real-space nuclear structure methods such as Green's function Monte Carlo, where the Fourier transform of the regulator will appear.

Consider a one-dimensional analogy. It is a well known fact that the Fourier transform of a Gaussian is a Gaussian.

$$\int_{-\infty}^{\infty} \frac{dk}{2\pi} e^{ikx} e^{-\frac{\sigma^2}{2}k^2} = \frac{1}{\sqrt{2\pi\sigma^2}} e^{-\frac{x^2}{2\sigma^2}}. \quad (2.45)$$

However, if the integral is cut off at some largest momentum value k_{\max}

$$\int_{-k_{\max}}^{k_{\max}} \frac{dk}{2\pi} e^{ikx} e^{-\frac{\sigma^2}{2}k^2}, \quad (2.46)$$

the Fourier transform “rings” as in Fig. (2.3).

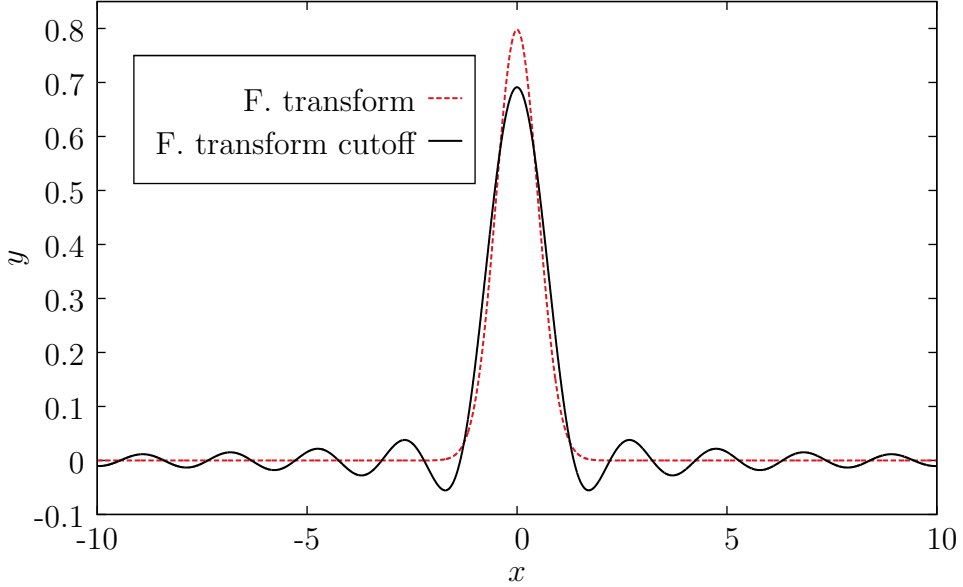


Figure 2.3: The Fourier transform of a Gaussian is a Gaussian (the red dashed curve). However, cutting off the integral at some largest momentum value k_{\max} results in “ringing” (the solid black curve). The dimensions are arbitrary here. $\sigma = 0.5$. $k_{\max} = 3$.

Now we examine the one-dimensional equivalent of the N³LO regulator Eq. (2.44) for ease of visualization.

Define the one-dimensional regulator function as $\tilde{f}_n(k) = e^{-(\hbar k/\Lambda)^{2n}}$. Taylor series expanding about zero, we find $\tilde{f}_n(k) \approx 1 - \left(\frac{\hbar k}{\Lambda}\right)^{2n} + \dots$ Clearly this choice does not generate powers of $k < k^{2n}$. However, despite the fact that this regulator function meets this condition and is smooth, it is relatively sharp, and therefore, the Fourier transform is likely to ring. The best-case scenario occurs for $n = 2$ and is shown in Fig. (2.4).

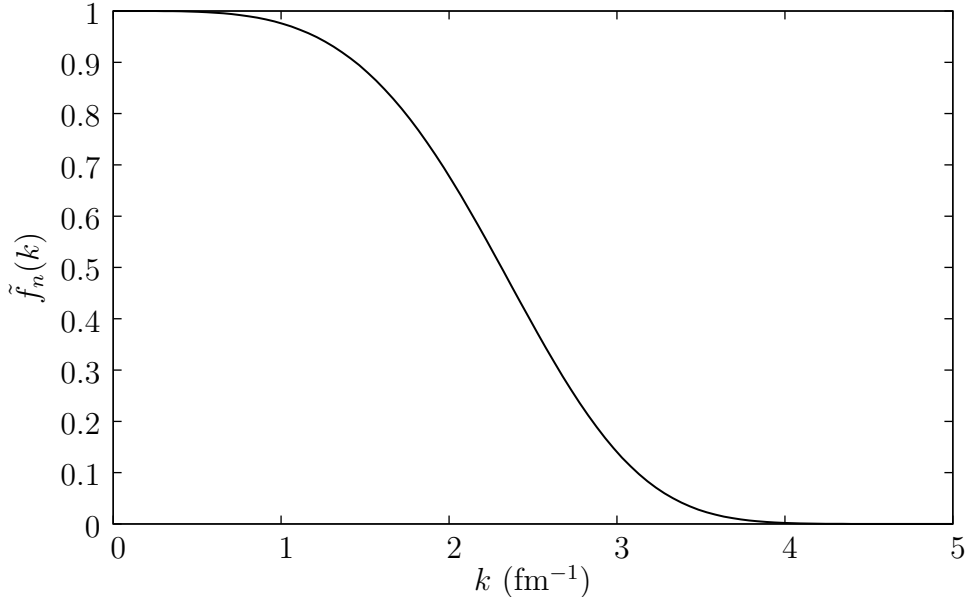


Figure 2.4: The one-dimensional regulator function for $n = 2$.

The Fourier transform to real space is

$$f_n(x) = \int \frac{dk}{2\pi} e^{ikx} \tilde{f}_n(k). \quad (2.47)$$

For comparison, we consider an alternate regulator. The properties we desire are as follows. 1) The regulator should generate powers of k beyond a certain order. 2) The regulator should be smooth. 3) The regulator should have a minimal impact on the

real-space results. A candidate is

$$\tilde{g}_n(k) = e^{-(\hbar k/\Lambda)^2} \left(\sum_{m=0}^{2n-2} \frac{(\hbar k/\Lambda)^{2m}}{m!} \right). \quad (2.48)$$

For example, for $n = 2$,

$$\tilde{g}_2(k) = e^{-(\hbar k/\Lambda)^2} \left(1 + \left(\frac{\hbar k}{\Lambda} \right)^2 + \frac{1}{2} \left(\frac{\hbar k}{\Lambda} \right)^4 \right) \quad (2.49)$$

This choice is obviously inspired by the fact that as $n \rightarrow \infty$, $\tilde{g}_n(k) \rightarrow 1$. If we series expand $\tilde{g}_n(k)$ for a given value of n , we find, just as for the original regulator, $\tilde{g}_n(k)$ does not generate powers of k below order $2n$. $\tilde{g}_n(k) \approx 1 - \frac{1}{n!} \left(\frac{\hbar k}{\Lambda} \right)^{2n} + \dots$ However, this alternate regulator is much more gradual of a cutoff and as Fig. (2.5) demonstrates, the ringing behavior in real space is reduced. The log-scale plot Fig. (2.6) is even

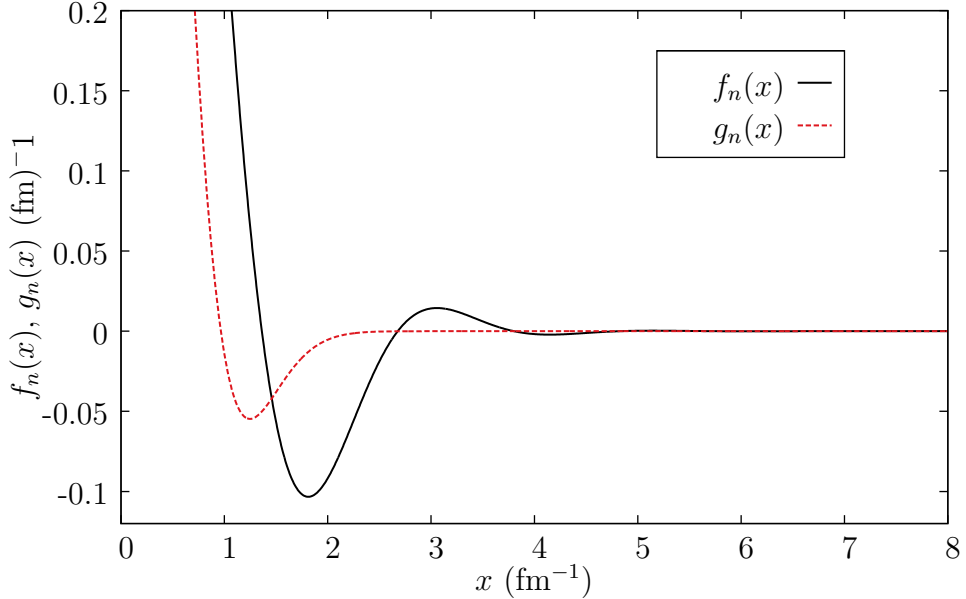


Figure 2.5: The one-dimensional regulator functions for $n = 2$, Fourier transformed to real space (normalized so that $f_n(0) = g_n(0) = 1$).

clearer. Each “crease” in the figure represents an oscillation. This figure shows just how long the regulator $f_2(x)$ rings.

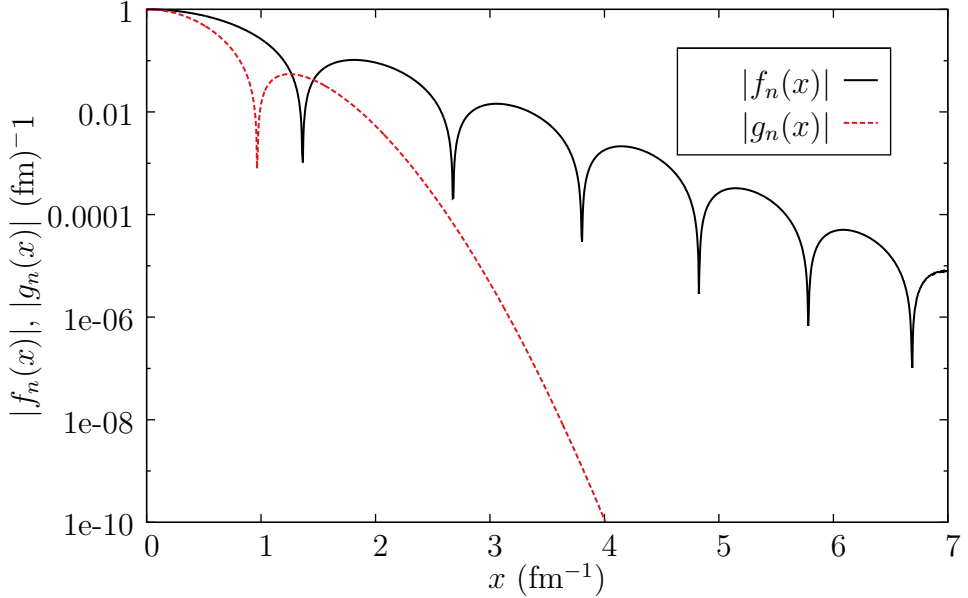


Figure 2.6: The absolute value of the one-dimensional regulator functions for $n = 2$, Fourier transformed to real space (normalized so that $f_n(0) = g_n(0) = 1$). The y axis is log scaled to emphasize the effect.

2.2.4 The CD-Bonn Interaction

We also briefly mention the CD-Bonn potential, a potential which is non-local but in an intermediate sense (less so than N³LO) and thus which serves as a useful proxy for N³LO during development of our methods. The specific version used here is the one from Machleidt (2001) which we refer to as CD-Bonn. The Bonn potential was the culmination of the efforts of several decades to construct a nucleon-nucleon potential from perturbative field theory of meson exchanges. A pedagogical review is available in Machleidt (1989). The theory largely reproduces the features of the nuclear force but at the cost of inventing spurious bosons such as the σ or ϵ bosons. With the advent of QCD, it is has been largely relegated to the status of a model, albeit a relatively successful one.

Chapter 3

PROPAGATORS FOR NON-LOCAL POTENTIALS

3.1 Introduction

Quantum Monte Carlo methods use propagation in imaginary time to project out the low-energy states of a quantum many-particle system. The propagation is performed by first writing the many-body short-imaginary-time propagator. Accurate methods use a pair-product approximation (Ceperley, 1995; Pudliner *et al.*, 1997) where the many-body propagator is written in terms of the propagator for each pair of particles. In order to perform a quantum Monte Carlo calculation using an arbitrary pair potential, we need to calculate the pair propagator in imaginary time.

The propagator ultimately depends on the initial and final relative coordinates, the imaginary time, and the spins and isospins of the pair:

$$\langle \mathbf{r}' S' M'_S T' T'_z | e^{-Ht} | \mathbf{r} S M_S T T_z \rangle. \quad (3.1)$$

The propagator is obtained by working in the standard channel basis where J^2 , J_z , L^2 , S^2 , S_z , T^2 and T_z are good quantum numbers, with the total spin, $\mathbf{S} = \mathbf{S}_1 + \mathbf{S}_2$, the total angular momentum $\mathbf{J} = \mathbf{L} + \mathbf{S}$, and total isospin $\mathbf{T} = \mathbf{T}_1 + \mathbf{T}_2$. The basis states are $|rJMLSTT_z\rangle$. Expressing the relative positions in spherical coordinates, the states are related by

$$|r\theta\phi S M_S T T_z\rangle = \sum_{JMLM_L} C_{SMLM_L}^{JM} Y_{LM}(\theta, \phi) |rJMLSTT_z\rangle, \quad (3.2)$$

with Y a spherical harmonic and C a Clebsch-Gordan coefficient. The two-body

Hamiltonian commutes with J^2 , J_z , S^2 , T^2 , and T_z . Therefore,

$$\begin{aligned} & \langle r'\theta'\phi' SM'_S TT_z | e^{-Ht} | r\theta\phi SM_S TT_z \rangle = \\ & \sum_{\alpha} C_{SM'_S L'M'_L}^{JM} Y_{L'M'_L}(\Omega') C_{SM_S LM_L}^{JM} Y_{LM_L}^*(\Omega) \langle r' JML' STT_z | e^{-Ht} | r JML STT_z \rangle, \end{aligned} \quad (3.3)$$

where $\alpha = \{JMLL'M_L M'_L\}$, and Ω stands for the angular coordinates (θ, ϕ) . The objects $\langle r' JML' STT_z | e^{-Ht} | r JML STT_z \rangle$ are the channel propagators.

The nuclear potential does not depend on the magnetic quantum number, M , and for any given isospin state $|TT_z\rangle$, there are two cases to consider. For $S = 0$, the spin singlet case, $J = L = L'$ and the channel propagators can be written as $g_L(r, r'; t)$. These obey the equation

$$\left(-\frac{\hbar^2}{2m_r} \left[\frac{\partial^2}{\partial r^2} - \frac{L(L+1)}{r^2} \right] + v_L(r) + \frac{\partial}{\partial t} \right) g_L(r, r'; t) = \delta(t)\delta(r - r'). \quad (3.4)$$

For $S = 1$, the spin triplet case, L' can differ from L as long as the triangle inequality is obeyed: $L' - S \leq J \leq L' + S$. So, in principle, L could couple to $L' = L$, $L' = L \pm 1$, and $L' = L \pm 2$. However, the nuclear interaction conserves parity and so can only couple together states with L to states with $L' = L, L \pm 2$. When L and L' differ, the (coupled-triplet) channel propagators obey the equations

$$\begin{pmatrix} -\frac{\hbar^2}{2m_r} \left[\frac{\partial^2}{\partial r^2} + \frac{(J-1)(J)}{r^2} \right] + v_J^{(-)}(r) + \frac{\partial}{\partial t} & v_J^{(+)}(r) \\ v_J^{(+)}(r) & -\frac{\hbar^2}{2m_r} \left[\frac{\partial^2}{\partial r^2} + \frac{(J+1)(J+2)}{r^2} \right] + v_J^{(++)}(r) + \frac{\partial}{\partial t} \end{pmatrix} \begin{pmatrix} g_J^{(-)}(r, r'; t) & g_J^{(+)}(r, r'; t) \\ g_J^{(+)}(r, r'; t) & g_J^{(++)}(r, r'; t) \end{pmatrix} = \begin{pmatrix} \delta(t)\delta(r - r') & 0 \\ 0 & \delta(t)\delta(r - r') \end{pmatrix}, \quad (3.5)$$

where the superscripts $+(-)$ refer to L or L' taking values $J+1(J-1)$. For $S = 1$, and $L = L' = J$, the channel propagators are uncoupled and obey equations analogous to Eq. (3.4).

There are two standard ways to calculate the channel propagators in imaginary time. The Trotter break-up methods of Schmidt and Lee (1995) and the matrix

squaring methods of Klemm and Storer (1973). The calculation comes down to the question of how to efficiently exponentiate a matrix. See Moler and Van Loan (2003) for a discussion of this mathematical problem: though the title is humorous (see References), the authors deftly illustrate the numerical complexities of the problem. Both of these standard methods exploit the locality of the potential to reduce the computational effort needed. We briefly review both here to point out why non-local potentials require a different approach.

The method of Schmidt and Lee (1995) uses a symmetrized break up of the channel propagators

$$e^{-Ht} = \lim_{N_t \rightarrow \infty} (e^{-H\Delta t})^{N_t}; \quad (3.6a)$$

$$e^{-H\Delta t} \approx e^{-V \frac{\Delta t}{2}} e^{-T_{\text{ke}} \Delta t} e^{-V \frac{\Delta t}{2}}, \quad (3.6b)$$

where the symmetrized break up of the small-imaginary-time propagator, Eq. (3.6b), introduces errors of order $(\Delta t)^3$. The numerical procedure is as follows. The exponential of the potential is formed and multiplies an initial position array. The result is Fourier transformed to momentum space, where the kinetic energy operator T_{ke} is diagonal. The exponential of the kinetic energy is computed and multiplies the array. A Fourier transform back to position space is computed, where the exponential of the potential again multiplies the array. This constitutes a propagation in imaginary time by one time step, Δt . If the Fourier transform is a fast Fourier transform (FFT) (Leforestier *et al.*, 1991), the FFT is an order $\ln N_S$ operation, where N_S is the dimension of the spatial grid used. The matrix-array multiplications are order N_S operations, but we must repeat for each of the N_S initial positions, and, as we repeat the small-time propagation N_t times, the calculation requires $N_t N_S^2 \ln N_S$ operations.

Matrix squaring also takes advantage of the fact that the small imaginary-time propagator can be broken up as in Eq. (3.6b) and the relationship $e^A = (e^{A/n})^n$ to

write

$$e^{-Ht} = \left(e^{-Ht/2^{N_t}} \right)^{2^{N_t}} = \underbrace{\left(\left(\cdots \left(e^{-Ht/2^{N_t}} \right)^2 \cdots \right)^2 \right)}_{N_t \text{ times}}^2. \quad (3.7)$$

The matrix squaring method requires order $\ln N_t$ operations for the squaring step, and order N_S^3 operations to form the N_S initial propagators. All together the calculation requires $N_S^3 \ln N_t$ operations.

Which of the above two methods to use, therefore, depends on the nature of the problem. If a smaller time t is necessary and a fine-resolution spatial grid, the methods of Schmidt and Lee (1995) may be more appropriate. However, if spatial resolution is less important and a large time is required, the matrix squaring technique is probably less computationally expensive.

In both cases, the fact that the potential $v(r)$ is local in space is exploited to easily write down the exponential $e^{-V\frac{\Delta t}{2}}$. For non-local potentials where $V = v(r, r')$, this exponential is no longer trivially calculated. If we were to follow the method of Schmidt and Lee (1995), we would be required to exponentiate the non-diagonal potential matrix to obtain the short-imaginary time propagator: a problem equally as computationally expensive as exponentiating the Hamiltonian to begin with. If, we instead used the matrix squaring technique of Klemm and Storer (1973), we would need a reasonably accurate approximation to the exponential of the Hamiltonian to begin with. The Taylor series $e^{-H\Delta t} \approx 1 - H\Delta t + \frac{1}{2}H^2\Delta t^2 + \cdots$ comes to mind, but would likely require a Δt so small, that rounding errors will begin to become problematic. This difficulty is addressed in the following section (Lynn and Schmidt, 2012).

3.2 Methods for Non-Local Potentials

Non-local potentials are typically generated in momentum space from an effective field theory. With a potential defined in momentum space, $V(k, k')$, it is natural that we proceed by constructing a Hamiltonian in momentum space as well. Our normalization and completeness conventions for our continuous real-space and momentum-space basis states are

$$1 = \int d^3r |\mathbf{r}\rangle\langle\mathbf{r}| = \int \frac{d^3k}{(2\pi)^3} |\mathbf{k}\rangle\langle\mathbf{k}|. \quad (3.8)$$

\mathbf{r} is the separation vector of the two nucleons and $\mathbf{p} = \hbar\mathbf{k}$ the conjugate momentum. The overlaps between the states are

$$\langle \mathbf{r} | \mathbf{k} \rangle = e^{i\mathbf{k} \cdot \mathbf{r}}. \quad (3.9)$$

We also work in the standard channel basis, choosing our basis states as $|rJMLST_z\rangle$ and $|kJMLST_z\rangle$, with normalization and completeness given by (suppressing J , S , T , and T_z)

$$\begin{aligned} 1 &= \sum_{LM} \int_0^\infty r^2 dr |rLM\rangle\langle rLM| \\ &= \sum_{LM} \int_0^\infty \frac{k^2 dk}{(2\pi)^3} |kLM\rangle\langle kLM|. \end{aligned} \quad (3.10)$$

The overlaps are

$$\langle rLM | kL'M' \rangle = 4\pi i^L j_L(kr) \delta_{LL'} \delta_{MM'}. \quad (3.11)$$

For numerical work, we compactify our real space to a sphere of radius R . We choose the Dirichlet boundary condition on the sphere which forces our momentum-space spectrum to be discrete, with $k_n^{(L)}R$ being the zeros of the spherical Bessel functions, $j_L(k_n^{(L)}R) = 0$. Below we often drop the superscript (L) when its value is clear from context. The discrete momentum states $|k_nLM\rangle$ are chosen with unit

normalization so that

$$\langle rLM|k_nL'M'\rangle = \sqrt{\frac{2}{R^3 j'_L(k_n R)^2}} j_L(k_n r) \delta_{LL'} \delta_{MM'}. \quad (3.12)$$

Our transformations can now be treated as orthogonal-matrix multiplications. Additional details about these methods can be found in Appendix A.

The momentum-space Hamiltonian for the uncoupled channels where $L = J$ (for a given set of the quantum numbers — J, M, L, S, T , and T_z — which we suppress below) is

$$\langle k_m | H | k_n \rangle = \frac{\hbar^2 k_n^2}{2m_r} \delta_{mn} + V(k_m, k_n), \quad (3.13)$$

with m_r the reduced mass. For the coupled channels, where the potentials couple the $L = J \pm 1$ states together, the Hamiltonian is

$$\begin{aligned} \langle k_m L | H | k_n L' \rangle = & \\ \left(\begin{array}{cc} \frac{\hbar^2 k_n^{(-)}{}^2}{2m_r} \delta_{mn} + V_{--}(k_m^{(-)}, k_n^{(-)}) & V_{-+}(k_m^{(-)}, k_n^{(+)}) \\ V_{+-}(k_m^{(+)}, k_n^{(-)}) & \frac{\hbar^2 k_n^{(+)}{}^2}{2m_r} \delta_{mn} + V_{++}(k_m^{(+)}, k_n^{(+)}) \end{array} \right), \end{aligned} \quad (3.14)$$

where the superscripts $(-)$ and $(+)$ correspond to L or L' having values of $J - 1$ and $J + 1$. We then construct the momentum-space, imaginary-time propagator by diagonalization of the Hamiltonian, giving

$$\langle k_m | e^{-Ht} | k_n \rangle = \sum_{i=1}^{N_k} \langle k_m | \psi_i \rangle e^{-E_i t} \langle \psi_i | k_n \rangle, \quad (3.15)$$

for the uncoupled channels, and

$$\langle k_m L | e^{-Ht} | k_n L' \rangle = \sum_{i=1}^{N_k} \langle k_m L | \psi_i \rangle e^{-E_i t} \langle \psi_i | k_n L' \rangle, \quad (3.16)$$

for the coupled channels. The $\{|\psi_i\rangle\}$ are eigenvectors of the Hamiltonian with corresponding eigenvalues $\{E_i\}$. N_k is the number of discrete momentum states we keep. We ensure that N_k is large enough such that the propagators converge. An estimate

of how large k_{\max} should be can be given by considering the kinetic energy alone. We want k_{\max} such that $\exp\left(-\frac{\hbar^2 k_{\max}^2}{2m}t\right)$ can be neglected. In practice, we check the convergence by increasing our estimate for k_{\max} and ensuring our results do not change to the desired precision. With these methods, it is easy to ensure that the numerical truncation errors are completely negligible. For example, for the results shown here, we use $k_{\max} = 40 \text{ fm}^{-1}$ ($N_k \sim 80$), and the propagators have truncation errors less than 10^{-10} .

After transforming to real space, we have the matrix elements (the real-space channel propagators)

$$\langle rJMLSTT_z | e^{-Ht} | r'JML'STT_z \rangle. \quad (3.17)$$

However, for use in Monte Carlo codes, we want the propagators in a 3D real-space basis, $|r\theta\phi SMSTT_z\rangle$, and so we use Eq. (3.2) to transform.

In quantum Monte Carlo calculations, the particle positions are typically sampled from the central part of the propagator. The non-central parts are then included in the spin-isospin samples (auxiliary field diffusion Monte Carlo) or sums (Green's function Monte Carlo). We will sample the propagators for these non-local potentials in the same way. Here, we define the central part of the propagator as the trace over all spins and isospins. For convenience we also choose a particular coordinate system where the initial separation lies along the z axis, and the final separation is in the xz plane such that we may take $\theta = \phi = \phi' = 0$ and we can visualize the central part of the propagator as a function of $r - r'$ and θ' . For any particular application, we can always rotate into this configuration, propagate, and rotate back and the Green's function Monte Carlo routines we use have been set up to perform these rotations.

The central part of the propagator is then written as

$$G(r, r', \theta'; t) = \sum_{SMSTT_z} \langle rSMSTT_z | e^{-Ht} | r'\theta' SMSTT_z \rangle. \quad (3.18)$$

3.3 Consistency of the Propagators at Large Imaginary Times

In the limit of large imaginary times, we expect that the propagators for different potentials should agree. The propagators are essentially density matrices for the two nucleon system:

$$\rho = \frac{\sum_i |\psi_i\rangle e^{-E_i t} \langle \psi_i|}{\sum_i e^{-E_i t}}; \quad \text{tr} \rho = 1, \quad (3.19)$$

corresponding to thermal equilibrium at the temperature $k_B T = t^{-1}$. Now, since any measurable quantity can be written as an expectation of a Hermitian operator O which can be obtained via $\langle O \rangle = \text{tr}(\rho O)$, the density matrices (propagators) we obtain for the various potentials contain all the measurable information for this system. If the position or momentum of the nucleons could be determined with arbitrary precision, the density matrix would be in principle measurable. Since the position and momentum are not well defined for arbitrary values, the propagator is not completely measurable. If the various potentials we use are phase-shift equivalent — meaning they reproduce the physical scattering data at or below $E_{\text{lab}} \approx 350$ MeV ($E_{\text{c.m.}} \approx 175$ MeV) — then we would expect that starting at imaginary times $t \approx (175 \text{ MeV})^{-1}$, the various propagators should begin to agree more and more. In fact, we find that for $t \approx (50 \text{ MeV})^{-1}$, the higher-energy modes not constrained by current experimental data do not contribute substantially to the propagator.

We see from Eq. (3.19) that at $t \approx (175 \text{ MeV})^{-1}$, energies of 175 MeV and above are suppressed by a factor of $1/e$. Therefore, it is not surprising that at $t \approx (50 \text{ MeV})^{-1}$, where energies of 175 MeV and above are suppressed by a factor of $1/e^3 \approx 0.0498$, we find relatively good agreement between the propagators with different potentials. This result is analogous to the renormalization group results

leading to the $V_{\text{low } k}$ potential of Bogner *et al.* (2003) and the similarity renormalization group results of Bogner *et al.* (2007), where the high energy modes are integrated out.

Figures 3.1–3.9 demonstrate these findings for three potentials: Argonne’s v_{18} (AV₁₈) Wiringa *et al.* (1995), N³LO, and N³LO(600) Entem and Machleidt (2003). The (600) in the second version of the N³LO potential refers to the value of Λ used for the cutoff $V(\mathbf{p}, \mathbf{p}') \rightarrow V(\mathbf{p}, \mathbf{p}') e^{-(\mathbf{p}/\Lambda)^{2n}} e^{-(\mathbf{p}'/\Lambda)^{2n}}$, where n is chosen according to the order of the calculation (see the discussion in Chapter 2 on N³LO). The N³LO interaction uses $\Lambda = 500$ MeV, whereas the N³LO(600) interaction uses $\Lambda = 600$ MeV. For the diagonal cases, where we take $k = k'$, we define a quantum potential, $V_q(k, k; t)$ through the equation

$$\langle k | e^{-Ht} | k \rangle = \langle k | e^{-H_0 \frac{t}{2}} e^{-V_q(k, k; t)t} e^{-H_0 \frac{t}{2}} | k \rangle, \quad (3.20)$$

with H_0 the free-particle Hamiltonian

$$H_0 = T_{\text{ke}} = \frac{p^2}{2m_r}. \quad (3.21)$$

In the off-diagonal cases ($k \neq k'$) we choose a particular k value and plot against k' . For visual comparison, we subtract the free-particle propagator, $g(k, k') - g_0(k, k')$, since at the point $k = k'$, the kinetic energy component is large and obscures the result.

Figures 3.1–3.4 show the quantum potential in the singlet (¹ S_0), uncoupled triplet (³ P_0), and coupled triplet (³ S_1 and ³ D_1) channels. The imaginary times chosen correspond to a typical time step used in Green’s function Monte Carlo calculations, $t = (2000 \text{ MeV})^{-1}$, and imaginary times that roughly correspond to center-of-mass energies of 350 MeV, 175 MeV, and 50 MeV. As we have discussed above, the imaginary time of $t = (50 \text{ MeV})^{-1}$ is the time at which the effects attributable to energies

of 175 MeV and above are effectively integrated out. It is interesting to note that the agreement of the quantum potentials is only good up to $k \approx 2 \text{ fm}^{-1}$: this is the approximate momentum value, k , one would associate with the corresponding kinetic energy: $\frac{\hbar^2 k^2}{2m} = 175 \text{ MeV}$. This relationship (better and better agreement — but only up to some cut off — as the potential is evolved) is precisely what is found in similarity renormalization group and $V_{\text{low } k}$ approaches.

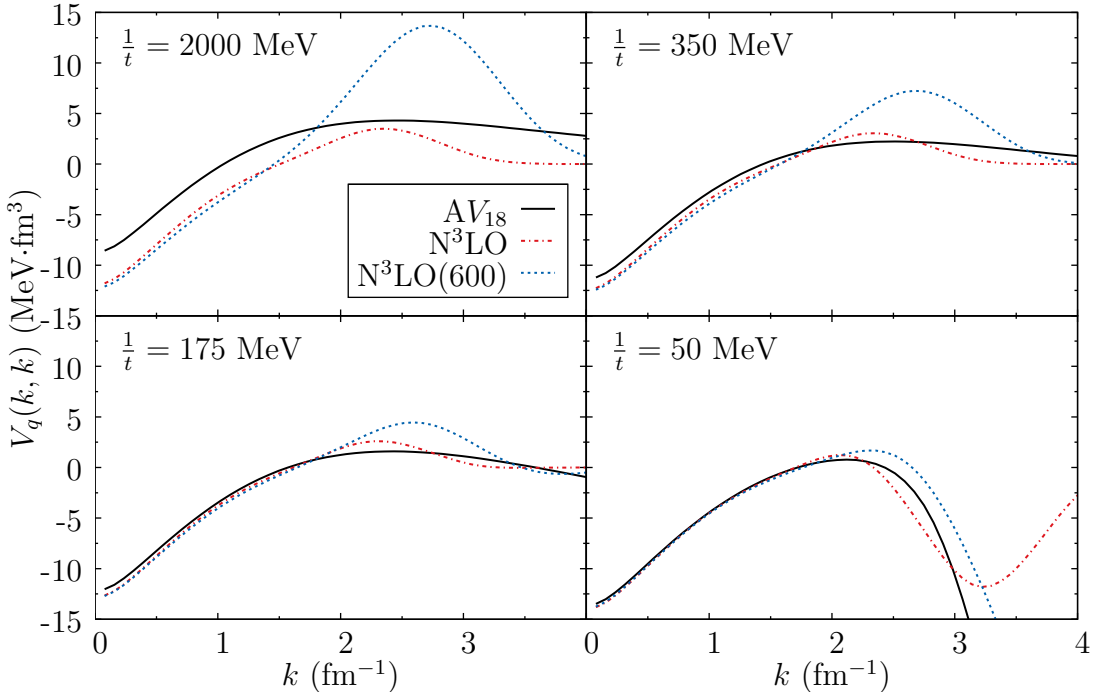


Figure 3.1: The quantum potential in the 1S_0 partial wave as the propagator is calculated for successively longer imaginary times.

It is tempting to interpret t as an evolution parameter for the quantum potential in the same sense that the similarity renormalization group approach has s or λ (see, for example, Bogner *et al.* (2007)). However, it is not clear if a direct comparison is at all trivial. In the similarity renormalization group approach, the evolution parameter s (and therefore λ , since $\lambda = 1/s^{1/4}$) is defined through the rather simple evolution

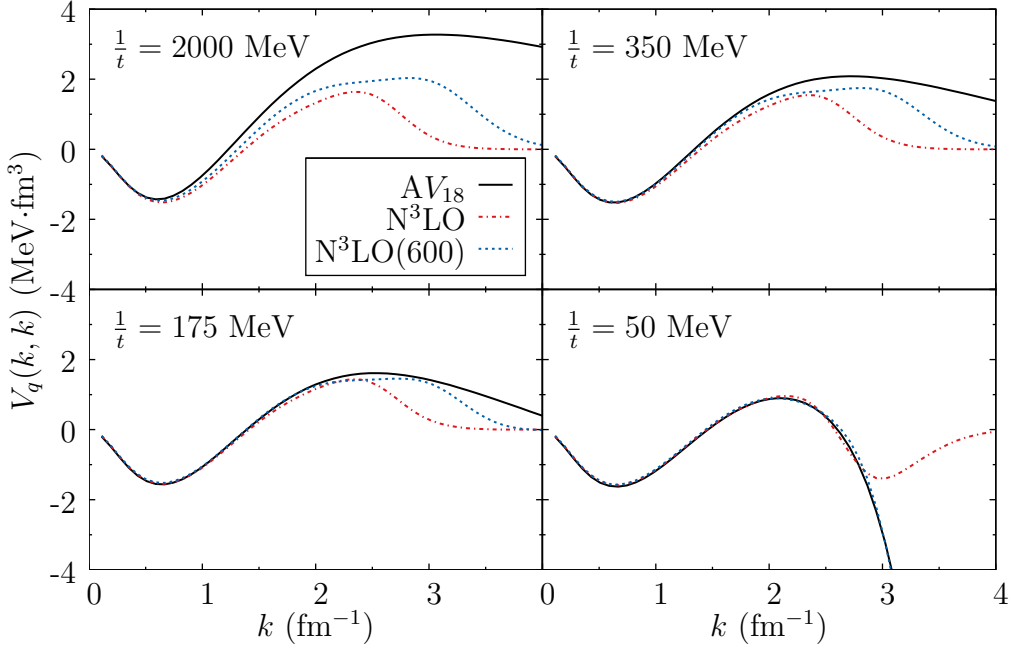


Figure 3.2: The quantum potential in the 3P_0 partial wave as the propagator is calculated for successively longer imaginary times.

equation for the potential

$$\frac{dH_s}{ds} = \frac{dV_s}{ds} = [[G_s, H_s], H_s], \quad (3.22)$$

where G_s is a Hermitian operator that generates the transformation. (G_s is often chosen to be T_{ke} , the kinetic energy). If we view our quantum potential akin to the similarity renormalization group's V_s , our defining equation is

$$e^{-Ht} = e^{-T_{\text{ke}}\frac{t}{2}} e^{-V_q(t)t} e^{-T_{\text{ke}}\frac{t}{2}}. \quad (3.23)$$

We can expand this using the Baker-Campbell-Hausdorff relation, which gives an infinite series of nested commutators.

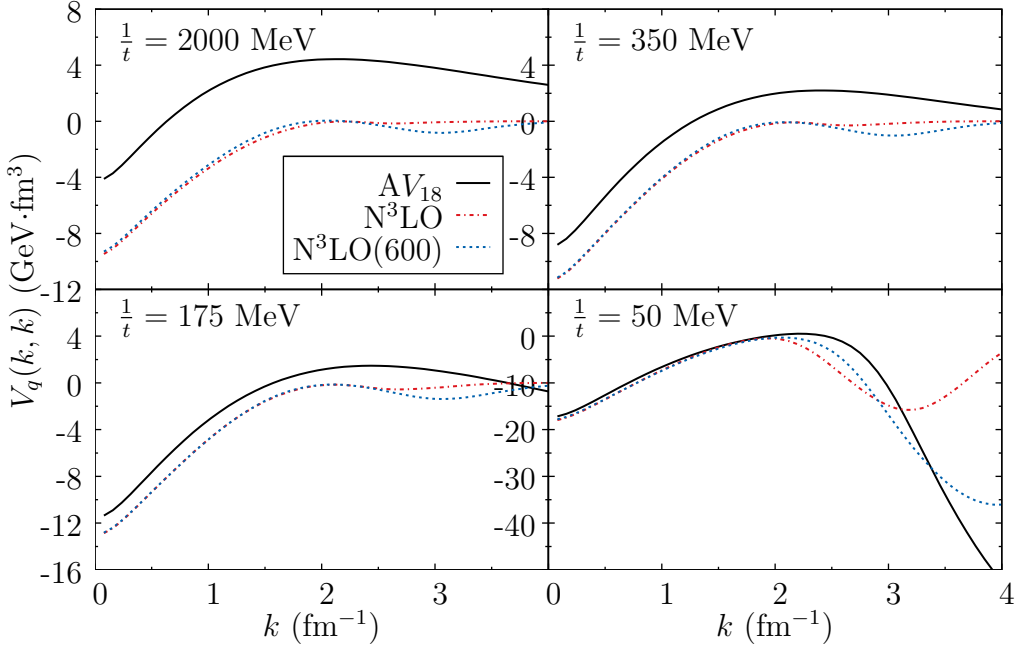


Figure 3.3: The quantum potential in the 3S_1 partial wave as the propagator is calculated for successively longer imaginary times.

The lowest order terms in an expansion in t are

$$V_q(t) = V - \frac{t^2}{12} ([V, [V, T_{\text{ke}}]] - \frac{1}{2}[T_{\text{ke}}, [T_{\text{ke}}, V]]) + \dots \quad (3.24)$$

where the double commutators are suggestive of Eq. (3.22), but clearly not the same.

The differential equation satisfied by $V_q(t)$ is not a simple, compact expression.

Figures 3.5-3.9, show the off-diagonal elements of the singlet (1S_0), uncoupled triplet, (3P_0), and coupled triplet (3S_1 , 3D_1 , and ${}^3S_1-{}^3D_1$) channel propagators. As discussed above, they are shifted by the free-particle result to make comparisons easier. What we can see from these figures is a general trend towards universality with at least two caveats. First, the propagators tend to converge most rapidly around the point where $k = k'$. Our interpretation of this result is that low momentum transfer behavior is constrained by the phase-shift equivalence of the various potentials,

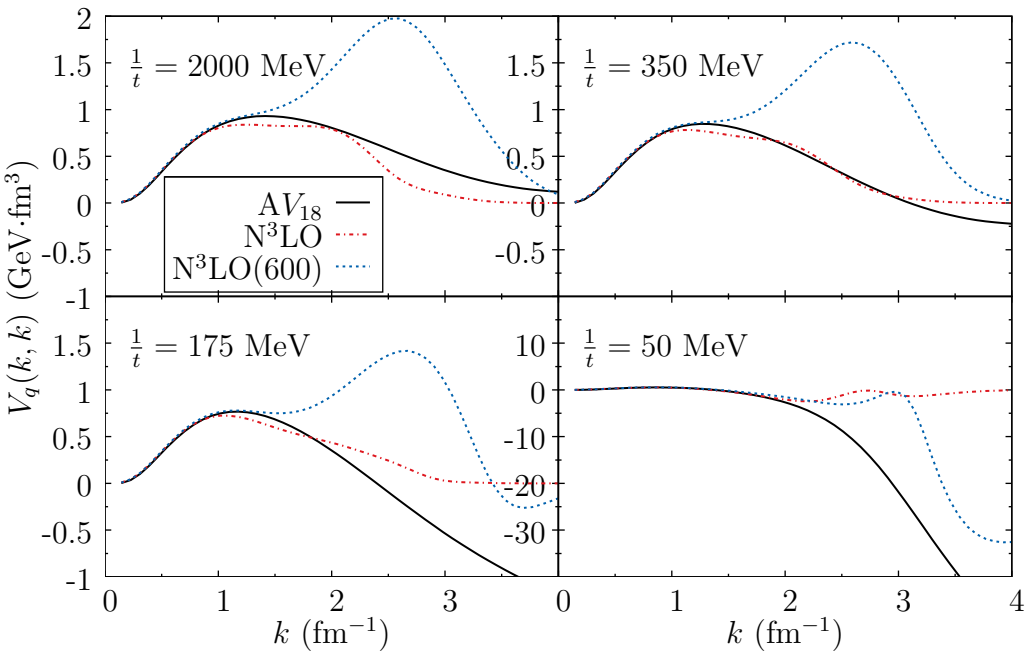


Figure 3.4: The quantum potential in the 3D_1 partial wave as the propagator is calculated for successively longer imaginary times.

whereas higher momentum transfer behavior is not. Second, some channels converge better than others. For example, Fig. 3.8 has still not converged at $t = (50 \text{ MeV})^{-1}$, and indeed, does not appear to converge well until $t = (10 \text{ MeV})^{-1}$. This may be due to this channel's sensitivity to the tensor part of the interaction, which the different potentials treat differently. These differences may point to true, quantifiable distinctions between the potentials.

Even though the potentials give propagators with the same sort of long imaginary time behavior, the many-body physics of the nucleus may not allow the use of the propagators in this regime. As mentioned above, in Green's function Monte Carlo calculations, the imaginary time step needed to accurately approximate the many-body Green's function by the pair-product is $t = (2000 \text{ MeV})^{-1}$ for the Argonne v_{18} potential. For larger time steps, commutator terms in the Trotter breakup spoil the

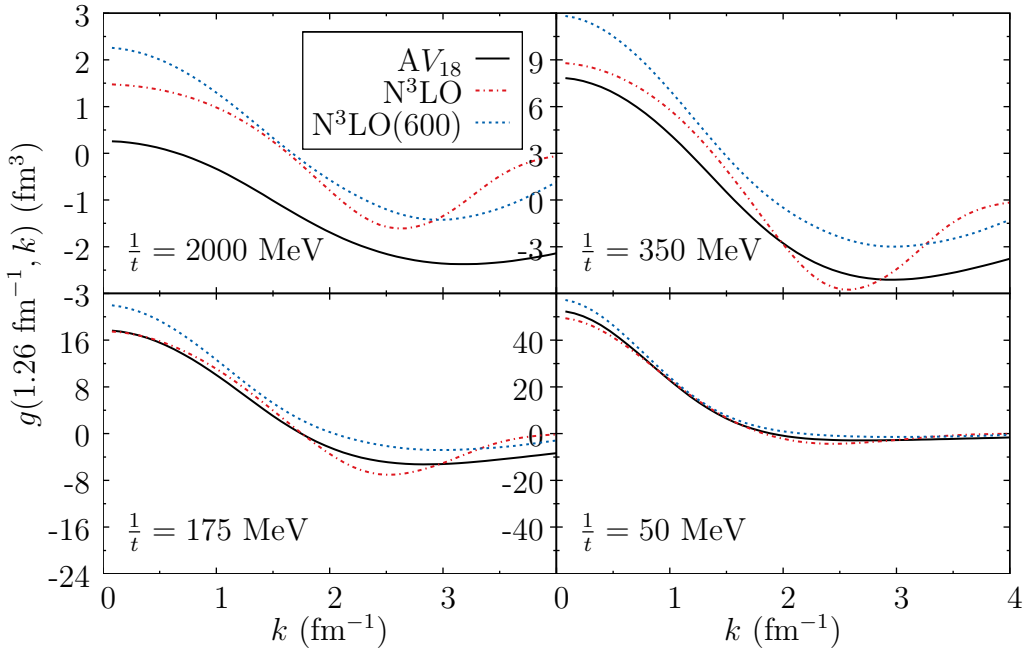


Figure 3.5: The off-diagonal propagator in the 1S_0 partial wave as the propagator is calculated for successively longer imaginary times.

approximation. Since, in the pair product approximation, these commutators occur only when three nucleons are close together, this indicates that three-body effects will also be important. That is, to be able to use the propagators in the limit where they become model independent, may require that three- and more-body terms in both the interaction and the propagators be included. This likely means that use of potentials like $V_{\text{low } k}$ for many-nucleon calculations will need to include many-body interactions. However, it is worth noting that for “softer” potentials like N³LO and other non-local potentials, the commutator terms may be smaller, allowing for a larger time step to be used and therefore, some possibility remains that “renormalized” potentials such

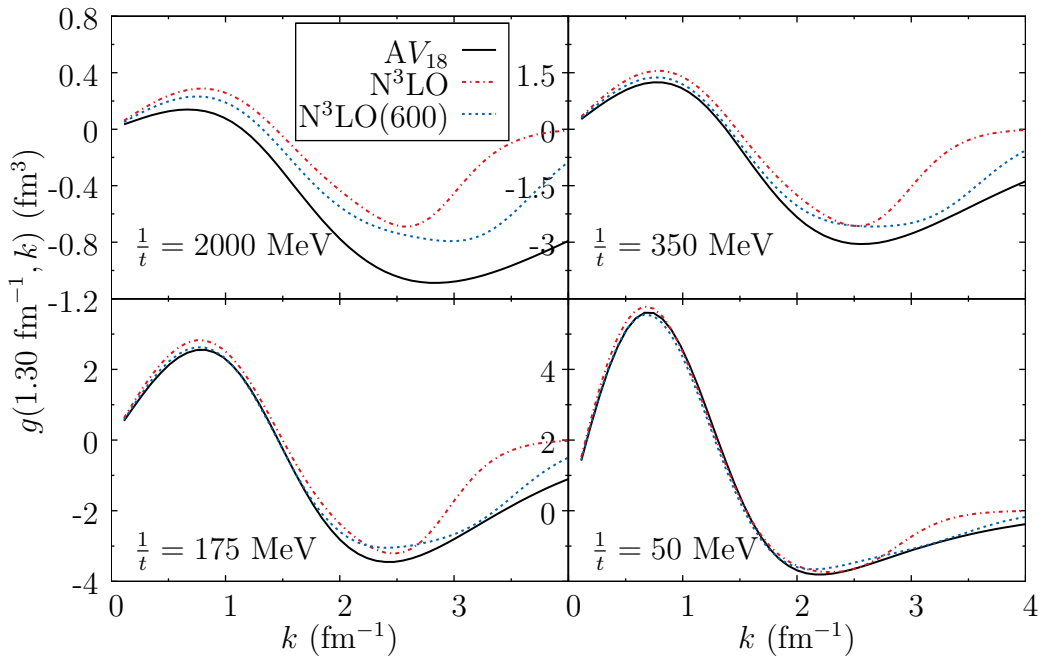


Figure 3.6: The off-diagonal propagator in the 3P_0 partial wave as the propagator is calculated for successively longer imaginary times.

as $V_{\text{low } k}$ potentials or similarity renormalization group potentials could be used in quantum Monte Carlo calculations.

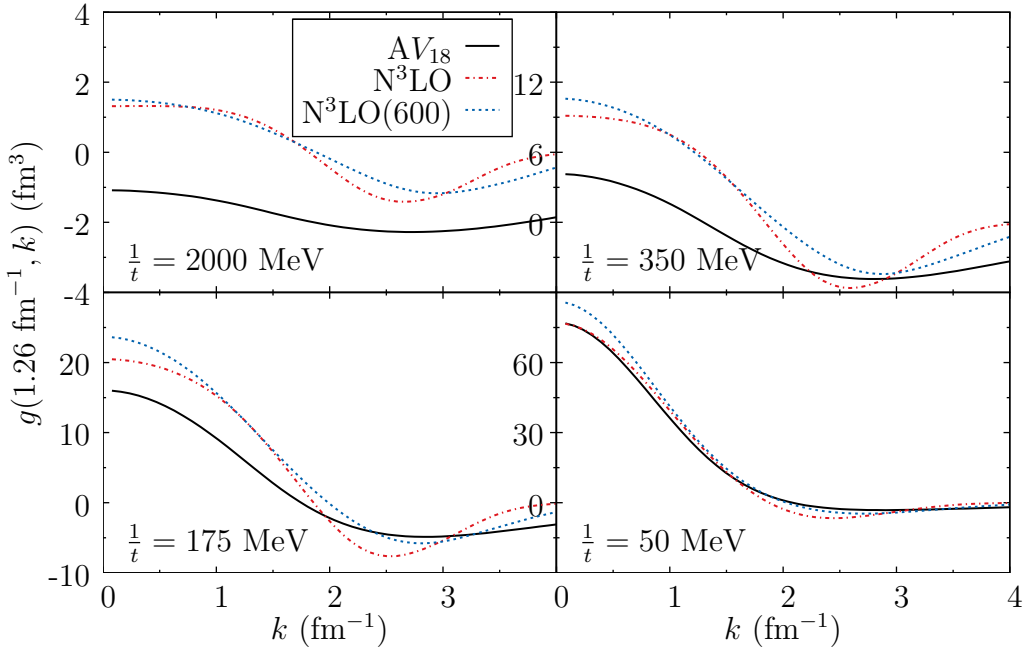


Figure 3.7: The off-diagonal propagator in the 3S_1 partial wave as the propagator is calculated for successively longer imaginary times.

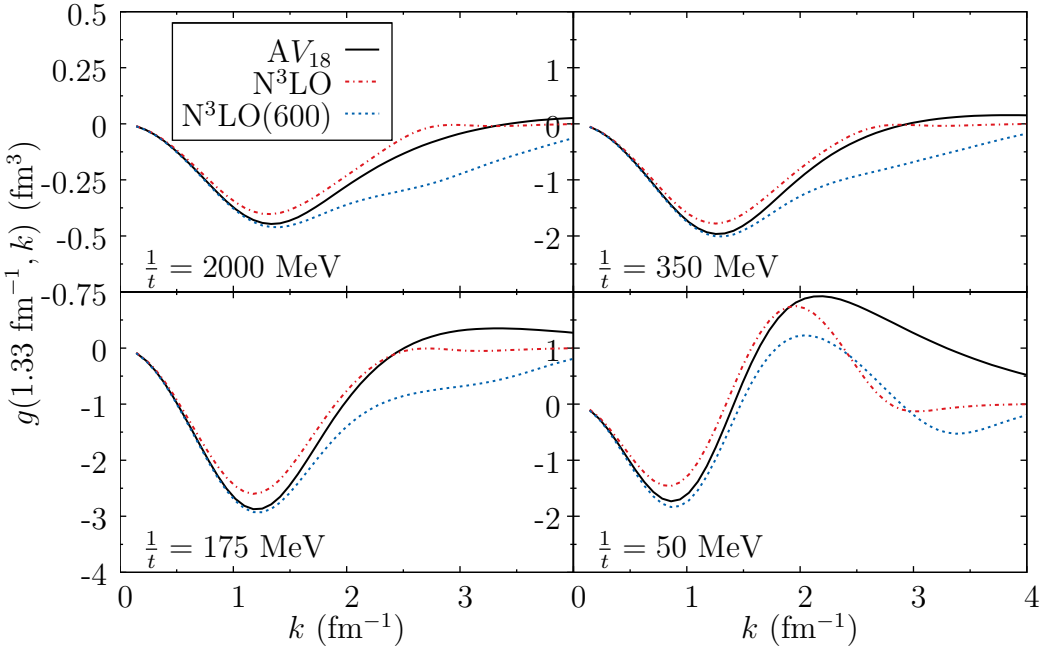


Figure 3.8: The off-diagonal propagator in the 3D_1 partial wave as the propagator is calculated for successively longer imaginary times.

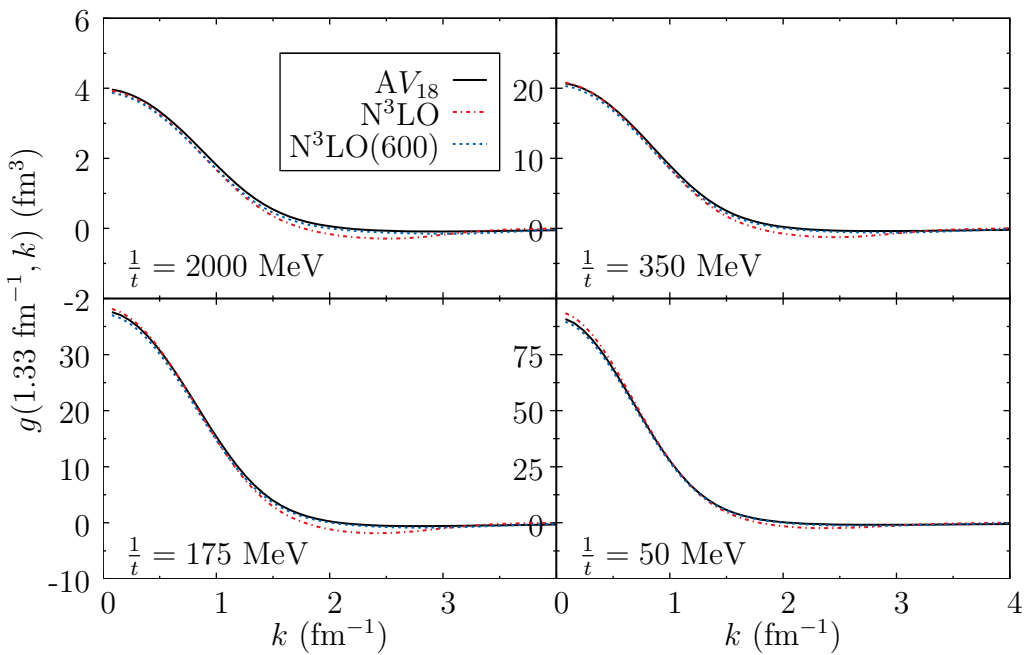


Figure 3.9: The off-diagonal propagator in the ${}^3S_1 - {}^3D_1$ partial wave as the propagator is calculated for successively longer imaginary times.

3.4 Quantum Monte Carlo with Non-Local Potentials

We now turn to the central parts of the propagators for the non-local N³LO and N³LO(600) potentials we have been considering throughout. Since the central part of the propagator is sampled in a quantum Monte Carlo calculation it should be positive-definite to avoid sign problems.

Figures 3.10 and 3.11 plot the central part of the propagator in real space, where the coordinates x' and z' are such that the origin corresponds to the final separation equal to the initial separation. That is, the relative coordinates are equal: $r = r'$. The precise transformation between the original coordinates, r , r' , and θ' and the new coordinates, x' and z' is given by

$$r'^2 = x'^2 + (r + z')^2 \quad (3.25a)$$

$$\cos \theta' = \frac{r + z'}{\sqrt{x'^2 + (r + z')^2}}, \quad (3.25b)$$

and can be visualized in Fig. 3.12.

The structure we can see is a Gaussian-like peak about the initial separation as well as an antisymmetric trough at the position that corresponds to the two nucleons undergoing a position interchange: $r' = -r$. The antisymmetric point is built in from tracing over the spins and isospins as in Eq. (3.18), and would be present even for Argonne v_{18} . This point gives no extra difficulty — since it comes from the fermion character of the nucleons, it will be dealt with in the same way that the fermion sign problem is dealt with in Green's function or auxiliary field diffusion Monte Carlo. That is, a path constraint (Wiringa *et al.*, 2000) is imposed that eliminates the fermion sign problem. The constraint can then be released and forward walking steps taken (Wiringa *et al.*, 2000; Pieper *et al.*, 2002) to improve the results and check the effect of the constraint.

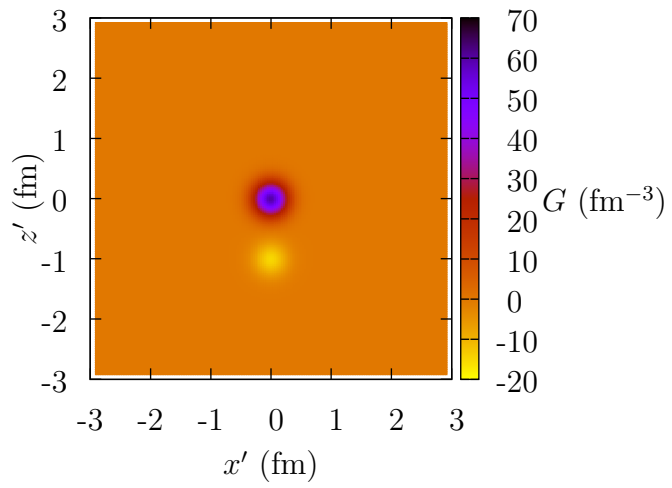


Figure 3.10: The N^3LO central propagator for initial separation, $r = 0.5$ fm, and imaginary time, $t = (2000 \text{ MeV})^{-1}$.

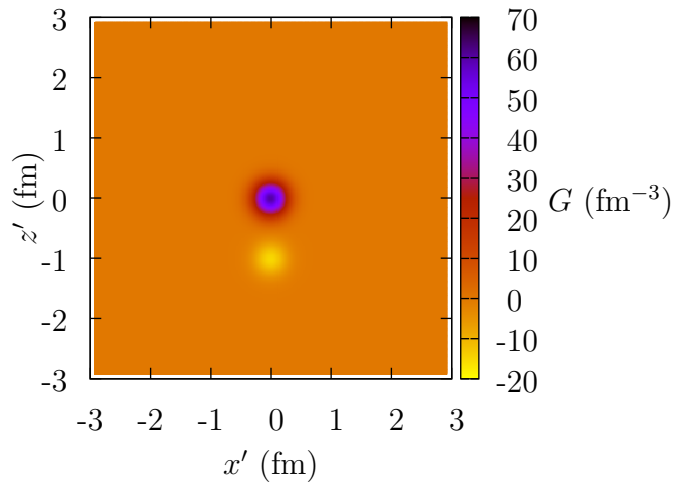


Figure 3.11: The $N^3LO(600)$ central propagator for initial separation, $r = 0.5$ fm, and imaginary time, $t = (2000 \text{ MeV})^{-1}$.

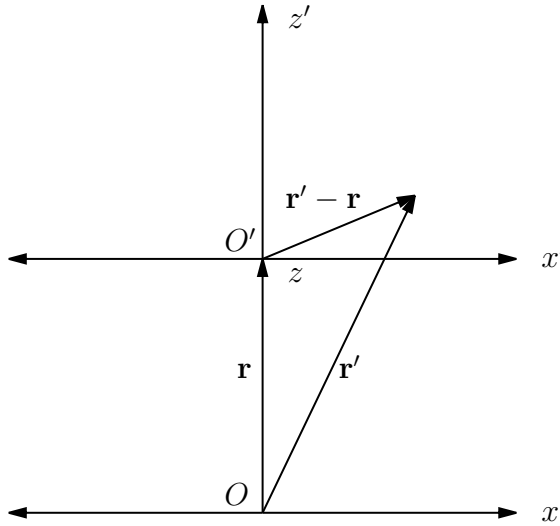


Figure 3.12: The coordinate system used to visualize the central propagators. O is the original origin, and O' is the shifted origin such that $r = r'$ corresponds to the shifted origin.

However, if we zoom in on the shifted origin, as in Figs. 3.13, and 3.14, setting any positive parts of the propagator to zero, and make sure we are clear of the antisymmetric region, we find that the propagators appear to be “ringing”, much like Friedel oscillations. These negative parts may make it more difficult to perform quantum Monte Carlo calculations and keep the sign problem under control. However, these negative parts are quite small, of order 10^{-1} fm^{-3} , whereas the peak of the propagator is of order 10^2 fm^{-3} . In fact, a typical slice through the propagator in the x' direction looks like Figs. 3.15 and 3.16. In many cases, the negative parts are negligible.

A straightforward method to take the small negative regions into account, is to first set any negative part (not associated with the antisymmetry) to zero, run a quantum Monte Carlo calculation until it converges, and then add the negative parts

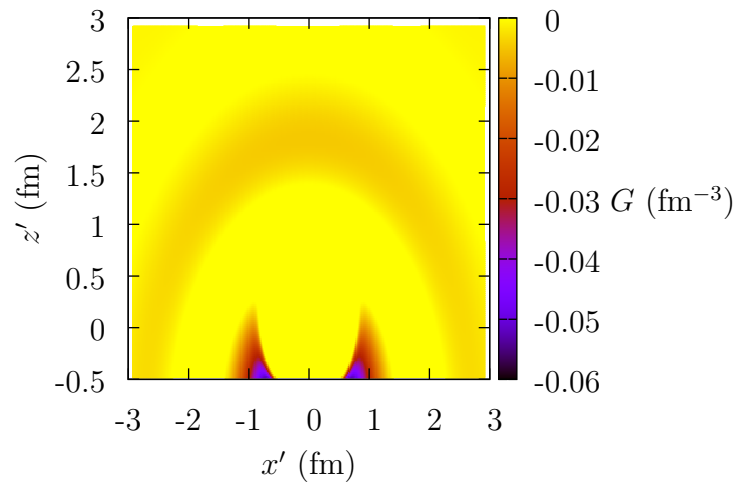


Figure 3.13: The negative parts of the N^3LO central propagator for an initial separation, $r = 0.5$ fm, and imaginary time, $t = (2000 \text{ MeV})^{-1}$.

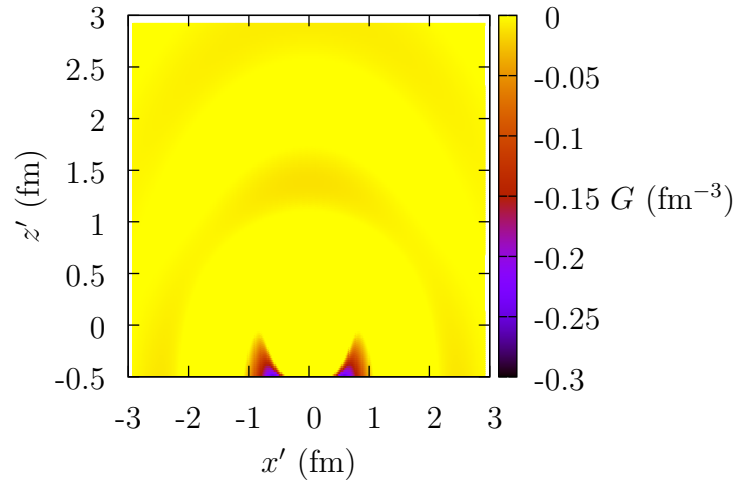


Figure 3.14: The negative parts of the $N^3LO(600)$ central propagator for an initial separation, $r = 0.5$ fm, and imaginary time, $t = (2000 \text{ MeV})^{-1}$.

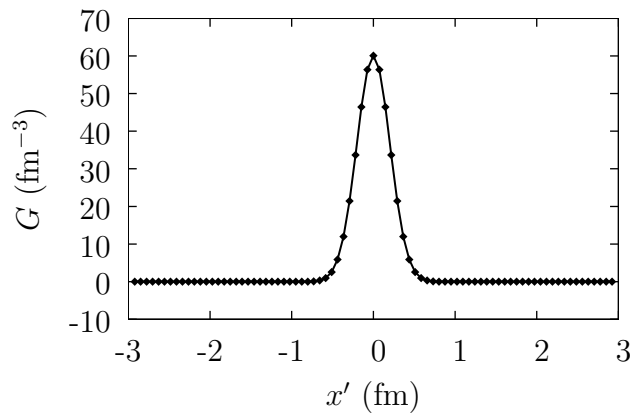


Figure 3.15: A typical slice through the N^3LO central propagator for an initial separation, $r = 0.5$ fm, and imaginary time, $t = (2000 \text{ MeV})^{-1}$.

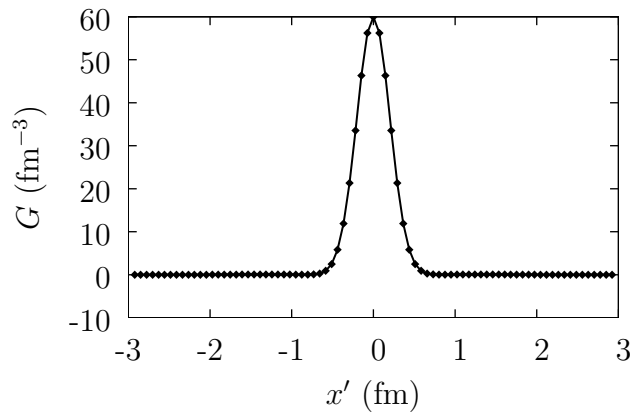


Figure 3.16: A typical slice through the $N^3LO(600)$ central propagator for an initial separation, $r = 0.5$ fm, and imaginary time, $t = (2000 \text{ MeV})^{-1}$.

back in, in a perturbative fashion, using forward walking exactly as for the fermion sign problem. The extra sign changes from the propagator are handled in the same way as sign changes from the fermion character.

We can estimate the fraction of walkers in the initial time step that may be given negative weights by comparing the integral of the absolute value of the propagators to the integral of the propagators. That is, we estimate the fraction of walkers with negative weights, f by

$$f = \frac{\int d^3r' \frac{1}{2} [|G(\mathbf{r}, \mathbf{r}'; t)| - G(\mathbf{r}, \mathbf{r}'; t)]}{\int d^3r' |G(\mathbf{r}, \mathbf{r}'; t)|}. \quad (3.26)$$

We calculate the integral over the upper half volume to exclude the interchange. For N³LO with an initial separation of 1.0 fm, we find $f \sim \mathcal{O}(10^{-2})$. If we now take the very conservative estimate for the alpha particle that all six pairs may be this close at one time and that the negative weights are acceptable so long as the fraction of walkers with negative weights is less than $1/e$, we find we can take approximately ten steps for N³LO [with time step $(2000 \text{ MeV})^{-1}$]. Green's function Monte Carlo typically uses forward walking of about 10 to 20 steps of $(2000 \text{ MeV})^{-1}$ (Pieper *et al.*, 2002; Wiringa *et al.*, 2000). Therefore forward walking will allow us to remove any bias from the negative parts of the propagator. This can be compared to forward walking keeping the propagator constraint, but releasing the fermion constraint to separate the two effects.

In the above analysis, we have assumed that the imaginary time step used will be the same as that used in Green's function Monte Carlo calculations with the Argonne family of potentials. Since the N³LO potentials are softer, the relevant commutator terms will be smaller, and longer time steps may be possible. For longer time steps there is much less ringing, and the calculations will be substantially easier.

3.5 Conclusions

We have shown how to calculate the imaginary time pair propagators needed for quantum Monte Carlo calculations of nuclei and nuclear matter using non-local potentials in momentum space. The method is general enough to handle any non-local potential in momentum or real space, but in this dissertation, we focus on those derived from effective field theory (N^3LO).

We find that the propagators display a universal behavior at large imaginary times, consistent with our expectations from renormalization group methods and the fact that the potentials are phase-shift equivalent, meaning that they reproduce the scattering data at or below laboratory energies of 350 MeV.

The central propagators sampled during Monte Carlo simulations for local potentials are expected to be positive-definite. Without this property, sign problems can develop. We find that for N^3LO with a 500 MeV or 600 MeV cutoff in momentum space, the central propagator is not positive definite. However, the negative parts consist of “rings” reminiscent of Friedel oscillations and their magnitude is quite small compared with the overall shape of the central propagator. Since these potentials were developed in momentum space, no attempt was made to influence their behavior in position space. It should be possible to modify the N^3LO potentials in such a way that they continue to reproduce the Nijmegen data with a low χ^2 , are still relatively soft, but have reduced ringing behavior. A modification of the choice of the regulator function used in the calculation of the N^3LO potentials:

$$V(k, k') \rightarrow V(k, k') e^{-(k/\Lambda)^{2n}} e^{-(k'/\Lambda)^{2n}}, \quad (3.27)$$

where Λ is the cutoff value, and n is an integer large enough such that powers of k are not generated less than the order of the calculation, ($n \geq 2$ for N^3LO), may help. In any case, quantum Monte Carlo calculations should still be possible by

using a modified path constraint as described above. We are implementing these calculations.

While we have concentrated on calculating the imaginary time pair propagators from phenomenological potentials, it is amusing to note that since the few-body imaginary time propagators are simply imaginary-time correlations of the appropriate nucleon operators, they might eventually be directly extracted from lattice QCD calculations.

Chapter 4

GREEN'S FUNCTION MONTE CARLO WITH NON-LOCAL POTENTIALS

4.1 Introduction

In this chapter we present our results for constructing a good trial wave function for non-local potentials and how to perform Green's function Monte Carlo calculations for non-local potentials. We begin by discussing the standard techniques for each and then discuss what modifications we have made to accommodate non-local potentials.

4.2 The Wave Function: Standard Form and Techniques

In Green's function Monte Carlo calculations, the wave function contains spatial, spin, and isospin degrees of freedom. The most important part of the wave function — and the part on which we will concentrate, since our focus is the two-body interaction — is the pair wave function

$$|\Psi_P\rangle = \left[\mathcal{S} \prod_{i < j} (1 + U_{ij}) \right] |\Psi_J\rangle, \quad (4.1)$$

where \mathcal{S} is a symmetrization operator, the U_{ij} are non-commuting two-body correlation operators, and $|\Psi_J\rangle$ is the so-called Jastrow wave function, which is a product of central pair-correlation functions $f_c(r_{ij})$ multiplying an antisymmetric single-particle wave function $|\Phi_A\rangle$ (Jastrow, 1955).

$$|\Psi_J\rangle = \prod_{i < j} f_c(r_{ij}) |\Phi_A\rangle. \quad (4.2)$$

The single-particle wave functions $|\Phi_A\rangle$ are nucleus specific. For s -shell nuclei, for example, they are often merely antisymmetrized spin-isospin states.

$$|\Phi_3\rangle = \mathcal{A} |p\uparrow p\downarrow n\uparrow\rangle, \text{ or } |\Phi_3\rangle = \mathcal{A} |p\uparrow n\downarrow n\uparrow\rangle; \quad (4.3a)$$

$$|\Phi_4\rangle = \mathcal{A} |p\uparrow p\downarrow n\uparrow n\downarrow\rangle, \quad (4.3b)$$

where \mathcal{A} is an antisymmetrizing operator. For larger nuclei into the p shell, a significantly more complicated Jastrow wave function is used, since some of the nucleons must be placed in the p shell (Pieper and Wiringa, 2001).

The correlation operators are

$$U_{ij} = \sum_{p=2}^m u_p(r_{ij}) O_{ij}^p, \quad (4.4)$$

where m can represent as many operators from the two-body interaction as is desired and practical. Because these two-body correlation operators do not commute, the symmetrization operator \mathcal{S} is used in Eq. (4.1) to keep the wave function overall antisymmetric as is required by the fermion nature of the nucleons. It does this by summing over all $\left[\frac{A(A-1)}{2}\right]!$ orderings of the terms in the product using Monte Carlo methods. This *ansatz* for the wave function is motivated by the idea that each operator present in the interaction can induce a correlation in the wave function.

We note that for the more general case, where three-body forces are included, an improved wave function is often used

$$|\Psi_T\rangle = \left[1 + \sum_{i < j < k} (U_{ijk} + U_{ijk}^{\text{TNI}}) + \sum_{i < j} U_{ij}^{LS} \right] |\Psi_P\rangle, \quad (4.5)$$

where U_{ijk} and U_{ijk}^{TNI} are non-commuting three-body correlations coming from the two- and three-body interactions, respectively. U_{ij}^{LS} is a two-body correlation stemming from the two-body spin-orbit interaction. An extensive discussion of this form and its origins is given by Arriaga *et al.* (1995). This more general form breaks the cluster

decomposition but the additional correlations are sufficiently weak that this can be neglected.

The central f_c and non-central u_p correlation functions are obtained by solving two-body Schrödinger-like equations with a modified phenomenological interaction that gives the correct short- and long-distance behavior of the nuclear system. That is, at short distances, the two-body interaction should be dominant; at long distances, the central correlation should decay exponentially like the separation energy of one nucleon from the remaining cluster of nucleons. We discuss here the simplest example, where only the dominant effect of one-pion exchange is considered, and only the central, spin, and spin-tensor/isospin correlations contribute. For s -shell nuclei, these are the most important pieces. For this, we follow the treatment detailed in Lomnitz-Adler *et al.* (1981). Details for the more involved cases (including those which involve the p -shell nuclei) may be found in Wiringa (1991) and Pieper and Wiringa (2001).

For this simplest case, the pair wave function Eq. (4.1), becomes

$$|\Psi_P\rangle = \left[\mathcal{S} \prod_{i < j} (1 + u_\sigma(r_{ij}) \boldsymbol{\sigma}_i \cdot \boldsymbol{\sigma}_j + u_{t\tau}(r_{ij}) S_{ij} \boldsymbol{\tau}_i \cdot \boldsymbol{\tau}_j) f_c(r_{ij}) \right] |\Phi_A\rangle. \quad (4.6)$$

The correlations f_c , u_σ , and $u_{t\tau}$ can be obtained by solving the following two-body equations in the 1S_0 , and 3S_1 - 3D_1 channels (m_r is the reduced mass of the two nucleons).

$$\left[-\frac{\hbar^2}{2m_r} \nabla^2 + v_c^{(1,0)} + \lambda^{(1,0)} \right] f_c^{(1,0)} = 0, \quad (4.7a)$$

$$\left[-\frac{\hbar^2}{2m_r} \nabla^2 + v_c^{(0,1)} + \lambda^{(0,1)} \right] f_c^{(0,1)} + 8v_t^{(0,1)} f_t^{(0,1)} = 0, \quad (4.7b)$$

$$\left[-\frac{\hbar^2}{2m_r} \left(\nabla^2 - \frac{6}{r^2} \right) + v_c^{(0,1)} + \lambda^{(0,1)} - 2v_t^{(0,1)} - 3v_b^{(0,1)} \right] f_t^{(0,1)} + v_t^{(0,1)} f_c^{(0,1)} = 0. \quad (4.7c)$$

These are essentially the Schrödinger equation in the channels with additional phenomenological potentials $\lambda^{(T,S)}(r)$, which are used to enforce physical boundary conditions. The subscripts of $f_p^{(T,S)}$ with $p = c, t$, and b refer to the central, tensor and

spin-orbit portions of the interaction. The superscripts (T, S) are the pair isospin and spin. The $f_p^{(T,S)}$ are related to the correlations f_c , u_σ , and $u_{t\tau}$ of Eq. (4.6) by

$$f_c = \frac{1}{4} (f_c^{(1,0)} + 3f_c^{(0,1)}), \quad (4.8a)$$

$$u_\sigma = \frac{1}{4f_c} (f_c^{(0,1)} - f_c^{(1,0)}), \quad (4.8b)$$

$$u_{t\tau} = -\frac{1}{3f_c} f_t^{(0,1)}. \quad (4.8c)$$

The $\lambda^{(T,S)}$ are chosen so that the boundary conditions

$$[f_c(r \rightarrow \infty)]^{A-1} = \frac{e^{-\kappa r}}{r}, \quad (4.9a)$$

$$rf_c(r \rightarrow 0) = 0, \quad (4.9b)$$

are satisfied, where,

$$\kappa = \sqrt{\frac{2M_r}{\hbar^2} E_S}, \quad (4.10a)$$

$$M_r = \frac{A-1}{A} m. \quad (4.10b)$$

E_S is the separation energy of one nucleon from the $A-1$ others, and M_r is the reduced mass of the separated nucleon with the cluster of the $A-1$ others. With these boundary conditions, the correlations have the following three properties. 1) When two nucleons are close together the dominant interaction is just the two-body nucleon-nucleon interaction. 2) When one nucleon separates from the cluster of the remaining $A-1$ nucleons, the product of $A-1$ central correlations decays exponentially like the separation energy E_S . 3) The correlations are regular at the origin.

The $\lambda^{(T,S)}$ are given by

$$\lambda^{(T,S)}(r) = \frac{\hbar^2}{2m_r} \left(\kappa^2 - \frac{2(1-\alpha)\kappa}{r} + \frac{\alpha(\alpha-1)}{r^2} \right) \left(1 - e^{-\left(\frac{r}{C}\right)^2} \right) + \frac{\gamma^{(T,S)}}{1 + e^{\frac{r-R}{\mu}}}, \quad (4.11)$$

where $\alpha = \frac{1}{A-1}$, and C , R , and μ (and in principle E_S) are variational parameters which are adjusted to minimize the variational energy. Though, it is found that in

practice E_S is close to the separation energy. The first term ensures the asymptotic behavior of Eq. (4.9a); the exponential regulates the $\frac{1}{r^2}$ singularity. The strength of the Woods-Saxon term $\gamma^{(T,S)}$ is adjusted so that the small- r behavior of Eq. (4.9b) is met. The standard method solves the differential equations Eqs. (4.7) using numerical techniques such as Numerov integration (Koonin and Meredith, 1998) with $\gamma^{(T,S)}$ adjusted to satisfy the boundary conditions to obtain the correlations. However, such numerical techniques are not practical when the potential is non-local.

4.3 The Wave Function: Non-Local Potentials

The point of departure for non-local potentials from the standard methods is the numerical solution of Eqs. (4.7) when the potential is no longer local. As in the case of the propagator, we turn to momentum space, where non-local potentials are typically defined.

We recast the differential equations in the discrete momentum space as

$$\langle k_m TS | H + \tilde{\lambda}^{(T,S)} | \tilde{f}_p^{(T,S)} \rangle = 0, \quad (4.12)$$

where H is the nuclear Hamiltonian in the discrete momentum space, and $\tilde{\lambda}^{(T,S)}$ and $\tilde{f}_p^{(T,S)}$ are the phenomenological potentials Eq. (4.11) and the correlations, respectively, in the discrete momentum space. Now, the various $\tilde{f}_p^{(T,S)}$ are the eigenvectors with zero eigenvalue of the modified Hamiltonians: $H + \tilde{\lambda}^{(T,S)}$. Therefore, we can obtain them by diagonalization.

We numerically construct the singlet channel (1S_0) Hamiltonian

$$\begin{aligned} & \langle k_m, T = 1, S = 0 | H + \tilde{\lambda}^{(T=1,S=0)} | k_n, T = 1, S = 0 \rangle \\ &= \frac{\hbar^2 k_n^2}{2m_r} \delta_{mn} + V(k_m, k_n) + \tilde{\lambda}^{(T=1,S=0)}(k_m, k_n), \end{aligned} \quad (4.13)$$

and the triplet channel (3S_1 - 3D_1) Hamiltonian

$$\langle k_m, T = 0, S = 1, L' | H + \tilde{\lambda}^{(T=0,S=1)} | k_n, T = 0, S = 1, L \rangle = \begin{pmatrix} H_{--} + \tilde{\lambda}^{(T=0,S=1)}(k_m^{(-)}, k_n^{(-)}) & H_{-+} \\ H_{+-} & H_{++} + \tilde{\lambda}^{(T=0,S=1)}(k_m^{(+)}, k_n^{(+)}) \end{pmatrix}, \quad (4.14)$$

where $H_{\pm,\pm}$ are the discrete-momentum-space Hamiltonian as in Eq. (3.14).

Now, we choose a value $\gamma^{(T,S)}$ for the Woods-Saxon strength, which can be zero to start, and using the nuclear energy scale, $\mathcal{O}(1)$ MeV, we find upper and lower bounds. Then we use the simple bisection method (Koonin and Meredith, 1998) to determine the value of $\gamma^{(T,S)}$ which forces the lowest eigenvalue of the modified Hamiltonian to zero (within some specified relative tolerance usually chosen to be $\mathcal{O}(10^{-10})$). The bisection method works by bracketing the root of a continuous function f in some interval $a < x < b$. That interval is repeatedly bisected, selecting a new subinterval bracketing the root in each iteration. Bracketing the root means we have two values in the domain a and b such that $f(a)$ and $f(b)$ have opposite signs, then by the intermediate value theorem f has a root on the interval. There are more sophisticated numerical root-finding methods that could be used, but bisection is quite robust, simple to implement, and guaranteed to converge to machine precision in about 50 iterations.

Once the lowest eigenvalue is zero within the specified tolerance, the lowest accompanying eigenvector is the discrete-momentum-space correlation: $\tilde{f}_p^{(T,S)}(k_n) = \langle k_n TSL | f_p^{(T,S)} \rangle$, and the real-space correlation we desire is obtained as an eigenfunction expansion in the discrete momentum space as detailed in Appendix A. One additional subtlety must be addressed. We want to ensure that the asymptotic behavior of the correlation is the boundary-condition exponential Eq. (4.9a), even though the basis goes to zero at $r = R$. Thus we scale the correlation such that the logarithmic derivative of the correlation and the boundary-condition exponential agree at some

point beyond the range of the potential (typically beyond 8 fm). This ensures that the correlation and the boundary-condition exponential are smoothly “attached” in the asymptotic region.

We present results for ${}^4\text{He}$ below. Table (4.1) shows the values of the variational parameters used. E_S is taken to be the approximate difference in the two-body binding energies between ${}^4\text{He}$ and ${}^3\text{H}$: $E_S \approx 24 \text{ MeV} - 8 \text{ MeV} = 16 \text{ MeV}$. Fig. (4.1) shows the singlet channel correlation, $f_c^{(1,0)}(r)$ for three different potentials using our diagonalization method outlined above. The plots themselves are of interest,

Table 4.1: Wave function parameters for ${}^4\text{He}$.

C	1.0 fm
R	1.0 fm
μ	0.5 fm
E_S	16.0 MeV

since they demonstrate some of the words that are often used to describe differences between the potentials. For example, non-local potentials are typically described as “softer” than the local AV_{18} . This is visible in the differences in the plots at small r . Two nucleons interacting via Argonne’s v_{18} potential are less likely to be separated by distances $r \lesssim 1 \text{ fm}$ than two nucleons interacting via the CD-Bonn or $N^3\text{LO}$ potentials. The boundary-condition exponential, Eq. (4.9a), is also displayed, which demonstrates that the correlations obey the correct asymptotic behavior.

Fig. (4.2) displays the central and tensor correlations, $f_c^{(0,1)}(r)$ and $f_t^{(0,1)}(r)$. The upper set of curves are the central correlations, $f_c^{(0,1)}(r)$. These are essentially modified S -state deuteron wave functions for the three different potentials. These three

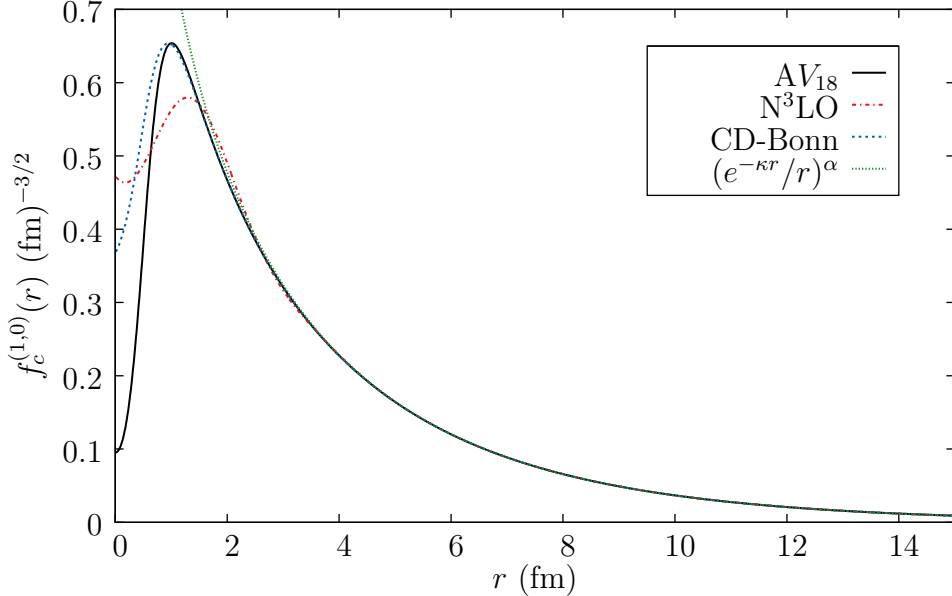


Figure 4.1: The correlation $f_c^{(1,0)}(r)$ (the 1S_0 channel) calculated using our diagonalization method for three different potentials: the boundary-condition exponential is also displayed, where $\alpha = \frac{1}{A-1} = \frac{1}{3}$.

curves also obey the same asymptotic boundary condition as the singlet correlations above. As in the case of the singlet correlations, it is clear that the two non-local potentials have a softer “core”.

The lower set of curves are modified D -state deuteron wave functions. The contrast between the N^3LO wave function and the others is noteworthy. Even in Fig. (4.2), one can see that the D -state wave function for the N^3LO potential is oscillating about the others. But, the subsequent figure makes it clear: Fig. (4.3) shows a portion of the D -state wave functions for the three different potentials with the y axis log scaled to emphasize the effect. This figure, taken seriously, suggests that there is non-trivial physics happening out as far as $\sim 8 - 10$ fm in the N^3LO potential. The

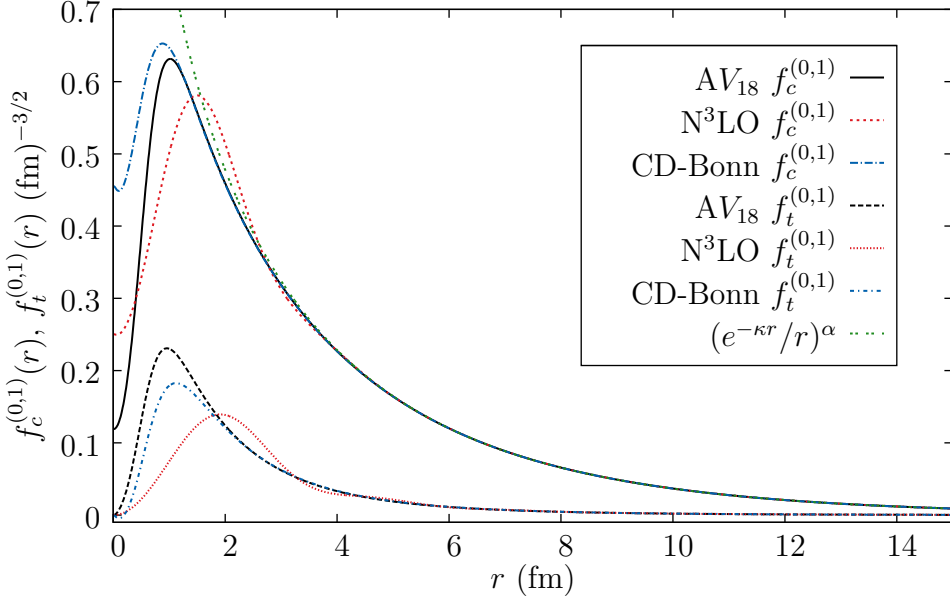


Figure 4.2: The correlations $f_c^{(0,1)}(r)$ and $f_t^{(0,1)}(r)$ (the ${}^3S_1 - {}^3D_1$ channel) calculated using our diagonalization method for three different potentials: the boundary-condition exponential is also displayed, where $\alpha = \frac{1}{A-1} = \frac{1}{3}$. The upper curves are the central correlations; the lower curves are the tensor correlations.

more likely explanation is the choice of the regulator used in the N^3LO potential: see Chapter 2, Section 2.2.3 for a discussion of the regulator.

Since this method of obtaining the correlations is distinct from the method typically used, it is worthwhile to make certain checks to ensure that we agree with previous calculations in certain limits. For example, if we consider the two-body ($A = 2$) nucleus, the deuteron, we can set $\lambda^{(T,S)}(r)$ to zero, and the correlations $f_c^{(0,1)}(r)$ and $f_t^{(0,1)}(r)$ thus obtained in the ${}^3S_1 - {}^3D_1$ channel are the S - and D -state contributions to the deuteron wave function:

$$\psi_D^{(M)}(\mathbf{r}) = \left[f_c^{(0,1)}(r) + \frac{S_{12}(\hat{\mathbf{r}})}{\sqrt{8}} f_t^{(0,1)}(r) \right] \frac{\chi_M}{\sqrt{4\pi}}, \quad (4.15)$$

where χ_M is the spin wave function, and S_{12} the tensor operator. The wave function

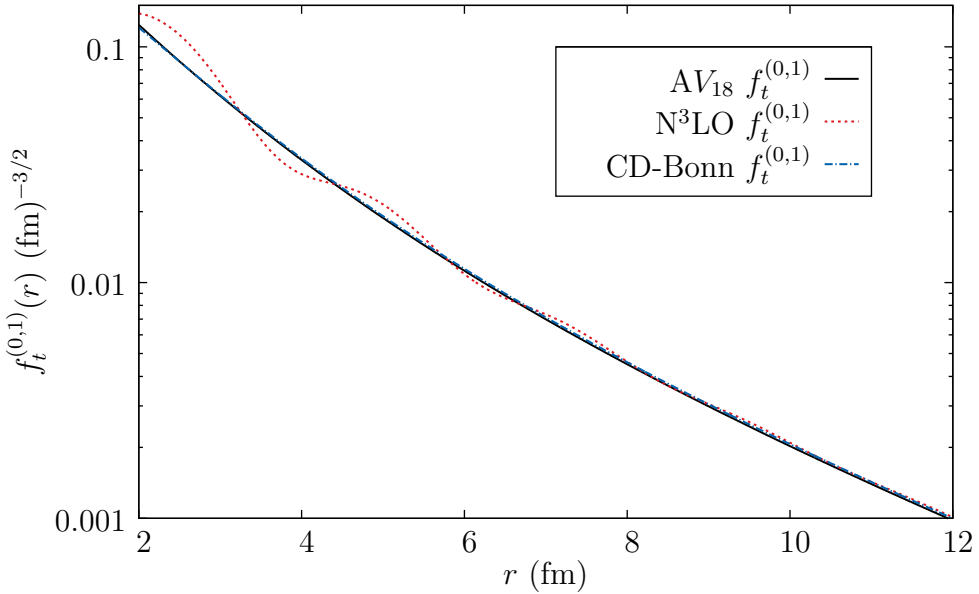


Figure 4.3: A portion of the correlation $f_t^{(0,1)}(r)$ calculated using our diagonalization method for three different potentials. The y axis is log scaled to make the “ringing” effect of the N^3LO wave function clearer.

is often written in terms of the reduced S - and D -state wave functions $u(r)$ and $w(r)$.

$$\psi_D^{(M)}(\mathbf{r}) = \left[\frac{u(r)}{r} + \frac{S_{12}(\hat{\mathbf{r}})}{\sqrt{8}} \frac{w(r)}{r} \right] \frac{\chi_M}{\sqrt{4\pi}}, \quad (4.16)$$

which leads to the identification, $u(r) = rf_c^{(0,1)}(r)$, and $w(r) = rf_t^{(0,1)}(r)$. With the deuteron wave function, we can calculate several observables and compare with previous calculations.

We choose the quadrupole moment, Q defined as

$$Q = \frac{1}{\sqrt{50}} \int dr r^2 Q(r), \quad (4.17)$$

where $Q(r) = u(r)w(r) - w^2(r)/\sqrt{8}$, the matter radius, $\langle r^2 \rangle_D$, defined as

$$\langle r^2 \rangle_D = \frac{1}{4} \int dr r^2 (u^2(r) + w^2(r)), \quad (4.18)$$

and the D -state probability (not quite an observable (Friar, 1979)), defined as

$$P_D = \int dr w^2(r) \quad (4.19)$$

(Garçon and Orden, 2001), and display the results in Table (4.2).

Table 4.2: Deuteron properties for three different potentials as calculated from our wave functions obtained via diagonalization compared with experiment.

	AV ₁₈	N ³ LO	CD-Bonn	Experiment
Deuteron properties:				
Quadr. moment Q (fm ²)	0.270 ^a	0.275 ^a	0.270 ^a	0.2860(15) ^b
Matter radius $\langle r^2 \rangle_D$ (fm)	1.97 ^a	1.974 ^a	1.965 ^a	1.971(6) ^c
D -state probab. P_D (%)	5.76	4.51	4.85	—

^a Without meson current contributions or relativistic corrections.

^b (Bishop and Cheung, 1979)

^c (Ericson and Rosa-Clot, 1983)

4.4 Green's Function Monte Carlo

Now we would like to present the Green's function Monte Carlo method in more detail, highlighting what changes must be made to accommodate non-local potentials. We begin by presenting a more detailed explanation of the variational Monte Carlo method used to prepare a set of walkers to be used in the Green's function Monte Carlo method.

4.4.1 Variational Monte Carlo and Non-Local Potentials

As was summarized in Chapter 2, variational Monte Carlo calculations begin with a trial wave function which contains variational parameters. The wave function

has the form described in this chapter. Expectation values are calculated by Monte Carlo sampling in both configuration space and in the order of the operators in the symmetrized product of Eq. (4.1).

$$\langle O \rangle = \frac{\sum_{\alpha\beta} \sum_{pq} \int d\mathbf{R} \Psi_{\alpha p}^\dagger(\mathbf{R}) O \Psi_{\beta q}(\mathbf{R}) / W_{pq}(\mathbf{R})}{\sum_{\alpha\beta} \sum_{pq} \int d\mathbf{R} \Psi_{\alpha p}^\dagger(\mathbf{R}) \Psi_{\beta q}(\mathbf{R}) / W_{pq}(\mathbf{R})}, \quad (4.20)$$

where the weight function $W_{pq}(\mathbf{R})$ is given by

$$W_{pq}(\mathbf{R}) = \text{Re} \left(\sum_{\alpha\beta} \Psi_{\alpha p}^\dagger(\mathbf{R}) \Psi_{\beta q}(\mathbf{R}) \right). \quad (4.21)$$

The sums on α and β (the spin-isospin sums) are carried out explicitly, while the integral and sums on the orderings of the operators in the symmetric product (p and q represent different orderings) are carried out with Monte Carlo sampling using a Metropolis random walk, where samples are drawn from the distribution $W_{pq}(\mathbf{R})$. Monte Carlo expectation values have statistical errors which are estimated by the standard deviation

$$\sigma = \sqrt{\frac{\langle O^2 \rangle - \langle O \rangle^2}{N - 1}}, \quad (4.22)$$

where N is the number of samples which are statistically independent from one another. This often means that the number of configurations actually sampled is larger than N since $\mathcal{O}(10)$ samples, or more, are generated between each statistically-independent sample.

Perhaps the most interesting operator is the Hamiltonian to obtain the variational energy. For local potentials where the two-body Hamiltonian is the sum of the Laplacian operator and a local potential operator, $\langle \mathbf{r}'_{ij} | v | \mathbf{r}_{ij} \rangle = v_{ij}(r) \delta^{(3)}(\mathbf{r} - \mathbf{r}')$ (plus, at most, one or two derivatives associated with linear and quadratic spin-orbit operators) obtaining the local energy (the energy at the position \mathbf{R}) requires calculating the first and second derivatives. As detailed by Wiringa (1991), the first and second derivatives are obtained by moving each nucleon a small distance ϵ in the positive

and negative directions along each axis, and then forming the finite differences

$$\begin{aligned}\frac{\partial \Psi_q(\mathbf{R})}{\partial r_i^m} &= \frac{1}{2\epsilon} [\Psi_q(\mathbf{R} + \epsilon r_i^m) - \Psi_q(\mathbf{R} - \epsilon r_i^m)], \\ \frac{\partial^2 \Psi_q(\mathbf{R})}{\partial (r_i^m)^2} &= \frac{1}{\epsilon} [\Psi_q(\mathbf{R} + \epsilon r_i^m) - 2\Psi_q(\mathbf{R}) + \Psi_q(\mathbf{R} - \epsilon r_i^m)],\end{aligned}\tag{4.23}$$

where r_i^m is the m th spatial component of nucleon coordinate \mathbf{r}_i . This amounts to $6A + 1$ evaluations of the wave function. Additional evaluations of the wave function are necessary for quadratic spin-orbit operators from the Hamiltonian, where mixed second derivatives are used. These additional complications are discussed in detail in Wiringa (1991). The effect is that the number of evaluations is $\mathcal{O}(10P)$, where $P = A(A - 1)/2$ is the number of pairs.

For non-local potentials, there are not just first and second derivatives to contend with. The potential has a complicated momentum-dependent structure. In configuration space it depends non-trivially on the relative separation of a pair at this moment and the relative separation of that pair in the next moment. Thus, the evaluation of the local energy requires an additional integration for each pair over the pair separation. That is, for each pair we have a contribution to the local energy of the form

$$\frac{\sum_{\alpha\beta} \sum_{pq} \int d^3r_{ij} \int d^3r'_{ij} \Psi_{\alpha p}(\mathbf{r}_{ij}) H(\mathbf{r}_{ij}, \mathbf{r}'_{ij}) \Psi_{\beta q}(\mathbf{r}'_{ij})}{\sum_{\alpha\beta} \sum_{pq} \int d^3r_{ij} \Psi_{\alpha p}(\mathbf{r}_{ij}) \Psi_{\beta q}(\mathbf{r}_{ij})}.\tag{4.24}$$

The most straightforward approach would be to treat the additional integral $\int d^3r'_{ij}$ numerically, but not with Monte Carlo. However, this would likely lead to large computational cost. Each pair requires this additional three-dimensional integral. Suppose the number of integration points required is n , where based on the range of the potential we might conservatively expect $n \sim \mathcal{O}(10^3)$. Then the cost of evaluating the local energy is $nP \sim 10^3 P$. This is orders of magnitude more than for a local potential. However, it is possible that this additional integral can be done using Monte Carlo sampling if the variance of the integral over the pair separation is comparable to

the variance of the other integrations, in which case it is conceivable that the number of samples could reduce n to $\mathcal{O}(100)$ or even $\mathcal{O}(10)$, which would be comparable to the evaluation of the local energy for the full local AV_{18} potential.

4.4.2 Green's Function Monte Carlo and Non-Local Potentials

We begin by providing more details on the standard Green's function Monte Carlo method and then discuss what changes need to be made to accommodate non-local potentials. An analysis of the method may begin with the understanding that we want the wave function at an imaginary time $t + \Delta t$ supposing we already have it at an imaginary time t . To obtain the wave function at the later imaginary time, we propagate in imaginary time

$$|\Psi(t + \Delta t)\rangle = e^{-H\Delta t} |\Psi(t)\rangle. \quad (4.25)$$

Inserting a complete set of states and projecting onto a state $\langle \mathbf{R}\alpha|$ we obtain

$$\langle \mathbf{R}\alpha | \Psi(t + \Delta t) \rangle = \sum_{\beta} \int d\mathbf{R}' \langle \mathbf{R}\alpha | e^{-H\Delta t} | \mathbf{R}'\beta \rangle \langle \mathbf{R}'\beta | \Psi(t) \rangle. \quad (4.26)$$

However, because the integral $\int d\mathbf{R}'$ is done using Monte Carlo, it is a waste of effort to compute the integral for regions where the integrand is small or negligible. Thus, we introduce and importance sampling function $\Psi_I(\mathbf{R})$ which is often taken to be the trial wave function $\Psi_{T\alpha}(\mathbf{R})$.

$$\langle \mathbf{R}\alpha | \Psi(t + \Delta t) \rangle = \sum_{\beta} \int d\mathbf{R}' \frac{\langle \mathbf{R}\alpha | e^{-H\Delta t} | \mathbf{R}'\beta \rangle}{\Psi_{T\beta}^*(\mathbf{R}')} \langle \mathbf{R}'\beta | \Psi(t) \rangle \Psi_{T\beta}^*(\mathbf{R}'). \quad (4.27)$$

Samples are now drawn from $(\langle \mathbf{R}'\beta | \Psi \rangle_{T\beta}^*(\mathbf{R}'))$, and to make the equation a consistent integral equation for this function, we multiply both sides by the importance sampling function.

$$\langle \mathbf{R}\alpha | \Psi(t + \Delta t) \rangle \Psi_{T\alpha}^*(\mathbf{R}) = \sum_{\beta} \int d\mathbf{R}' \Psi_{T\alpha}^*(\mathbf{R}) \frac{\langle \mathbf{R}\alpha | e^{-H\Delta t} | \mathbf{R}'\beta \rangle}{\Psi_{T\beta}^*(\mathbf{R}')} \langle \mathbf{R}'\beta | \Psi(t) \rangle \Psi_{T\beta}^*(\mathbf{R}). \quad (4.28)$$

Now, to propagate forward, we sample

$$\frac{\Psi_{T\alpha}^*(\mathbf{R})}{\Psi_{T\beta}^*(\mathbf{R}')}\langle \mathbf{R}\alpha|e^{-H\Delta t}|\mathbf{R}'\beta\rangle. \quad (4.29)$$

This is achieved by expressing the propagator in the pair product form of Eq. (2.18):

$$\langle \mathbf{R}\alpha|e^{-H\Delta t}|\mathbf{R}'\beta\rangle = G_0(\mathbf{R}, \mathbf{R}')\langle \alpha|\mathcal{S} \prod_{i < j} \frac{g_{ij}(\mathbf{r}_{ij}, \mathbf{r}'_{ij}; \Delta t)}{g_{0,ij}(\mathbf{r}_{ij}, \mathbf{r}'_{ij}; \Delta t)} |\beta\rangle. \quad (4.30)$$

where $G_0(\mathbf{R}, \mathbf{R}') = \langle \mathbf{R}|e^{-H_0\Delta t}|\mathbf{R}'\rangle$ is the many-body free-particle propagator, and $\langle \alpha|g_{ij}(\mathbf{r}_{ij}, \mathbf{r}'_{ij}; \Delta t)|\beta\rangle$ and $\langle \alpha|g_{0,ij}(\mathbf{r}_{ij}, \mathbf{r}'_{ij}; \Delta t)|\beta\rangle$, are the interacting and free-particle pair propagators, respectively. In the short imaginary time limit, we can use the primitive approximation for the interacting pair propagator

$$\begin{aligned} \langle \alpha|g_{ij}(\mathbf{r}_{ij}, \mathbf{r}'_{ij}; \Delta t)|\beta\rangle &= \langle \mathbf{r}_{ij}\alpha|e^{-H\Delta t}|\mathbf{r}'_{ij}\beta\rangle \\ &\approx \int d^3 r''_{ij} \sum_{\gamma} \langle \mathbf{r}_{ij}\alpha|e^{-V\Delta t}|\mathbf{r}''_{ij}\gamma\rangle \langle \mathbf{r}''_{ij}\gamma|e^{T_{\text{ke}}\Delta t}|\mathbf{r}'\beta\rangle. \end{aligned} \quad (4.31)$$

The potential is local, so the exponential of the potential gives a delta function, and the kinetic energy is diagonal in spin-isospin space, giving a Kronecker delta:

$$\langle \alpha|g_{ij}(\mathbf{r}_{ij}, \mathbf{r}'_{ij}; \Delta t)|\beta\rangle \approx \langle \mathbf{r}_{ij}\alpha|e^{-V\Delta t}|\mathbf{r}_{ij}\beta\rangle \langle \mathbf{r}_{ij}\beta|e^{T_{\text{ke}}\Delta t}|\mathbf{r}'\beta\rangle. \quad (4.32)$$

Therefore, in this limit the ratio

$$\frac{g_{ij}(\mathbf{r}_{ij}, \mathbf{r}'_{ij}; \Delta t)}{g_{0,ij}(\mathbf{r}_{ij}, \mathbf{r}'_{ij}; \Delta t)} \approx \langle \mathbf{r}_{ij}\alpha|e^{-V\Delta t}|\mathbf{r}_{ij}\beta\rangle, \quad (4.33)$$

and the many-body propagator is therefore

$$\begin{aligned} \langle \mathbf{R}\alpha|e^{-H\Delta t}|\mathbf{R}'\beta\rangle &= G_0(\mathbf{R}, \mathbf{R}')\langle \alpha|\mathcal{S} \prod_{i < j} \frac{g_{ij}(\mathbf{r}_{ij}, \mathbf{r}'_{ij}; \Delta t)}{g_{0,ij}(\mathbf{r}_{ij}, \mathbf{r}'_{ij}; \Delta t)} |\beta\rangle \\ &\approx \langle \mathbf{R}|e^{-T_{\text{ke}}\Delta t}|\mathbf{R}'\rangle \langle \mathbf{R}\alpha|e^{-V\Delta t}|\mathbf{R}'\beta\rangle, \end{aligned} \quad (4.34)$$

which demonstrates that for local potentials the pair product form is correct at short imaginary times. For non-local potentials a similar but more careful form will need

to be used which divides by the free-particle pair propagator for $\alpha = \beta$, but not when $\alpha \neq \beta$.

Then, new positions \mathbf{R} are proposed from G_0 . One way to accomplish this is to take as possible new positions for each pair, the 6 at $r_i \pm x_i$, where x_i are sampled from G_0 . Then a weight is calculated which is given by

$$W_i = \frac{w_i}{\sum_i w_i}, \quad (4.35)$$

where the w_i are given by

$$w_{\alpha\beta}(\mathbf{R}, \mathbf{R}') = \frac{\Psi_{T\alpha}^*(\mathbf{R})}{\Psi_{T\beta}^*(\mathbf{R}')} \langle \alpha | \mathcal{S} \prod_{i < j} \frac{g_{ij}(\mathbf{r}_{ij}, \mathbf{r}'_{ij}; \Delta t)}{g_{0,ij}(\mathbf{r}_{ij}, \mathbf{r}'_{ij}; \Delta t)} | \beta \rangle. \quad (4.36)$$

The value of this weight is used to determine which of the 6 proposed new positions for each pair is chosen. With this method, mixed estimates of operators, including the Hamiltonian to obtain the local energy are calculated. Evaluating the local energy now proceeds exactly as described in our discussion of variational Monte Carlo above.

In addition to the local energy, it is possible to calculate a value known as the growth energy. That is, by averaging the Green's function itself, we can often extract an estimate for the energy of the system. Using the cumulant expansion, we can write

$$-\frac{1}{\Delta t} \log \langle e^{-H\Delta t} \rangle = \langle H \rangle - \frac{1}{2} \sigma_H^2 \Delta t + \dots, \quad (4.37)$$

where σ_H^2 is the variance. To see this, start with the expectation value of the exponential of some operator and expand in a Taylor series

$$\langle e^{-O\Delta t} \rangle = 1 - \langle O \rangle \Delta t + \frac{1}{2} \langle O^2 \rangle \Delta t^2 + \mathcal{O}(\Delta t^3). \quad (4.38)$$

Now, compare this to the exponential of the expectation value and the exponential of the variance.

$$e^{-\langle O \rangle \Delta t} = 1 - \langle O \rangle \Delta t + \frac{1}{2} \langle O \rangle^2 \Delta t^2 + \mathcal{O}(\Delta t^3) \quad (4.39a)$$

$$e^{\frac{1}{2}[\langle O^2 \rangle - \langle O \rangle^2]\Delta t^2} = 1 + \frac{1}{2} \langle O^2 \rangle \Delta t^2 - \frac{1}{2} \langle O \rangle^2 \Delta t^2 + \mathcal{O}(\Delta t^3) \quad (4.39b)$$

Comparing the two, we see that, to order Δt^2 ,

$$\langle e^{-O\Delta t} \rangle = e^{-\langle O \rangle \Delta t + \frac{1}{2} [\langle O^2 \rangle - \langle O \rangle^2] \Delta t^2}. \quad (4.40)$$

And therefore, to order Δt ,

$$-\frac{1}{\Delta t} \log \langle e^{-O\Delta t} \rangle = \langle O \rangle - \frac{1}{2} [\langle O^2 \rangle - \langle O \rangle^2] \Delta t. \quad (4.41)$$

This allows for the possibility that we can calculate a “one-step” Green’s function Monte Carlo calculation, without addressing the additional three-dimensional integral necessary for calculating the local energy. This would proceed as follows. A set of configurations (walkers) is generated from a variational Monte Carlo calculation. Then a single Green’s function Monte Carlo step in Δt is taken. The weight is calculated and the walkers are then returned to their initial configurations. This is repeated many times, generating an average for the expectation value $\langle e^{-H\Delta t} \rangle$. In Chapter 5, we present results for this one-step Green’s function Monte Carlo method for several cases.

A complication that arises that must be addressed is the choice of the importance function G_0 in the sampling of the new positions during the propagation. For local potentials, such as Argonne’s v_{18} , G_0 is the many-body free-particle propagator, and this choice works well. For non-local potentials, we have found this choice to be inadequate for at least two reasons.

The interacting pair propagator for non-local potentials g_{ij} typically extends well past the free-particle pair propagator $g_{0,ij}$, such that the division $g_{ij}/g_{0,ij}$ yields large values out in the tail regions of the propagator. This gives rise to large variance in the calculation. Therefore, an alternative must be found. One choice, as discussed in Chapter 3, would be the central part of the pair propagator (the trace over spins and isospins of the pair propagator), although as discussed in Chapter 3 there are

complications which arise there, because of the fact that the central part of the pair propagator for a non-local potential is not positive definite. One solution is as proposed in Chapter 3, to set the small negative regions to zero and add them back in perturbatively. Another solution may be to add in unphysical channels (which are projected out when the propagator acts on the antisymmetric wave function) which will ensure the positive-definite character of the central part. These options are currently under investigation. A second reason the free-particle propagator G_0 is likely to be inadequate is the fact that the binding energy for Argonne's v_{18} largely appears to come from integrating over regions very close to the initial separation of a pair. For non-local potentials it appears that this is no longer the case. Evidence for this assertion is presented in Chapter 5.

Chapter 5

CHECKING THE METHODS AND CURRENT STATUS

With the development of any new method which is a generalization of a currently used and successful method, it is prudent to check that the new agrees in certain limits with the old: a sort of correspondence principle for methods. Therefore, in this chapter we present various checks we have carried out to be sure we can reproduce calculations using local potentials but using our diagonalization method to produce the imaginary-time pair propagator. In this chapter we also discuss the current status of the project to calculate the ground-state energy of ${}^4\text{He}$ with N³LO and challenges that remain.

5.1 Checks

The simplest case to consider is the construction of the free-particle propagator. Here, $V = 0$, and the momentum-space Hamiltonian is already diagonal. Still, we use our routines for diagonalizing the Hamiltonian in the channel basis, and then re-sum the partial waves to obtain the full pair propagator. Now, if we use this pair propagator in the one-step Green's function Monte Carlo codes with a deuteron wave function, then, the growth energy

$$-\frac{1}{\Delta t} \log \langle e^{-T_{\text{ke}} \Delta t} \rangle = \langle T_{\text{ke}} \rangle - \frac{1}{2} [\langle T_{\text{ke}}^2 \rangle - \langle T_{\text{ke}} \rangle^2] \Delta t + \mathcal{O}(\Delta t)^2, \quad (5.1)$$

should be the kinetic energy of the deuteron up to the variance of the kinetic energy operator

$$\sigma_{\text{ke}}^2 = \langle T_{\text{ke}}^2 \rangle - \langle T_{\text{ke}} \rangle^2. \quad (5.2)$$

The deuteron is not an eigenstate of the kinetic energy operator, and so we should not expect the variance of the kinetic energy to be a trivial correction. We emphasize here that this is not a Monte Carlo variance we are discussing, but the variance of the operator itself in this state. We can calculate both the kinetic energy expectation value and its variance directly in the channel basis in the discrete momentum space, where the kinetic energy and its square are diagonal.

$$\begin{aligned} T_{\text{ke}} &= \langle \psi | \hat{T}_{\text{ke}} | \psi \rangle = \sum_{mn} \psi^\dagger(k_m) \left(\frac{\hbar^2 k_m^2}{2m_r} \delta_{mn} \right) \psi(k_n); \\ T_{\text{ke}}^2 &= \langle \psi | \hat{T}_{\text{ke}}^2 | \psi \rangle = \sum_{mn} \psi^\dagger(k_m) \left[\left(\frac{\hbar^2 k_m^2}{2m_r} \right)^2 \delta_{mn} \right] \psi(k_n). \end{aligned} \quad (5.3)$$

$\psi(k_n)$ is the lowest eigenvector of the ${}^3S_1 - {}^3D_1$ channel Hamiltonian (the deuteron channel) in the discrete momentum space,

$$\begin{aligned} \langle k_m, L' = 1 \pm 1 | H | k_n, L = 1 \pm 1 \rangle \\ = \begin{pmatrix} \frac{\hbar^2 k_n^{(0)2}}{2m_r} \delta_{mn} + V_{00}(k_m^{(0)}, k_n^{(0)}) & V_{02}(k_m^{(0)}, k_n^{(2)}) \\ V_{20}(k_m^{(2)}, k_n^{(0)}) & \frac{\hbar^2 k_n^{(2)2}}{2m_r} \delta_{mn} + V_{22}(k_m^{(2)}, k_n^{(2)}) \end{pmatrix} \end{aligned} \quad (5.4)$$

making it the discrete momentum-space deuteron wave function. Or, in the language of Chapter 4, $\psi(k_m)$ is made up of the discrete-momentum space correlations $\tilde{f}_c^{(0,1)}(k_m)$ and $\tilde{f}_t^{(0,1)}(k_m)$ calculated with the additional phenomenological potentials $\lambda^{(T,S)}$ set to zero:

$$\psi(k_m) = \begin{pmatrix} \tilde{f}_c^{(0,1)}(k_m) \\ \tilde{f}_t^{(0,1)}(k_m) \end{pmatrix}. \quad (5.5)$$

This will allow for two independent checks: the one-step Green's function Monte Carlo routine calculates the growth energy and the kinetic energy of the wave function using finite differences.

The results for the three different determinations of the kinetic energy for three different potentials are summarized in Table (5.1). The growth energy calculations

are corrected by the variance of the kinetic energy as calculated in the channels in accordance with Eq. (5.1). These calculations are done by taking 50 single Green's function Monte Carlo steps (returning to the original configuration after each step) with 4000 configurations generated from a variational Monte Carlo calculation. This procedure is repeated 20 times to generate good statistics. The growth energy results are within 1% of the values calculated in the channels.

Table 5.1: A comparison of the deuteron kinetic energy as calculated by three different methods for three different potentials. The channel calculation is as described in Eq. (5.3). The growth energy calculation is our one-step Green's function Monte Carlo calculation. The finite difference calculation is also done by the Green's function Monte Carlo code. The values in parentheses are the Monte Carlo statistical errors. Δt is $(2000 \text{ MeV})^{-1}$.

	N ³ LO	AV ₁₈	CD-Bonn
Channel T_{ke} (MeV)	14.63	19.81	15.60
Growth T_{ke} (MeV)	14.72(7) ^a	19.98(5) ^b	15.68(9) ^c
Finite difference T_{ke} (MeV)	14.65(7)	19.78(6)	15.56(8)

^a Corrected with $\frac{1}{2}\sigma_{\text{ke}}^2\Delta t$ in the amount of 0.29 MeV.

^b Corrected with $\frac{1}{2}\sigma_{\text{ke}}^2\Delta t$ in the amount of 1.09 MeV.

^c Corrected with $\frac{1}{2}\sigma_{\text{ke}}^2\Delta t$ in the amount of 0.49 MeV.

A less trivial check is to calculate the imaginary-time pair propagator for Argonne's v_{18} potential and use it in our one-step Green's function Monte Carlo code to calculate the growth energy for ${}^2\text{H}$ and ${}^4\text{He}$. As discussed in Appendix A, we must first calculate the discrete-momentum-space matrix elements of the channel potentials.

$$\tilde{v}_{nm}^{(LL')} = \sum_{ij} T_{ni}^{(L)} v_{ij}^{(LL')} T_{jm}^{(L')}, \quad (5.6)$$

where the $T_{ni}^{(L)}$ are transformation matrices (Eq. (A.38)) which numerically perform the integrals

$$\langle k_m L | v | k_n L' \rangle = \int_0^R dr r^2 \int_0^R dr' r'^2 \langle k_m L | r L \rangle \langle r L | v | r' L' \rangle \langle r' L' | k_n L' \rangle. \quad (5.7)$$

Then, we proceed as outlined in Chapter 3, to calculate the pair propagator using our diagonalization routines. We calculate a wave function for ${}^2\text{H}$ and ${}^4\text{He}$ as outlined in Chapter 4. And we calculate the one-step Green's function Monte Carlo growth energy as outlined in Chapter 4. Table (5.2) summarizes the results for ${}^2\text{H}$ and ${}^4\text{He}$ calculations. For each, we create 4000 initial configurations via a variational Monte Carlo calculation. Then, each configuration is propagated forward one step in Δt and then returned to its original configuration; this is repeated 50 times. The entire procedure, from variational calculation to the one-step Green's function Monte Carlo calculation, is repeated 20 times to generate good statistics.

A different check, which verifies the diagonalization methods we have developed for calculating the wave functions and propagators for non-local potentials, is to calculate the growth energy for the deuteron directly in the channel basis. The deuteron wave function $|\psi\rangle$ is an eigenstate of the two-body Hamiltonian.

$$e^{-Ht} |\psi\rangle = e^{-E_0 t} |\psi\rangle. \quad (5.8)$$

It is useful to write it in terms of the channels. The deuteron is a $J = 1, S = 1, T = 0$ mixture of $L = 0$ and $L = 2$ states. So, we can write this equation as

$$e^{-Ht} |\psi\rangle \rightarrow \begin{pmatrix} e^{-H^{(--)}t} & e^{-H^{(-+)}t} \\ e^{-H^{(+-)}t} & e^{-H^{(++)t}} \end{pmatrix} \begin{pmatrix} |\psi_S\rangle \\ |\psi_D\rangle \end{pmatrix}, \quad (5.9)$$

where the elements of the Hamiltonian $H^{(\pm\pm)}$ are as in Eq. (5.4). If we insert a complete set of position states and project the results onto position space we have

Table 5.2: A comparison of Green's function Monte Carlo results with experiment for AV₁₈. The propagator is calculated using our diagonalization routines. The growth energy is our one-step Green's function Monte Carlo estimate of the energy. We also include the local energy calculation for comparison. For the Monte Carlo calculations, the values in parentheses are the Monte Carlo statistical errors. For the experimental energies, the values in parentheses are the experimental uncertainties.

	² H	⁴ He
Growth E (MeV)	-2.23(3)	-23.03(7) ^a
Local E (MeV)	-2.225(1)	-21.63(5) ^a
Experiment E (MeV)	-2.224575(9) ^b	-28.296 ^c

^a Our results are in relative agreement with previous work using only the two-body interaction: -24.07(4) MeV (Pieper and Wiringa, 2001).

^b (Leun and Alderliesten, 1982)

^c (Tilley *et al.*, 1992)

the two equations

$$\begin{aligned} \int_0^R dr' r'^2 \langle r | e^{-H^{(--)} t} | r' \rangle \langle r' | \psi_S \rangle + \int_0^R dr' r'^2 \langle r | e^{-H^{(-+)} t} | r' \rangle \langle r' | \psi_D \rangle &= e^{-E_0 t} \langle r | \psi_S \rangle, \\ \int_0^R dr' r'^2 \langle r | e^{-H^{(+-)} t} | r' \rangle \langle r' | \psi_S \rangle + \int_0^R dr' r'^2 \langle r | e^{-H^{(++)} t} | r' \rangle \langle r' | \psi_D \rangle &= e^{-E_0 t} \langle r | \psi_D \rangle. \end{aligned} \quad (5.10)$$

We can write the channel propagators as $\langle r | e^{-H^{(\pm\pm)} t} | r' \rangle = g^{(\pm,\pm)}(r, r')$, suppressing the imaginary time argument. Then, two independent evaluations of the growth energy are given by

$$\begin{aligned} E_0(r) &= -\frac{1}{t} \log \left\{ \frac{\int_0^R dr' r'^2 [g^{(--)}(r, r') \psi_S(r') + g^{(-+)}(r, r') \psi_D(r')]}{\psi_S(r)} \right\}, \\ E_0(r) &= -\frac{1}{t} \log \left\{ \frac{\int_0^R dr' r'^2 [g^{(+-)}(r, r') \psi_S(r') + g^{(++)}(r, r') \psi_D(r')]}{\psi_D(r)} \right\}. \end{aligned} \quad (5.11)$$

At each and (in principle every) point r , the energy should be the deuteron binding energy. Since we are working in a compact space, we are sure to evaluate the energy at points sufficiently far from the upper boundary, $r \ll R$, where the boundary conditions enforce $\psi_{S,D}(R) = 0$. Table (5.3) summarizes the results of these calculations for three different potentials. The values reported here are averages over r for $0 \leq r \ll R \approx 50$ fm.

Table 5.3: Growth energy averages as calculated in the channels according to Eq. (5.11).

AV_{18}	N^3LO	CD-Bonn	Experiment
-2.2246	-2.2246	-2.2232 ^a	-2.224575(9) ^b

^a CD-Bonn uses relativistic kinematics in the fit of the deuteron binding energy which explains the discrepancy (Machleidt, 2001).

^b (Leun and Alderliesten, 1982)

5.2 Current Status and Challenges

The quantum Monte Carlo methods as laid out in Chapter 4 and as applied in a few cases in this chapter run into some challenges when the non-local potential is included in the propagator. In particular, as discussed in Chapter 4, Green's function Monte Carlo routines typically use the free-particle propagator (a Gaussian) to sample new positions from. For non-local potentials this introduces two complications. One is that propagators for the non-local potentials used here, CD-Bonn and N^3LO , have longer tails than does a Gaussian. This means that the free-particle propagator is likely not as good a choice for an importance sampling function for non-local potentials.

Considering a toy problem with features similar to the research problem helps to illustrate the issue. 1) Consider an integral of a function which is decaying but oscillating. 2) The integral extends to infinity in principle, but can be well approximated at some finite upper limit. 3) The integral can be evaluated using Monte Carlo and importance sampling. A function with these properties is

$$f(x) = \frac{\sin(x)}{x} e^{-x}. \quad (5.12)$$

The value of the integral we seek is

$$I = \int_0^\infty dx f(x) = \frac{\pi}{4} \approx 0.7854. \quad (5.13)$$

As desired, if we replace the upper limit by $L \approx 15.0$, we still get the integral correct to one part in a billion. Now, we would like to perform this integral with Monte Carlo and importance sampling. We would like the importance sampling function to take a parameter that we can adjust to see if we can “ruin” the importance sampling by mismatching the importance sampling function to the desired integrand $f(x)$.

We can take the importance sampling function as $w(k, x) = ke^{-kx}$, where k can be adjusted. Then, our integral becomes

$$I = \int_0^L dx \frac{f(x)}{w(k, x)} w(k, x). \quad (5.14)$$

We sample from $w(k, x)$, and average $\frac{f(x)}{w(k, x)}$ to get our Monte Carlo evaluation of I . To sample from $w(k, x)$, we can use the inversion sampling technique (Hammond *et al.*, 1994). Suppose u is a random number drawn from a uniform distribution on the interval $(0, 1)$ then we can generate x drawn from $w(k, x)$ by inverting

$$1 - u = \int_0^x dx' k e^{-kx'}. \quad (5.15)$$

That is, if we generate uniform random numbers u on $(0, 1)$, then the random numbers $x = -\frac{1}{k} \log(1 - u)$ will be drawn from $w(k, x)$.

Now we can explore the parameter space. We find for $k \approx 1.4$ the variance is optimal with the result $I = 0.785(3)$, whereas, for values of $k \gtrsim 5.0$, we find $I = 0.812 \pm 0.795$. That is, the variance is as large as the average. The importance sampling function works best when the ratio $\frac{f(x)}{w(x)}$ that we average is as constant as possible. Compare Fig. (5.1) to Fig. (5.2), where we plot the ratio f/w for the two values of k in the ranges mentioned above. The majority of the integral I comes from the region $0 \leq x \leq 2$. Comparing the two ratios over this region, we see that for $k = 1.4$, the ratio certainly varies, but only on the order of $\mathcal{O}(10^{-1})$. For $k = 6.0$, however, the ratio varies from 1 to 10000.

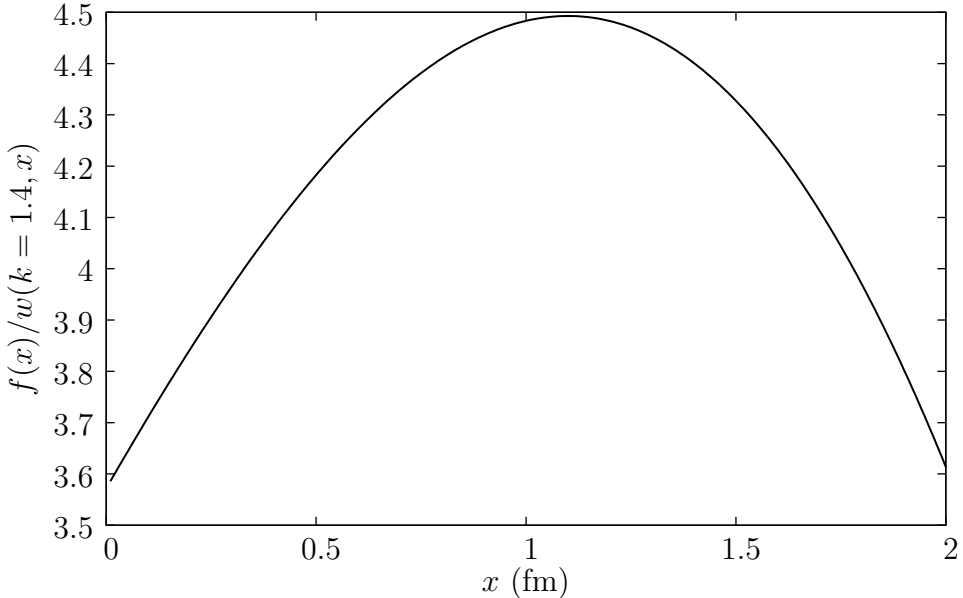


Figure 5.1: The ratio f/w for $k = 1.4$ in the region that contributes 98% of the integral: $0 \leq x \leq 2$.

Choosing $k = 6.0$ clearly is a poor choice for an importance sampling function, and this is akin to the choice of the free-particle propagator as an importance sampling function for the non-local potentials. A different choice will have to be made. Possibilities include the central part of the propagator — the trace over spins and isospins

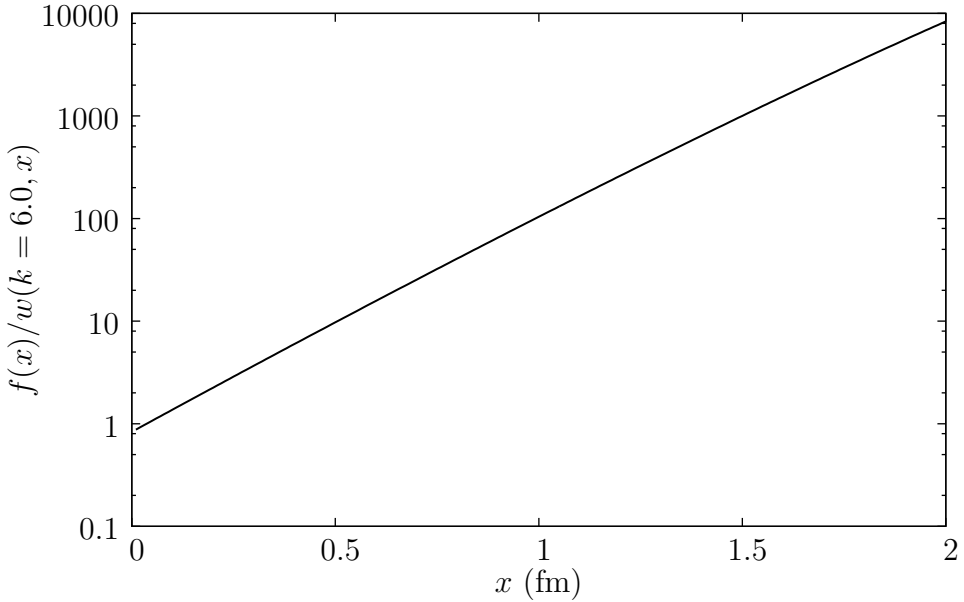


Figure 5.2: The ratio f/w for $k = 6.0$ in the region that contributes 98% of the integral: $0 \leq x \leq 2$.

(although this is complicated by the fact that this function is not positive-definite for non-local potentials) — or a free-particle propagator but evaluated at a later imaginary time, so that the tails of the non-local propagator and the later-imaginary-time free-particle propagator match better.

Even if the variance were not a problem, the second reason that the standard choice of the free-particle propagator for the importance sampling function is inadequate is that non-local potentials are not “local”. That is, for a local potential like Argonne’s v_{18} , it has proved sufficient to sample the space for a given pair of nucleons roughly with ~ 1 fm of the original separation of the pair. However, perhaps not surprisingly, this does not appear to hold true for the non-local potentials under consideration here. We provide two examples to clarify.

The first example is provided by the Figs. (5.3)–(5.5), which plot the imaginary-time propagators for Argonne’s v_{18} , the CD-Bonn potential, and the N³LO potential

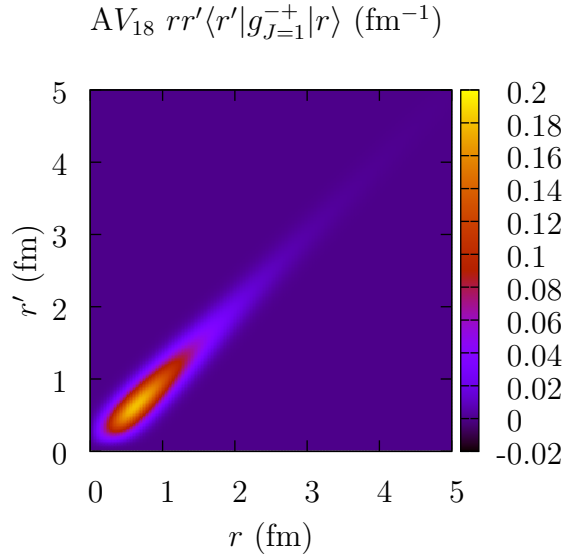


Figure 5.3: The AV_{18} channel propagator $\langle r'L'JS|e^{-Ht}|rLJS\rangle$ with $L' = 0$, $L = 0$, $J = 1$, $S = 1$, and $t = (2000 \text{ MeV})^{-1}$.

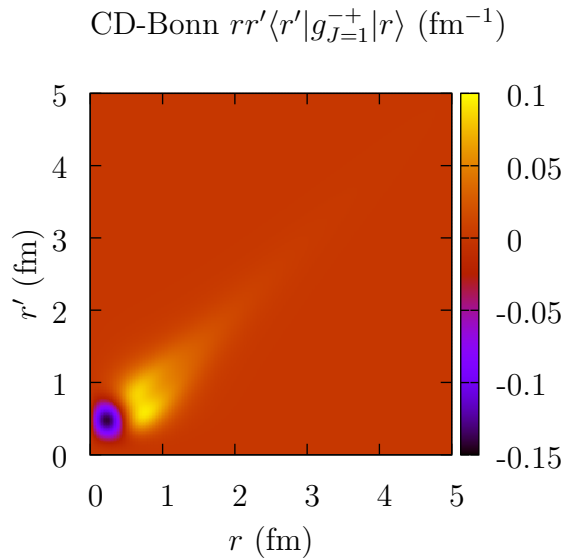


Figure 5.4: The CD-Bonn channel propagator $\langle r'L'JS|e^{-Ht}|rLJS\rangle$ with $L' = 0$, $L = 0$, $J = 1$, $S = 1$, and $t = (2000 \text{ MeV})^{-1}$.

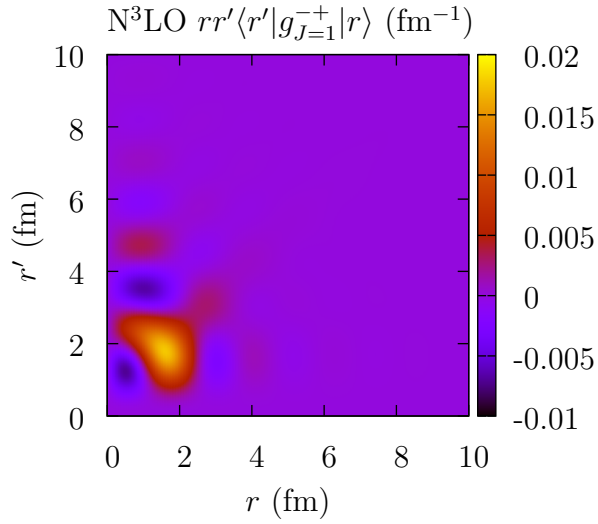


Figure 5.5: The N^3LO channel propagator $\langle r'L'JS|e^{-Ht}|rLJS\rangle$ with $L' = 0$, $L = 0$, $J = 1$, $S = 1$, and $t = (2000 \text{ MeV})^{-1}$.

in the deuteron channel where $J = 1$, $L = 2$, $L' = 0$, and $t = (2000 \text{ MeV})^{-1}$. The propagators are scaled by the product of the initial and final relative separations rr' and are plotted as functions of r and r' . For AV_{18} , the propagator is nearly diagonal: all of the contributions from the propagator in this channel come from within ~ 1 fm of the initial separation r . For CD-Bonn this is still mostly true, although the propagator is a bit wider and as we expect from the non-local nature of the potential, the propagator fluctuates between positive and negative values. For N^3LO , the propagator shows non-trivial contributions may come from as far as $\sim 4 - 6$ fm from the initial separation, and (likely due to the choice of regulator used in N^3LO — see Chapter 2 for a discussion) the propagator oscillates dramatically.

The second example comes from reconsidering our growth energy calculation of the deuteron in the channels Eq. (5.11). Since we are investigating what values of the separation contribute to the binding energy, that is, how non-local the non-local

potentials are, we instead carry out the integrations in the channels over a finite range Δ . This defines two (now distinct) “energies”, which in the limit of large Δ are identically the deuteron binding energy.

$$E_0^{(S)}(r, \Delta) = -\frac{1}{t} \log \left\{ \frac{\int_{r-\Delta}^{r+\Delta} dr' r'^2 [g^{(--)}(r, r') \psi_S(r') + g^{(-+)}(r, r') \psi_D(r')]}{\psi_S(r)} \right\}; \quad (5.16)$$

$$E_0^{(D)}(r, \Delta) = -\frac{1}{t} \log \left\{ \frac{\int_{r-\Delta}^{r+\Delta} dr' r'^2 [g^{(+-)}(r, r') \psi_S(r') + g^{(++)}(r, r') \psi_D(r')]}{\psi_D(r)} \right\}.$$

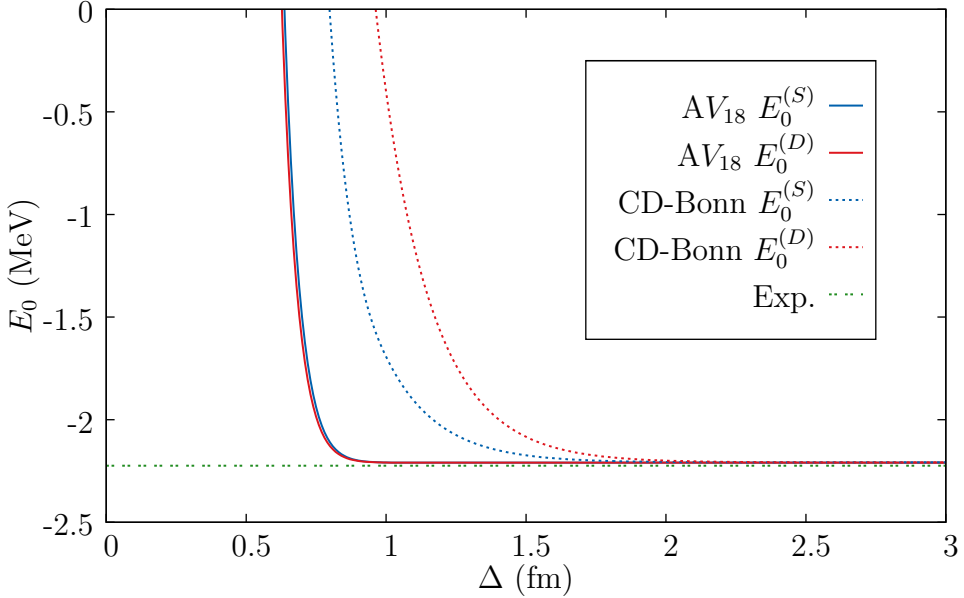


Figure 5.6: The S - and D -wave energies of Eq. (5.16) for an initial separation of $r = 1.0$ fm as a function of Δ for AV₁₈ and CD-Bonn.

Fig. (5.6) and Fig. (5.7) plot these S - and D -wave energies as a function of the integration range Δ for an initial separation of $r = 1.0$ fm. What we see is further clear indications that the local Argonne potential receives much of its binding energy from regions within ~ 1.0 fm from the initial separation. The non-local CD-Bonn potential needs to be integrated out to ~ 2.0 fm at this initial separation to get a good value of the binding energy, while the non-local N³LO potential appears to

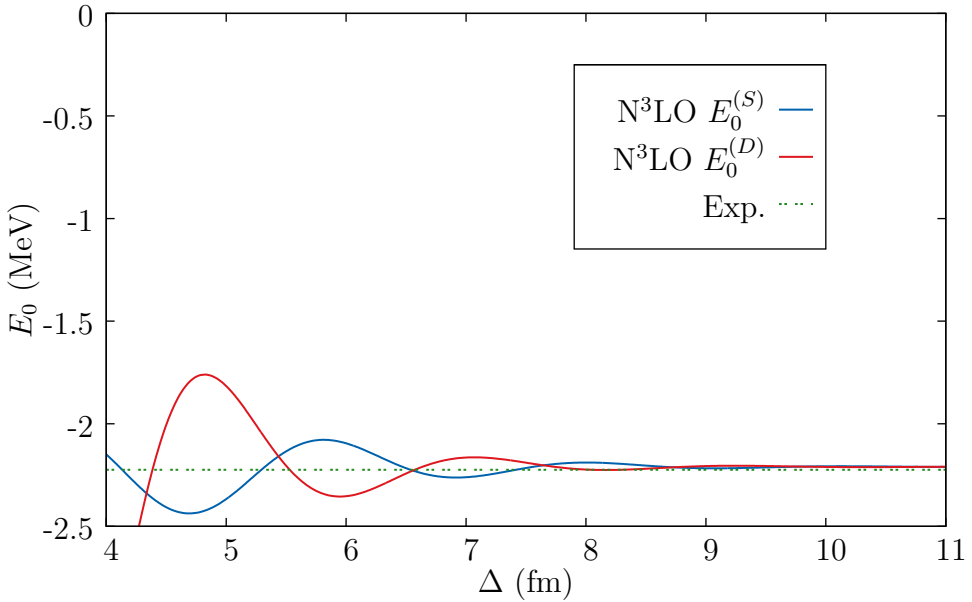


Figure 5.7: The S - and D -wave energies of Eq. (5.16) for an initial separation of $r = 1.0$ fm as a function of Δ for $N^3\text{LO}$.

need integrated out to ~ 8 or 9 fm before good convergence is reached. The dashed horizontal line is the experimental value $E_0 = -2.224575(9)$ of Leun and Alderliesten (1982).

These challenges are in the process of being addressed by finding a better importance sampling function for the non-local potentials. It is worth pointing out, that in the case of $N^3\text{LO}$, if the Monte Carlo sampling for larger nuclei is required to reach out to 8 or 9 fm, other problems may develop since large propagations for local potentials are found to give high variance. At least some of the non-locality of $N^3\text{LO}$ comes from the choice of the regulator used in the construction of the potential. A refitting of the potential with a better choice of the regulator may be called for as we continue to investigate further.

Chapter 6

CONCLUSION

6.1 Summary

Nuclear structure calculations form an important part of the goal of a complete understanding of atomic nuclei. Nuclear structure calculations can have significant impact on questions about the origin of matter, how complex phenomena emerge from underlying principles, the nature of the fundamental force between nucleons, and how nuclear physics can be used to benefit society. In this thesis, we have pushed the science of nuclear structure calculations forward by demonstrating the need and the means for including non-local potentials (some of which are derived from chiral perturbation theory and so make a more direct connection to QCD than has been possible before) in quantum Monte Carlo calculations of nuclei.

The most challenging hurdle to overcome is the calculation of the imaginary time pair propagator for non-local potentials, which was not possible using previous methods. In Chapter 3 we have presented a method for calculating this propagator which is highly accurate and general enough to handle both local and non-local potentials with a comparable computational cost to previous methods. In the process, we have demonstrated universality in imaginary-time propagators for different potentials, making a connection with research into universal low-energy nuclear potentials such as those calculated in the $V_{\text{low } k}$ and similarity renormalization group approaches. We have shown that while similar results are obtained using our long-imaginary time limit, it is not trivially related to the similarity renormalization group flow equations. This may help in understanding the flow equations themselves or suggest new gen-

erators of the flow. Because similarity renormalization group potentials and $V_{\text{low } k}$ potentials are also non-local, we have opened up the possibility of quantum Monte Carlo calculations with such renormalized potentials which would also not have been possible before this work.

In Chapter 4 we have demonstrated how our method of diagonalization can be used to generate correlations from non-local potentials which are necessary to calculate good trial wave functions used in Monte Carlo calculations. We present the correlations calculated by this method for three different potentials and compare and contrast them. We have discussed what changes are needed in the variational and Green's function Monte Carlo routines themselves to accommodate non-local potentials and have proposed an intermediate method — the one-step Green's function Monte Carlo method — to estimate the ground state energy of a nucleus with the growth energy.

In Chapter 5 we have presented various qualitative and quantitative checks on our methods including using the growth energy estimate of a one-step Green's function Monte Carlo calculation to calculate the kinetic energy of the deuteron for three different two-body potentials and compared it to different methods of obtaining the kinetic energy. We have used the one-step Green's function Monte Carlo calculation and our diagonalization method to obtain the pair propagator to estimate the ground-state energy for ${}^2\text{H}$ and ${}^4\text{He}$ using the AV₁₈ interaction. In Chapter 5 we have also laid out the challenges that remain in working with non-local potentials and quantum Monte Carlo.

Throughout, we have attempted to present evidence that the choice of regulator used in the N³LO in chiral perturbation theory potential of Entem and Machleidt (2003) has unintended consequences for real-space nuclear structure methods like quantum Monte Carlo. In Chapter 2 we propose an alternative regulator that still

meets the desired qualifications for momentum space, but likely will have significantly less impact on real-space quantities where the Fourier transform of the regulator appears. Evidence for this behavior is seen in the ringing central propagators of Chapter 3, the ringing correlations of Chapter 4, and in the integration of the deuteron in the channel basis in Chapter 5.

6.2 Outlook

Quantum Monte Carlo calculations of light nuclei with non-local potentials are now a real possibility, suggesting many avenues of further research. Further modifications of the methods to calculate the local energy (a better estimate of the ground-state energy) and other operators would be useful and would allow for comparative studies of quantum Monte Carlo with other nuclear structure methods such as the no-core shell model and coupled-cluster techniques using identical potentials. This would also allow for comparative studies of potentials. One could pursue precision calculations of light nuclei with Argonne’s v_{18} plus a phenomenological three-body potential such as the Illinois II potential compared to the same calculations using the chiral N³LO two-body and chiral N²LO three-body interactions.

Auxiliary field diffusion Monte Carlo is a method that samples the spin-isospin states instead of explicitly summing them and so can calculate neutron matter for larger numbers of neutrons than Green’s function Monte Carlo can. Such calculations can help constrain the nuclear equation of state used in astrophysical models and simulations. Currently such calculations use Argonne’s v_{18} interaction for the two-body potential and either a phenomenological three-body potential or the chiral three-body potential. Therefore, a related line of research would be to adapt our methods to auxiliary field diffusion Monte Carlo. This would allow for a fully chiral calculation

of neutron matter, which may help constrain the equation of state of nuclear matter, or may give some insight into the chiral expansion and its convergence.

Light nuclear reaction calculations have been carried out as a pseudo-bound state problem using Green's function Monte Carlo and the standard phenomenological two- and three-body potentials. These calculations demonstrated clear distinctions between different phenomenological three-body potentials. With the methods we have developed here, fully consistent chiral potentials could be used in such scattering calculations, which could help verify or test the chiral expansion.

An interesting project that suggests itself from our work in this thesis would be a collaboration to refit the chiral two-body N³LO potential using either the alternative regulator we propose in Chapter 2, or something similar which has less effect on real-space behavior of various quantities computed from the potential. This should be able to be done in a way that leaves the desired properties in momentum space intact or improves upon them.

Another idea touched upon in Chapter 3 and this conclusion is to consider the relationship between the long-imaginary time consistency of the pair propagators calculated with different phase-shift equivalent potentials and renormalization group methods such as the similarity renormalization group or $V_{\text{low } k}$. Such a study could try to make a more concrete connection between the two methods or directly attempt to use a renormalized potential in a Green's function Monte Carlo calculation. This is unexplored territory since all such renormalized potentials are non-local. We have argued that the limit in which a renormalized potential is valid may be the same as the long imaginary-time limit, which, at least for a local potential such Argonne's v_{18} , spoils the pair-product approximation typically used in Green's function Monte Carlo. However, it is also true that non-local potentials may tolerate a larger time step than do local potentials, in which case, this idea may succeed.

This is a very exciting time in nuclear physics. The possibility of chiral perturbation theory providing a bridge between QCD and low-energy nuclear structure calculations using quantum Monte Carlo is now nearly a reality. Our work takes the first quantitative steps in this direction and provides a fertile grounds for future investigations.

REFERENCES

- Arriaga, A., V. R. Pandharipande and R. B. Wiringa, “Three-body correlations in few-body nuclei”, Phys. Rev. C **52**, 2362–2368, URL <http://link.aps.org/doi/10.1103/PhysRevC.52.2362> (1995).
- Barnea, N., W. Leidemann and G. Orlandini, “State dependent effective interaction for the hyperspherical formalism”, Phys. Rev. C **61**, 054001, URL <http://link.aps.org/doi/10.1103/PhysRevC.61.054001> (2000).
- Barnea, N., W. Leidemann and G. Orlandini, “State-dependent effective interaction for the hyperspherical formalism with non-central forces”, Nuclear Physics A **693**, 3-4, 565 – 578, URL <http://www.sciencedirect.com/science/article/pii/S0375947401007941> (2001).
- Bergervoet, J. R., P. C. van Campen, R. A. M. Klomp, J.-L. de Kok, T. A. Rijken, V. G. J. Stoks and J. J. de Swart, “Phase shift analysis of all proton-proton scattering data below $T_{\text{lab}}=350$ MeV”, Phys. Rev. C **41**, 1435–1452, URL <http://link.aps.org/doi/10.1103/PhysRevC.41.1435> (1990).
- Bishop, D. M. and L. M. Cheung, “Quadrupole moment of the deuteron from a precise calculation of the electric field gradient in D_2 ”, Phys. Rev. A **20**, 381–384, URL <http://link.aps.org/doi/10.1103/PhysRevA.20.381> (1979).
- Blankenbecler, R. and R. Sugar, “Linear integral equations for relativistic multichannel scattering”, Phys. Rev. **142**, 1051–1059, URL <http://link.aps.org/doi/10.1103/PhysRev.142.1051> (1966).
- Bogner, S., R. Furnstahl and R. Perry, “Similarity Renormalization Group for Nucleon-Nucleon Interactions”, Phys. Rev. **C75**, 061001 (2007).
- Bogner, S., T. Kuo, A. Schwenk, D. Entem and R. Machleidt, “Towards a model-independent low momentum nucleon-nucleon interaction”, Physics Letters B **576**, 3-4, 265 – 272, URL <http://www.sciencedirect.com/science/article/pii/S0370269303015594> (2003).
- Carlson, J., “Green’s function Monte Carlo study of light nuclei”, Phys. Rev. C **36**, 5, 2026–2033 (1987).
- Carlson, J., “Alpha particle structure”, Phys. Rev. C **38**, 1879–1885, URL <http://link.aps.org/doi/10.1103/PhysRevC.38.1879> (1988).
- Ceperley, D. M., “Path integrals in the theory of condensed helium”, Rev. Mod. Phys. **67**, 279–355, URL <http://link.aps.org/doi/10.1103/RevModPhys.67.279> (1995).
- Ceperley, D. M. and B. J. Alder, “Ground state of the electron gas by a stochastic method”, Phys. Rev. Lett. **45**, 566–569, URL <http://link.aps.org/doi/10.1103/PhysRevLett.45.566> (1980).

- Coester, F., "Bound states of a many-particle system", Nuclear Physics **7**, 0, 421 – 424, URL <http://www.sciencedirect.com/science/article/pii/0029558258902803> (1958).
- Coester, F. and H. Kümmel, "Short-range correlations in nuclear wave functions", Nuclear Physics **17**, 0, 477 – 485, URL <http://www.sciencedirect.com/science/article/pii/0029558260901401> (1960).
- Courant, R. and D. Hilbert, *Methods of Mathematical Physics*, vol. I, chap. V, pp. 291 – 295 (Interscience Publishers, Inc. a division of John Wiley & Sons, 1965), first edn.
- Crawford, T. D. and H. F. Schaefer III, *An Introduction to Coupled Cluster Theory for Computational Chemists*, vol. 14 of *Reviews in Computational Chemistry*, chap. 2, pp. 33–125 (Wiley-VCH, Inc., NY, 2000).
- de la Ripelle, M. F., "The potential harmonic expansion method", Annals of Physics **147**, 2, 281 – 320, URL <http://www.sciencedirect.com/science/article/pii/0003491683902129> (1983).
- Dean, D. J. and M. Hjorth-Jensen, "Coupled-cluster approach to nuclear physics", Phys. Rev. C **69**, 054320, URL <http://link.aps.org/doi/10.1103/PhysRevC.69.054320> (2004).
- Entem, D. and R. Machleidt, "Accurate nucleon-nucleon potential based upon chiral perturbation theory", Physics Letters B **524**, 1-2, 93 – 98, URL <http://www.sciencedirect.com/science/article/pii/S0370269301013636> (2002a).
- Entem, D. R. and R. Machleidt, "Chiral 2π exchange at fourth order and peripheral nn scattering", Phys. Rev. C **66**, 014002, URL <http://link.aps.org/doi/10.1103/PhysRevC.66.014002> (2002b).
- Entem, D. R. and R. Machleidt, "Accurate charge-dependent nucleon-nucleon potential at fourth order of chiral perturbation theory", Phys. Rev. C **68**, 041001, URL <http://link.aps.org/doi/10.1103/PhysRevC.68.041001> (2003).
- Ericson, T. and M. Rosa-Clot, "The deuteron asymptotic D-state as a probe of the nucleon-nucleon force", Nuclear Physics A **405**, 3, 497 – 533, URL <http://www.sciencedirect.com/science/article/pii/037594748390516X> (1983).
- Fettes, N., U. Meißner, M. Mojžiš and S. Steininger, "The chiral effective pion-nucleon Lagrangian of order p^4 ", Annals of Physics **283**, 2, 273 – 307, URL <http://www.sciencedirect.com/science/article/pii/S0003491600960597> (2000).
- Fettes, N., U. Meißner, M. Mojžiš and S. Steininger, "The chiral effective pion-nucleon Lagrangian of order p^4 : Volume 283, number 2 (2000), pages 273 - 307", Annals of Physics **288**, 1, 249 – 250, URL <http://www.sciencedirect.com/science/article/pii/S0003491601961342> (2001).
- Feynman, R. P. and A. R. Hibbs, *Quantum Mechanics and Path Integrals*, chap. 3, pp. 62 – 73 (McGraw-Hill Book Company, 1965).

- Forssén, C., J. P. Vary, E. Caurier and P. Navrátil, “Converging sequences in the *ab initio* no-core shell model”, Phys. Rev. C **77**, 024301, URL <http://link.aps.org/doi/10.1103/PhysRevC.77.024301> (2008).
- Friar, J. L., “Measurability of the deuteron D state probability”, Phys. Rev. C **20**, 325–330, URL <http://link.aps.org/doi/10.1103/PhysRevC.20.325> (1979).
- Garçon, M. and J. W. V. Orden, “The deuteron: Structure and form factors”, in “Advances in Nuclear Physics”, edited by J. W. Negele and E. W. Vogt, no. 26, pp. 293 – 378 (Kluwer Academic Publishers, 2001).
- Glöckle, W. and H. Kamada, “Alpha-particle binding energies for realistic nucleon-nucleon interactions”, Phys. Rev. Lett. **71**, 971–974, URL <http://link.aps.org/doi/10.1103/PhysRevLett.71.971> (1993).
- Gray, A., G. B. Mathews and T. M. MacRobert, *A Treatise on Bessel functions and their applications to physics*, chap. VI, pp. 69 – 71 (Macmillan and Co. Limited, 1952), second edn.
- Hagen, G., T. Papenbrock, D. J. Dean and M. Hjorth-Jensen, “Medium-mass nuclei from chiral nucleon-nucleon interactions”, Phys. Rev. Lett. **101**, 092502, URL <http://link.aps.org/doi/10.1103/PhysRevLett.101.092502> (2008).
- Hammond, B. L., J. W. A. Lester and P. J. Reynolds, *Monte Carlo Methods in Ab Initio Quantum Chemistry*, vol. 1 of *World Scientific Lecture and Course Notes in Chemistry* (World Scientific, 1994).
- Hastings, W. K., “Monte Carlo sampling methods using Markov chains and their applications”, Biometrika **57**, 1, pp. 97–109, URL <http://www.jstor.org/stable/2334940> (1970).
- Heisenberg, J. H. and B. Mihaila, “Ground state correlations and mean field in ^{16}O ”, Phys. Rev. C **59**, 1440–1448, URL <http://link.aps.org/doi/10.1103/PhysRevC.59.1440> (1999).
- Hiyama, E., M. Kamimura, K. Miyazaki and T. Motoba, “ γ transitions in $A = 7$ hypernuclei and a possible derivation of hypernuclear size”, Phys. Rev. C **59**, 2351–2360, URL <http://link.aps.org/doi/10.1103/PhysRevC.59.2351> (1999).
- Hiyama, E., M. Kamimura, T. Motoba, T. Yamada and Y. Yamamoto, “ ΛN spin-orbit splittings in $^9\Lambda\text{Be}$ and $^{13}\Lambda\text{C}$ studied with one-boson-exchange ΛN interactions”, Phys. Rev. Lett. **85**, 270–273, URL <http://link.aps.org/doi/10.1103/PhysRevLett.85.270> (2000).
- Jastrow, R., “Many-body problem with strong forces”, Phys. Rev. **98**, 1479–1484, URL <http://link.aps.org/doi/10.1103/PhysRev.98.1479> (1955).
- Jenkins, E. and A. V. Manohar, “Baryon chiral perturbation theory using a heavy fermion Lagrangian”, Physics Letters B **255**, 4, 558 – 562, URL <http://www.sciencedirect.com/science/article/pii/037026939190266S> (1991).

- Kamada, H. and W. Glöckle, “Solutions of the Yakubovsky equations for four-body model systems”, Nuclear Physics A **548**, 2, 205 – 226, URL <http://www.sciencedirect.com/science/article/pii/0375947492900099> (1992).
- Kamada, H., A. Nogga, W. Glöckle, E. Hiyama, M. Kamimura, K. Varga, Y. Suzuki, M. Viviani, A. Kievsky, S. Rosati, J. Carlson, S. C. Pieper, R. B. Wiringa, P. Navrátil, B. R. Barrett, N. Barnea, W. Leidemann and G. Orlandini, “Benchmark test calculation of a four-nucleon bound state”, Phys. Rev. C **64**, 044001, URL <http://link.aps.org/doi/10.1103/PhysRevC.64.044001> (2001).
- Kameyama, H., M. Kamimura and Y. Fukushima, “Coupled-rearrangement-channel Gaussian-basis variational method for trinucleon bound states”, Phys. Rev. C **40**, 974–987, URL <http://link.aps.org/doi/10.1103/PhysRevC.40.974> (1989).
- Kamimura, M., “Nonadiabatic coupled-rearrangement-channel approach to muonic molecules”, Phys. Rev. A **38**, 621–624, URL <http://link.aps.org/doi/10.1103/PhysRevA.38.621> (1988).
- Kamimura, M. and H. Kameyama, “Coupled rearrangement channel calculations of muonic molecules and $A = 3$ nuclei”, Nuclear Physics A **508**, 0, 17 – 28, URL <http://www.sciencedirect.com/science/article/pii/037594749090459Y> (1990).
- Kievsky, A., L. E. Marcucci, S. Rosati and M. Viviani, “High-precision calculation of the triton ground state within the hyperspherical-harmonics method”, Few-Body Systems **22**, 1–10, URL <http://dx.doi.org/10.1007/s006010050049> (1997).
- Klemm, A. D. and R. G. Storer, “The structure of quantum fluids: Helium and Neon”, Aust. J. Phys. **26**, 1, 43, URL <http://www.publish.csiro.au/paper/PH730043> (1973).
- Koonin, S. and D. Meredith, *Computational Physics: Fortran Version* (Westview Press, 1998).
- Kowalski, K., D. J. Dean, M. Hjorth-Jensen, T. Papenbrock and P. Piecuch, “Coupled cluster calculations of ground and excited states of nuclei”, Phys. Rev. Lett. **92**, 132501, URL <http://link.aps.org/doi/10.1103/PhysRevLett.92.132501> (2004).
- Leforestier, C., R. Bisseling, C. Cerjan, M. Feit, R. Friesner, A. Guldberg, A. Hammerich, G. Jolicard, W. Karrlein, H.-D. Meyer, N. Lipkin, O. Roncero and R. Kosloff, “A comparison of different propagation schemes for the time dependent Schrödinger equation”, J. of Comp. Phys. **94**, 1, 59 – 80, URL <http://www.sciencedirect.com/science/article/pii/002199919190137A> (1991).
- Leun, C. V. D. and C. Alderliesten, “The deuteron binding energy”, Nuclear Physics A **380**, 2, 261 – 269, URL <http://www.sciencedirect.com/science/article/pii/0375947482901051> (1982).
- Lomnitz-Adler, J., V. Pandharipande and R. Smith, “Monte Carlo calculations of Triton and ${}^4\text{He}$ nuclei with the Reid potential”, Nuclear Physics A **361**, 2, 399 – 411, URL <http://www.sciencedirect.com/science/article/pii/0375947481906424> (1981).

- Lovato, A., O. Benhar, S. Fantoni and K. E. Schmidt, “Comparative study of three-nucleon potentials in nuclear matter”, Phys. Rev. C **85**, 024003, URL <http://link.aps.org/doi/10.1103/PhysRevC.85.024003> (2012).
- Lynn, J. E. and K. E. Schmidt, “Real-space imaginary-time propagators for non-local nucleon-nucleon potentials”, Phys. Rev. C **86**, 014324, URL <http://link.aps.org/doi/10.1103/PhysRevC.86.014324> (2012).
- Machleidt, R., “The meson theory of nuclear forces and nuclear structure”, in “Advances in Nuclear Physics”, edited by J. W. Negele and E. W. Vogt, no. 19, pp. 189 – 380 (Plenum Press, 1989).
- Machleidt, R., “High-precision, charge-dependent Bonn nucleon-nucleon potential”, Phys. Rev. C **63**, 024001, URL <http://link.aps.org/doi/10.1103/PhysRevC.63.024001> (2001).
- Metropolis, N., A. W. Rosenbluth, M. N. Rosenbluth, A. H. Teller and E. Teller, “Equation of state calculations by fast computing machines”, The Journal of Chemical Physics **21**, 6, 1087–1092, URL <http://link.aip.org/link/?JCP/21/1087/1> (1953).
- Mihaila, B. and J. H. Heisenberg, “Center-of-mass corrections reexamined: A many-body expansion approach”, Phys. Rev. C **60**, 054303, URL <http://link.aps.org/doi/10.1103/PhysRevC.60.054303> (1999).
- Mihaila, B. and J. H. Heisenberg, “Ground state correlations and mean field in ^{16}O . II. Effects of a three-nucleon interaction”, Phys. Rev. C **61**, 054309, URL <http://link.aps.org/doi/10.1103/PhysRevC.61.054309> (2000a).
- Mihaila, B. and J. H. Heisenberg, “Microscopic calculation of the inclusive electron scattering structure function in ^{16}O ”, Phys. Rev. Lett. **84**, 1403–1406, URL <http://link.aps.org/doi/10.1103/PhysRevLett.84.1403> (2000b).
- Moler, C. and C. Van Loan, “Nineteen dubious ways to compute the exponential of a matrix, twenty-five years later”, SIAM Review **45**, 1, 3–49, URL <http://epubs.siam.org/doi/abs/10.1137/S00361445024180> (2003).
- Navrátil, P., “Local three-nucleon interaction from chiral effective field theory”, Few-Body Systems **41**, 117–140, URL <http://dx.doi.org/10.1007/s00601-007-0193-3> (2007).
- Navrátil, P. and B. R. Barrett, “Four-nucleon shell-model calculations in a Faddeev-like approach”, Phys. Rev. C **59**, 1906–1918, URL <http://link.aps.org/doi/10.1103/PhysRevC.59.1906> (1999).
- Navrátil, P., G. P. Kamuntavičius and B. R. Barrett, “Few-nucleon systems in a translationally invariant harmonic oscillator basis”, Phys. Rev. C **61**, 044001, URL <http://link.aps.org/doi/10.1103/PhysRevC.61.044001> (2000a).

- Navrátil, P., S. Quaglioni, I. Stetcu and B. R. Barrett, “Recent developments in no-core shell-model calculations”, Journal of Physics G: Nuclear and Particle Physics **36**, 8, 083101, URL <http://stacks.iop.org/0954-3899/36/i=8/a=083101> (2009).
- Navrátil, P., J. P. Vary and B. R. Barrett, “Large-basis *ab initio* no-core shell model and its application to ^{12}C ”, Phys. Rev. C **62**, 054311, URL <http://link.aps.org/doi/10.1103/PhysRevC.62.054311> (2000b).
- Navrátil, P., J. P. Vary and B. R. Barrett, “Properties of ^{12}C in the *Ab Initio* nuclear shell model”, Phys. Rev. Lett. **84**, 5728–5731, URL <http://link.aps.org/doi/10.1103/PhysRevLett.84.5728> (2000c).
- Nogga, A., H. Kamada and W. Glöckle, “Modern nuclear force predictions for the α particle”, Phys. Rev. Lett. **85**, 944–947, URL <http://link.aps.org/doi/10.1103/PhysRevLett.85.944> (2000).
- Ôkubo, S., “Diagonalization of Hamiltonian and Tamm-Dancoff equation”, Progress of Theoretical Physics **12**, 5, 603–622, URL <http://ptp.ipap.jp/link?PTP/12/603/> (1954).
- Pieper, S. C., “Quantum Monte Carlo calculations of light nuclei”, Nuclear Physics A **751**, 0, 516 – 532, URL <http://www.sciencedirect.com/science/article/pii/S0375947405001247>, Proceedings of the 22nd International Nuclear Physics Conference (Part 1) (2005).
- Pieper, S. C., V. R. Pandharipande, R. B. Wiringa and J. Carlson, “Realistic models of pion-exchange three-nucleon interactions”, Phys. Rev. C **64**, 014001, URL <http://link.aps.org/doi/10.1103/PhysRevC.64.014001> (2001).
- Pieper, S. C., K. Varga and R. B. Wiringa, “Quantum Monte Carlo calculations of $a = 9, 10$ nuclei”, Phys. Rev. C **66**, 044310, URL <http://link.aps.org/doi/10.1103/PhysRevC.66.044310> (2002).
- Pieper, S. C. and R. B. Wiringa, “Quantum Monte Carlo calculations of light nuclei”, Annual Review of Nuclear and Particle Science **51**, 1, 53–90, URL <http://www.annualreviews.org/doi/abs/10.1146/annurev.nucl.51.101701.132506> (2001).
- Pudliner, B. S., V. R. Pandharipande, J. Carlson, S. C. Pieper and R. B. Wiringa, “Quantum Monte Carlo calculations of nuclei with $A \lesssim 7$ ”, Phys. Rev. C **56**, 1720–1750, URL <http://link.aps.org/doi/10.1103/PhysRevC.56.1720> (1997).
- Salpeter, E. E. and H. A. Bethe, “A relativistic equation for bound-state problems”, Phys. Rev. **84**, 1232–1242, URL <http://link.aps.org/doi/10.1103/PhysRev.84.1232> (1951).
- Schmidt, K. E. and M. A. Lee, “High-accuracy Trotter-formula method for path integrals”, Phys. Rev. E **51**, 5495–5498, URL <http://link.aps.org/doi/10.1103/PhysRevE.51.5495> (1995).

- Stoks, V. G. J., R. A. M. Klomp, M. C. M. Rentmeester and J. J. de Swart, “Partial-wave analysis of all nucleon-nucleon scattering data below 350 mev”, Phys. Rev. C **48**, 792–815, URL <http://link.aps.org/doi/10.1103/PhysRevC.48.792> (1993).
- Suzuki, K. and S. Y. Lee, “Convergent theory for effective interaction in nuclei”, Progress of Theoretical Physics **64**, 6, 2091–2106, URL <http://ptp.ipap.jp/link?PTP/64/2091/> (1980).
- Suzuki, K. and R. Okamoto, “Degenerate perturbation theory in quantum mechanics”, Progress of Theoretical Physics **70**, 2, 439–451, URL <http://ptp.ipap.jp/link?PTP/70/439/> (1983).
- (The NP2010 Committee): The Committee on the Assessment of and Outlook for Nuclear Physics; Board on Physics and Astronomy; Division on Engineering and Physical Sciences; National Research Council, *Nuclear Physics: Exploring the Heart of Matter* (The National Academies Press, 2012), URL http://www.nap.edu/openbook.php?record_id=13438.
- Tilley, D., H. Weller and G. Hale, “Energy levels of light nuclei a = 4”, Nuclear Physics A **541**, 1, 1 – 104, URL <http://www.sciencedirect.com/science/article/pii/037594749290635W> (1992).
- Usukura, J., Y. Suzuki and K. Varga, “Stability of two- and three-dimensional excitonic complexes”, Phys. Rev. B **59**, 5652–5661, URL <http://link.aps.org/doi/10.1103/PhysRevB.59.5652> (1999).
- Usukura, J., K. Varga and Y. Suzuki, “Signature of the existence of the positronium molecule”, Phys. Rev. A **58**, 1918–1931, URL <http://link.aps.org/doi/10.1103/PhysRevA.58.1918> (1998).
- Varga, K., Y. Ohbayasi and Y. Suzuki, “Stochastic variational method with noncentral forces”, Physics Letters B **396**, 1-4, 1 – 6, URL <http://www.sciencedirect.com/science/article/pii/S0370269397000853> (1997).
- Varga, K. and Y. Suzuki, “Precise solution of few-body problems with the stochastic variational method on a correlated Gaussian basis”, Phys. Rev. C **52**, 2885–2905, URL <http://link.aps.org/doi/10.1103/PhysRevC.52.2885> (1995).
- Viviani, M., “Transformation coefficients of hyperspherical harmonic functions of an -body system”, Few-Body Systems **25**, 177–187, URL <http://dx.doi.org/10.1007/s006010050101> (1998).
- Viviani, M., A. Kievsky and S. Rosati, “Calculation of the α -particle ground state”, Few-Body Systems **18**, 25–39, URL <http://dx.doi.org/10.1007/s006010050002> (1995).
- Weinberg, S., “Phenomenological Lagrangians”, Physica A: Statistical Mechanics and its Applications **96**, 1-2, 327 – 340, URL <http://www.sciencedirect.com/science/article/pii/0378437179902231> (1979).

- Weinberg, S., “Nuclear forces from chiral Lagrangians”, Physics Letters B **251**, 2, 288 – 292, URL <http://www.sciencedirect.com/science/article/pii/0370269390909383> (1990).
- Weinberg, S., “Effective chiral Lagrangians for nucleon-pion interactions and nuclear forces”, Nuclear Physics B **363**, 1, 3 – 18, URL <http://www.sciencedirect.com/science/article/pii/055032139190231L> (1991).
- Wiringa, R. B., “Variational calculations of few-body nuclei”, Phys. Rev. C **43**, 1585–1598, URL <http://link.aps.org/doi/10.1103/PhysRevC.43.1585> (1991).
- Wiringa, R. B., S. C. Pieper, J. Carlson and V. R. Pandharipande, “Quantum Monte Carlo calculations of $A = 8$ nuclei”, Phys. Rev. C **62**, 014001, URL <http://link.aps.org/doi/10.1103/PhysRevC.62.014001> (2000).
- Wiringa, R. B., R. A. Smith and T. L. Ainsworth, “Nucleon-nucleon potentials with and without $\Delta(1232)$ degrees of freedom”, Phys. Rev. C **29**, 1207–1221, URL <http://link.aps.org/doi/10.1103/PhysRevC.29.1207> (1984).
- Wiringa, R. B., V. G. J. Stoks and R. Schiavilla, “Accurate nucleon-nucleon potential with charge-independence breaking”, Phys. Rev. C **51**, 38–51, URL <http://link.aps.org/doi/10.1103/PhysRevC.51.38> (1995).
- Yakubovsky, O., Soviet Journal of Nuclear Physics **5**, 937 (1967).
- York, R., S. Assadi, G. B. M. Doleans, T. Glasmacher, W. Hartung, M. J. Johnson, G. Machicoane, F. Marti, E. Pozdeyev, E. Tanke, X. Wu and Q. Zhao, “Status and plans for the facility for rare isotope beams at Michigan state university”, in “Proceedings of the XXV Linear Accelerator Conference (LINAC10), Tsukuba, Japan”, (2010).

APPENDIX A
EIGENFUNCTION EXPANSIONS OF VARIOUS QUANTITIES

In order to calculate the pair propagator, which we need as a basic ingredient for the Green's Function Monte Carlo method, we need to exponentiate the Hamiltonian. The details of this method are presented below. It is most straightforward to begin with a familiar example.

A.1 One-Dimensional Examples

Consider the one-dimensional time-independent Schrödinger equation for a free particle

$$\langle x|H|k\rangle = E\langle x|k\rangle \rightarrow -\frac{\hbar^2}{2m}\frac{d^2}{dx^2}\psi(x) = E\psi(x), \quad (\text{A.1})$$

where we label the eigenkets $|k\rangle$ in anticipation of the solution and we call the eigenfunctions $\psi(x) = \langle x|k\rangle$. Suppose we solve this equation on the interval $0 \leq x \leq L$. We impose the boundary conditions

$$\psi(0) = 0; \quad (\text{A.2a})$$

$$\psi(L) = 0. \quad (\text{A.2b})$$

The solution spectrum is discrete now and is given by

$$\psi_n(x) = A \sin(k_n x), \quad (\text{A.3})$$

with $k_n = \sqrt{\frac{2mE_n}{\hbar^2}} = \frac{n\pi}{L}$, n an integer, and A a normalization constant fixed by requiring $\int_0^L dx |\psi_n(x)|^2 = 1$. A choice with the overall phase real and positive is

$$\psi_n(x) = \sqrt{\frac{2}{L}} \sin(k_n x). \quad (\text{A.4})$$

These are the discrete free-particle eigenfunctions for this one-dimensional interval. It is a well-known fact that, since this is a Sturm-Liouville system, they form an orthonormal and complete set from which we can “build” any other function on the interval which obeys the same boundary conditions (Courant and Hilbert, 1965).

That is, if $f(x)$ also obeys $f(0) = 0$ and $f(L) = 0$, then we can write

$$\langle x|f\rangle = \sum_{n=1}^{\infty} \langle x|k_n\rangle \langle k_n|f\rangle = \sum_{n=1}^{\infty} c_n \psi_n(x), \quad (\text{A.5})$$

where the $c_n = \langle k_n|f\rangle$.

As an example, take a Gaussian distribution

$$f(x) = \frac{1}{\sqrt{2\pi\sigma^2}} \exp\left[-\frac{(x-a)^2}{2\sigma^2}\right], \quad (\text{A.6})$$

with $0 < a < L$. The Gaussian obeys $\lim_{x \rightarrow \pm\infty} f(x) = 0$, but, if the width, characterized by σ , is narrow enough compared with L , and a is well inside the interval, then we can say $f(0) \approx 0$ and $f(L) \approx 0$. The coefficients c_n are obtained by inserting a complete set of position states

$$\begin{aligned} c_n &= \langle k_n|f\rangle = \int_0^L dx \langle k_n|x\rangle \langle x|f\rangle \\ &= \frac{1}{\sqrt{2\pi\sigma^2}} \sqrt{\frac{2}{L}} \int_0^L dx \sin\left(\frac{n\pi x}{L}\right) \exp\left[-\frac{(x-a)^2}{2\sigma^2}\right]. \end{aligned} \quad (\text{A.7})$$

Under our assumptions about the position and width of the Gaussian, the integration limits can safely be extended to $\pm\infty$. In which case, by completing the square in the exponent and analytic continuation we find

$$c_n = \sqrt{\frac{2}{L}} \exp\left[-\frac{1}{2} \left(\frac{n\pi\sigma}{L}\right)^2\right] \sin\left(\frac{n\pi a}{L}\right). \quad (\text{A.8})$$

Therefore, we can write the eigenfunction expansion

$$f(x) = \frac{2}{L} \sum_{n=1}^{\infty} \exp\left[-\frac{1}{2} \left(\frac{n\pi\sigma}{L}\right)^2\right] \sin\left(\frac{n\pi a}{L}\right) \sin\left(\frac{n\pi x}{L}\right). \quad (\text{A.9})$$

An important feature of the expansion is that it can be truncated at some n_{\max} and

still faithfully reproduce $f(x)$ to some desired accuracy. If we assume that $\frac{2}{L}$ and the sines are all of $\mathcal{O}(1)$, and we want $f(x)$ accurate to N places, then we require

$$\exp \left[-\frac{1}{2} \left(\frac{n_{\max} \pi \sigma}{L} \right)^2 \right] < 10^{-N} \quad (\text{A.10})$$

$$\Rightarrow n_{\max} \geq \frac{L}{\pi \sigma} \sqrt{2N \log(10)}. \quad (\text{A.11})$$

For example, take (in arbitrary units) $L = 10$, $\sigma = 0.8$, $a = 5$ and $N = 8$. Then n_{\max} should be at least 24 and the root-mean-square (RMS) of the deviations between the eigenfunction expansion Eq. (A.9) truncated to $n_{\max} = 24$ and the analytic function Eq. (A.6) is $\mathcal{O}(10^{-11})$.

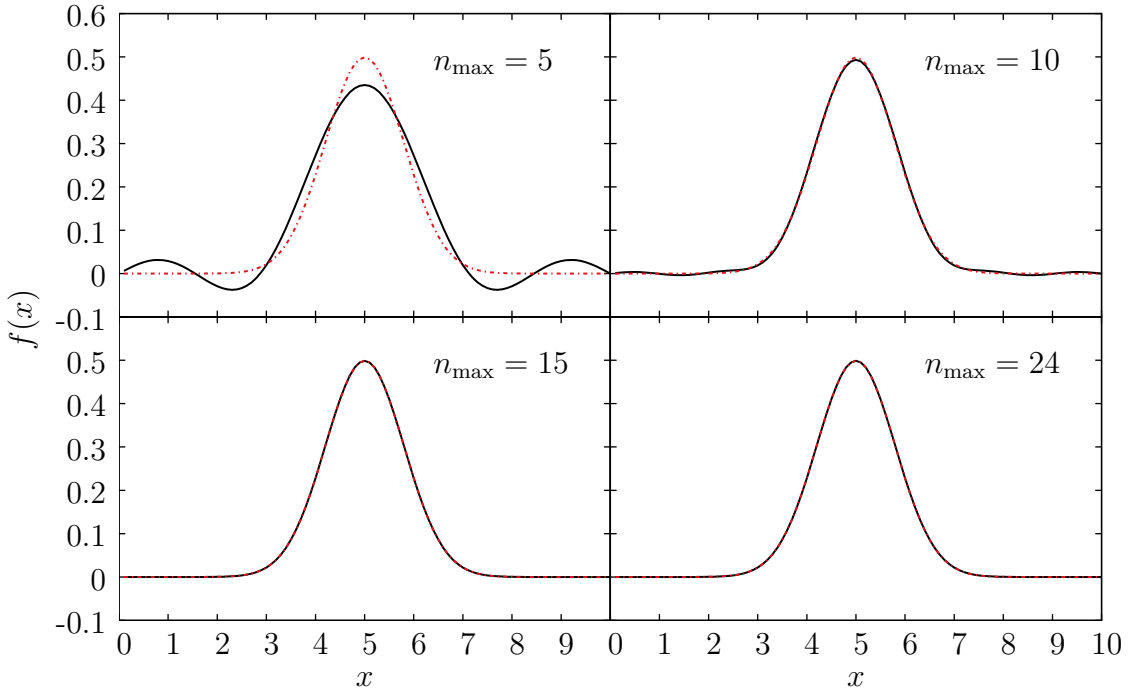


Figure A.1: The Gaussian Eq. (A.6) in red (dashed-dotted line), and the eigenfunction expansion Eq. (A.9) truncated to different values of n_{\max} in black (solid line) for comparison.

Let us consider now calculating an imaginary-time propagator for some potential $V(x)$ on this interval. We want the matrix elements $\langle x'|e^{-Ht}|x\rangle$. We can insert a complete set of discrete free-particle eigenstates on the interval

$$\langle x'|e^{-Ht}|x\rangle = \sum_{mn} \langle x'|k_m\rangle \langle k_m|e^{-Ht}|k_n\rangle \langle k_n|x\rangle. \quad (\text{A.12})$$

We must be able to write the Hamiltonian in this basis:

$$\langle k_m|H|k_n\rangle = H_{mn} = \frac{\hbar^2 k_n^2}{2m} \delta_{mn} + V(k_m, k_n). \quad (\text{A.13})$$

Then, our method consists of diagonalizing the Hamiltonian in this basis, and exponentiating:

$$\langle x'|e^{-Ht}|x\rangle = \sum_{mni} \underbrace{\langle x'|k_n\rangle}_{\substack{\text{transformation} \\ \text{matrix}}} \times \underbrace{\langle k_n|\psi_i\rangle}_{\substack{\text{eigenvector} \\ \text{momentum-space propagator}}} e^{-E_i t} \underbrace{\langle \psi_i|k_m\rangle}_{\substack{\text{eigenvector}}} \times \underbrace{\langle k_m|x\rangle}_{\substack{\text{transformation} \\ \text{matrix}}}. \quad (\text{A.14})$$

A simple non-trivial example is the harmonic-oscillator-in-a-box potential:

$$V(x) = \begin{cases} \infty, & x \leq 0 \\ \frac{1}{2}m\omega^2 x^2, & 0 < x < L \\ \infty, & x \geq L. \end{cases} \quad (\text{A.15})$$

We use a system of units commonly used in nuclear physics where $[m] = \text{MeV}$, $[x] = \text{fm}$, $[t] = (\text{MeV})^{-1}$, $[\hbar c] = \text{MeV} \cdot \text{fm}$, and $[k] = (\text{fm})^{-1}$. Then, $[\omega]$ must be in $(\text{fm})^{-1}$ so that $[V] = \text{MeV}$. If the initial position x is far from the hard walls, and the width of the propagator is not too great, then we can compare our numerical results to the analytic result for the entire real line (Feynman and Hibbs, 1965).

$$\langle x'|e^{-Ht}|x\rangle = \sqrt{\frac{m\omega}{2\pi\hbar \sinh(\hbar\omega t)}} \exp\left(-\frac{m\omega((x^2 + x'^2) \cosh(\hbar\omega t) - 2xx')}{2\hbar \sinh(\hbar\omega t)}\right). \quad (\text{A.16})$$

In order to use the method outlined in Eq. (A.14), we must express the potential in the discrete free-particle eigenbasis

$$\begin{aligned}\langle k_m | V | k_n \rangle &= \int_0^L dx \int_0^L dx' \langle k_m | x' \rangle \langle x' | V | x \rangle \langle x | k_n \rangle \\ &= \frac{m\omega^2}{L} \int_0^L dx \sin(k_m x) \sin(k_n x) x^2,\end{aligned}\tag{A.17}$$

where we have used the fact that $\langle x' | V | x \rangle \propto \delta(x - x')$. For $k_n \neq k_m$,

$$V(k_n, k_m) = (-1)^{n+m} m\omega^2 \left[\frac{1}{(k_n - k_m)^2} - \frac{1}{(k_n + k_m)^2} \right],\tag{A.18}$$

whereas for $k_n = k_m$,

$$V(k_n, k_n) = m\omega^2 \left[\frac{L^2}{6} - \frac{1}{(2k_n)^2} \right].\tag{A.19}$$

However, since we will be working with potentials which are not analytic, we really need a numerical way to do the integrals Eq. (A.17). We define transformation matrices from a set of uniformly-spaced points in real space ($\{x_i\}$ with spacing Δx) to the set of discrete free-particle eigenstates

$$T_{ni} = \sqrt{\frac{2\Delta x}{L}} \sin(k_n x_i).\tag{A.20}$$

Then, the potential in the discrete free-particle basis can be obtained by

$$V_{mn} = \sum_{ij} T_{mi} V_{ij} T_{jn}.\tag{A.21}$$

If we choose the nuclear-inspired values $m = 469.459$ MeV, $t = 0.0005$ (MeV) $^{-1}$, $L = 8$ fm, with the initial distance 1.0 fm $\lesssim x \lesssim 7.0$ fm, $\hbar = 197.3269718$ MeV · fm, and the eigenfunction expansion truncated at $n_{\max} \sim 200$, then the RMS of the deviations between our numerical result and the analytic result Eq. (A.16) is less than $\mathcal{O}(10^{-6})$. Higher-accuracy results are obtained with the initial separation deep inside the interval and can be obtained by taking larger values of L , for example.

A.2 Three-Dimensional Channel Basis

For the actual problem, we work in the channel basis as discussed in Chapter 3, where J^2 , J_z , L^2 , S^2 , S_z , T^2 and T_z are good quantum numbers, with the total spin, $\mathbf{S} = \mathbf{S}_1 + \mathbf{S}_2$, the total angular momentum $\mathbf{J} = \mathbf{L} + \mathbf{S}$, and total isospin $\mathbf{T} = \mathbf{T}_1 + \mathbf{T}_2$. The basis states are $|rJMLSTT_z\rangle$. The equivalent expression to Eq. (A.1) is the free radial time-independent Schrödinger equation in the channel basis (suppressing all quantum numbers except L and M)

$$\begin{aligned} \langle rLM|H|kLM\rangle &= E\langle rLM|kLM\rangle \\ \rightarrow -\frac{\hbar^2}{2m_r} \left[\frac{1}{r} \frac{d^2}{dr^2} r - \frac{L(L+1)}{r^2} \right] \psi_L(r) &= E\psi_L(r). \end{aligned} \quad (\text{A.22})$$

As in the one-dimensional example, we label the eigenkets $|kLM\rangle$ in anticipation of the solution, and we call the eigenfunctions $\psi_L(r) = \langle rLM|kLM\rangle$.

We solve the equation on the interval $0 \leq r \leq R$ and impose the boundary conditions that the eigenfunctions should be regular at the origin, and zero at the upper boundary.

$$\lim_{r \rightarrow 0} \psi_L(r) = \text{finite}; \quad (\text{A.23a})$$

$$\psi_L(R) = 0. \quad (\text{A.23b})$$

Then, the solution spectrum is discrete and is given by

$$\psi_{nL}(r) = A j_L(k_n r), \quad (\text{A.24})$$

with j_L a spherical Bessel function, $k_n = \sqrt{\frac{2m_r E_n}{\hbar^2}} = \frac{\beta_{nL}}{R}$, n an integer, β_{nL} the n th zero of the L th spherical Bessel function, and A , a normalization constant fixed by requiring $\int_0^R dr r^2 |\psi_{nL}(r)|^2 = 1$. The integral can be obtained by the Lommel method (Gray *et al.*, 1952).

We want the integral

$$\int_0^R dr r^2 j_L(k_n r) j_L(k_m r), \quad (\text{A.25})$$

where, ultimately, since we know that the $\{j_L(k_n r)\}$ are orthogonal, we want $m = n$. But for now, we treat them as distinct. In fact, it is useful to think of k_n as being one of the allowed k values in our compact r space, and k_m as being $k_n + \Delta k$, where we will eventually let $\Delta k \rightarrow 0$. Now we follow Lommel's method for evaluating integrals of products of Bessel functions.

We let $u = j_L(k_n r)$, and $v = j_L(k_m r)$. Then the two functions obey

$$r^2 u'' + 2ru' + (k_n^2 r^2 - L(L+1)) u = 0, \quad (\text{A.26})$$

$$r^2 v'' + 2rv' + (k_m^2 r^2 - L(L+1)) v = 0. \quad (\text{A.27})$$

Multiplying the first by v and the second by u and subtracting we find

$$r^2(u''v - uv'') + 2r(u'v - uv') = (k_m^2 - k_n^2)r^2uv. \quad (\text{A.28})$$

We can recognize the left hand side as

$$\frac{\partial}{\partial r} [r^2(u'v - uv')]. \quad (\text{A.29})$$

Thus, integrating both sides we find

$$(k_m^2 - k_n^2) \int_0^R dr r^2 uv = [r^2(u'v - uv')]_0^R. \quad (\text{A.30})$$

That is,

$$\begin{aligned} & (k_m^2 - k_n^2) \int_0^R dr r^2 j_L(k_n r) j_L(k_m r) \\ &= [r^2(k_n j'_L(k_n r) j_L(k_m r) - k_m j_L(k_n r) j'_L(k_m r))]_0^R. \end{aligned} \quad (\text{A.31})$$

The evaluations at the lower limit, 0, both vanish due to the leading r^2 , for all L and the fact that all of the j_L are finite at $r = 0$. This just leaves the upper limit

evaluations at R . But, the second of these, $-k_m j_L(k_n R) j'_L(k_m R)$ vanishes by the boundary condition we have in place that $j_L(k_n R) = 0$ if k_n is one of the allowed k values. (Note this argument does not work for the other k , k_m , since it is not quite one of the allowed values for k).

Thus, we have for $k_n \neq k_m$,

$$\int_0^R dr r^2 j_L(k_n r) j_L(k_m r) = \frac{R^2 k_n j'_L(k_n R) j_L(k_m R)}{k_m^2 - k_n^2}. \quad (\text{A.32})$$

And so,

$$\int_0^R dr r^2 j_L(k_n r)^2 = \lim_{m \rightarrow n} \frac{R^2 k_n j'_L(k_n R) j_L(k_m R)}{k_m^2 - k_n^2}. \quad (\text{A.33})$$

Rewrite the result as

$$\lim_{\Delta k \rightarrow 0} \int_0^R dr r^2 j_L(k_n r) j_L((k_n + \Delta k)r) = \lim_{\Delta k \rightarrow 0} \frac{R^2 k_n j'_L(k_n R) j_L((k_n + \Delta k)R)}{(k_n + \Delta k)^2 - k_n^2}, \quad (\text{A.34})$$

where $k_n R$ is a root of the L th spherical Bessel function. First, we recognize that the denominator can be written as $2\Delta k k_n + (\Delta k)^2$, where we can neglect the second order term in Δk since we are going to be taking the limit where $\Delta k \rightarrow 0$. We can then power series expand Bessel function $j_L((k_n + \Delta k)R)$ as

$$j_L((k_n + \Delta k)R) \approx j_L(k_n R) + j'_L(k_n R) \Delta k R + \dots \quad (\text{A.35})$$

Since the first term of this expansion is zero, and Δk can be taken small, we finally find for the complete result

$$\int_0^R dr r^2 j_L(k_n r)^2 = \frac{R^3}{2} j'_L(k_n R)^2. \quad (\text{A.36})$$

Therefore, a consistent normalization choice with the phase real and positive is

$$\psi_{nL}(r) = \sqrt{\frac{2}{R^3 j'_L(k_n R)^2}} j_L(k_n r). \quad (\text{A.37})$$

Now we have an orthonormal and complete set of functions on the interval $0 \leq r \leq R$. Unlike the one-dimensional examples presented above, (where for good convergence it was necessary that the function to be expanded go to zero at both the

origin and the upper limit) the boundary conditions are such that any function that is merely regular at the origin and is sufficiently small at $r = R$ can be expanded readily in this basis. (Other functions which do not obey these boundary conditions may of course be expanded in this basis. However, we will essentially be forcing the boundary condition upon them, which may lead to behavior near the boundary analogous to the Gibbs phenomenon of Fourier analysis. Away from the boundary, the convergence will be good. If, for example, we need to calculate a propagator for a potential which does not die off at large r , but perhaps even grows as r grows, the expansion of the potential may suffer from boundary condition effects, but if the propagator itself goes to zero at large r , the convergence in the expansion will still be good). Much like the one-dimensional examples presented above, we will have local real-space potentials (such as Argonne's v_{18} interaction) that we want to write in this discrete free-particle channel basis and so we define transformation matrices which will perform the necessary integrals numerically to take a set of evenly-spaced real-space values ($\{r_i\}$ with spacing Δr) to the discrete free-particle channel basis.

$$T_{ni}^{(L)} = \sqrt{\frac{2\Delta r r_i^2}{R^3 j_L'(k_n R)^2}} j_L(k_n r_i). \quad (\text{A.38})$$

In addition, we will work with potentials calculated in the continuous free-particle basis: that is, momentum-space basis states where the conjugate real space has not been compactified to a sphere of radius R but extends to infinity. These states are normalized not to a Kronecker delta but to the Dirac delta function:

$$\langle k' L' M' | k L M \rangle = \frac{(2\pi)^3 \delta(k - k')}{k^2} \delta_{LL'} \delta_{MM'}. \quad (\text{A.39})$$

These continuous free-particle basis states are given by

$$\langle r L M | k L M \rangle = 4\pi i^L j_L(kr). \quad (\text{A.40})$$

The normalization ($4\pi i^L$) can be obtained by inserting a complete set of three-dimensional real- and momentum-space states

$$\begin{aligned}\langle rLM|kLM \rangle &= \int d^3r' \int \frac{d^3k'}{(2\pi)^3} \langle rLM|\mathbf{r}'\rangle \langle \mathbf{r}'|\mathbf{k}'\rangle \langle \mathbf{k}'|kLM \rangle \\ &= \int d^3r' \int \frac{d^3k'}{(2\pi)^3} \frac{\delta(r-r')}{r^2} Y_{LM}^*(\theta, \phi) e^{i\mathbf{k}' \cdot \mathbf{r}'} \frac{(2\pi)^3 \delta(k-k')}{k^2} Y_{LM}(\theta_k, \phi_k).\end{aligned}\tag{A.41}$$

We use the plane-wave expansion and the orthogonality of the spherical harmonics to obtain

$$\begin{aligned}\langle rLM|kLM \rangle &= \sum_{L'M'} \int d\Omega d\Omega_k Y_{LM}^*(\Omega) Y_{L'M'}(\Omega) Y_{L'M'}^*(\Omega_k) Y_{LM}(\Omega_k) 4\pi i^{L'} j_{L'}(kr) \\ &= 4\pi i^L j_L(kr).\end{aligned}\tag{A.42}$$

Now we answer the question of how to obtain the potential in the discrete free-particle basis if it is originally in the continuous free-particle basis. We want the matrix elements $\langle k_m|V|k_n \rangle$ and we know the matrix elements $\langle k'|V|k \rangle$. We begin with the former and insert complete sets of real-space states, suppressing the quantum numbers

$$\langle k_m|V|k_n \rangle = \int dr' r'^2 \int dr r^2 \langle k_m|r'\rangle \langle r'|V|r\rangle \langle r|k_n \rangle.\tag{A.43}$$

We further insert complete sets of continuous momentum-space states

$$\begin{aligned}\langle k_m|V|k_n \rangle &= \int dr' r'^2 \int dr r^2 \int \frac{dk' k'^2}{(2\pi)^3} \int \frac{dk k^2}{(2\pi)^3} \langle k_m|r'\rangle \langle r'|k'\rangle \langle k'|V|k\rangle \langle k|r\rangle \langle r|k_n \rangle.\end{aligned}\tag{A.44}$$

The $\langle k_m|r'\rangle$ and $\langle r|k_n \rangle$ are given by $\sqrt{\frac{2}{R^3 j_L'(k_m R)^2}} j_L(k_m r')$ and $\sqrt{\frac{2}{R^3 j_L'(k_n R)^2}} j_L(k_n r)$ respectively, which we abbreviate as $A_{mL} j_L(k_m r')$ and $A_{nL} j_L(k_n r)$ respectively. The $\langle r'|k'\rangle$ and $\langle k|r\rangle$ are given by $4\pi i^L j_L(k'r')$ and $4\pi i^{-L} j_L(kr)$ respectively. Thus, we

can write

$$\begin{aligned} \langle k_m | V | k_n \rangle &= (4\pi)^2 A_{nL} A_{mL} \int \frac{dk' k'^2}{(2\pi)^3} \int \frac{dk k^2}{(2\pi)^3} \int dr' r'^2 j_L(k_m r') j_L(k' r') \times \\ &\quad \times \int dr r^2 j_L(k_n r) j_L(kr) \langle k' | V | k \rangle. \end{aligned} \quad (\text{A.45})$$

The r and r' integrals are closure relations for the spherical Bessel functions, which yield $\frac{\pi}{2k_n^2} \delta(k - k_n)$ and $\frac{\pi}{2k_m^2} \delta(k' - k_m)$ respectively. We can write the final relationship between the continuous momentum-space and discrete momentum-space matrix elements as

$$\langle k_m | V | k_n \rangle = \frac{1}{(4\pi)^2} \sqrt{\frac{2}{R^3 j'_L(k_m R)^2}} \sqrt{\frac{2}{R^3 j'_L(k_n R)^2}} \langle k' = k_m | V | k = k_n \rangle. \quad (\text{A.46})$$

Now we have all of the ingredients we need to calculate numerically the channel propagators needed in Chapter 3 as laid out schematically in Eq. (A.14).